

REPUBLIQUE DU CAMEROUN

UNIVERSITE DE YAOUNDE I

FACULTE DES SCIENCES

CENTRE DE RECHERCHE ET DE
FORMATION DOCTORALE EN
SCIENCES TECHNOLOGIE ET
GEOSCIENCES

UNITE DE RECHERCHE ET DE
FORMATION DOCTORALE EN
PHYSIQUES ET APPLICATIONS

DEPARTEMENT DE PHYSIQUE



REPUBLIC OF CAMEROON

THE UNIVERSITY OF YAOUNDE I

FACULTY OF SCIENCE

POST GRADUATE SCHOOL OF
SCIENCES, TECHNOLOGY
GEOSCIENCES

DOCTORAL RESEARCH UNIT AND
TRAINING IN PHYSICS AND
APPLICATIONS

DEPARTMENT OF PHYSICS

LABORATOIRE DE MECANIQUE, MATERIAUX ET STRUCTURES
LABORATORY OF MECHANICS, MATERIALS AND STRUCTURES

ON VIBRATION CONTROL OF MECHANICAL STRUCTURE WITH BOUC-WEN HYSTERESIS

Thesis submitted and defended in partial fulfillment of the requirements for the award of
degree of Doctor of Philosophy (Ph.D.) in Physics.
Speciality : **Mechanics, Materials and Structures**

By

YOUTH A NGOUOKO Octave Nathaniel

Registration number : 10W0906

Master of Science in Physics

Option : Fundamental Mechanics and Complex Systems

Under the supervision of

NANA NBENDJO Blaise Roméo

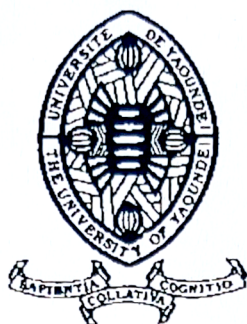
Professor

University of Yaoundé I

© Year 2023



UNIVERSITÉ DE YAOUNDÉ
THE UNIVERSITY OF YAOUNDE I



FACULTÉ DES SCIENCES
FACULTY OF SCIENCE

DÉPARTEMENT DE PHYSIQUE
DEPARTMENT OF PHYSICS

ATTESTATION DE CORRECTION DE LA THÈSE DE DOCTORAT/Ph.D

Nous, Professeur **DJUIDJE KENMOE Germaine** et Professeur **WOAFO Paul**, respectivement Examineur et Président du jury de la Thèse de Doctorat/PhD de Monsieur **YOUTH A NGOUOKO Octave Nathaniel**, Matricule **10W0906**, préparée sous la direction du Professeur **NANA NBENDJO Blaise Roméo** (Université de Yaoundé I), intitulée : « **ON VIBRATION CONTROL OF MECHANICAL STRUCTURE WITH BOUC-WEN HYSTERESIS** », soutenue le Mardi, **25 Avril 2023**, en vue de l'obtention du grade de Docteur/PhD en Physique, Spécialité **Mécanique, Matériaux et Structures**, option **Mécanique Fondamentale et Systèmes Complexes** attestons que toutes les corrections demandées par le jury de soutenance ont été effectuées.

En foi de quoi, la présente attestation lui est délivrée pour servir et valoir ce que de droit.

Examineur

Le Président du jury

Le Chef de Département de Physique



11 MAI 2023

Fait à Yaoundé, le

Pr. DJUIDJE KENMOE Germaine

Pr. WOAFO Paul

Pr. NDJAKA Jean-Marie Bienvenu

DEPARTMENT OF PHYSICS

On vibration control of mechanical structure with
Bouc-Wen hysteresis

Thesis

Submitted and defended for the award of
Doctorat/ PhD in Physics

Specialty: Mechanics, Materials and Structures

Option: Fundamental Mechanics and Complex Systems

By

YOUTHIA NGOUOKO Octave Nathaniel

Registration Number: 10W0906

Master degree in Physics

supervised by

NANA NBENDJO Blaise Roméo

Professor

e-mail address: ynonl@yahoo.fr

Year 2023

Contents

Dedications	viii
Acknowledgements	x
List of abbreviations	xiii
Abstract	xv
Résumé	xvii
General Introduction	1
1 Literature review	4
1.1 Introduction	5
1.2 Generality on mechanical hysteresis and its applications	5
1.2.1 History of hysteresis	5
1.2.2 Mechanical hysteresis	7
1.2.3 Some applications of hysteresis	8
1.3 Some mechanical hysteresis models	9
1.3.1 Coulomb model	10
1.3.2 Preisach model	10
1.3.3 Dahl model	11
1.3.4 Duhem model	11
1.3.5 Bouc-Wen model	12
1.4 General formalism of vibration control	13
1.4.1 Structural control systems	13
1.4.2 The Self-vibration control	16

1.5	Problematic of the thesis	17
1.6	Conclusion	18
2	Material and methods	19
2.1	Introduction	20
2.2	Bouc-Wen model: Considerations	20
2.2.1	The memory operators	21
2.2.2	Presentation of the model	21
2.2.3	Physical and mathematical consistency of the Bouc-Wen model	23
2.2.4	Characteristic of Bouc-Wen parameters model	26
2.3	Mathematical formalisms and numerical methods	29
2.3.1	Mathematical formalisms	29
2.3.2	Numerical methods	32
2.3.3	Hardware and software	34
2.4	Computational tools for the characterization of the dynamical states of non-linear systems	34
2.4.1	Phase portraits diagrams	34
2.4.2	Bifurcation Diagrams	35
2.4.3	Lyapunov exponents	35
2.5	Conclusion	36
3	Results and discussion	37
3.1	Introduction	38
3.2	On the appearance of horseshoe chaos in a nonlinear hysteretic systems with negative stiffness	38
3.2.1	Bouc-Wen model: Description	38
3.2.2	Appearance of separatrix	41
3.2.3	Melnikov analysis	43
3.2.4	Numerical investigation	47
3.3	On Appearance of homoclinic chaos in a SDoF oscillator with Bouc-Wen hysteresis: Mathematical formalism and dynamics explanation	50
3.3.1	Bouc-Wen hysteresis model: New consideration	50
3.3.2	Fixed points and their stability	50
3.3.3	Appearance of separatrix	52

3.3.4	Melnikov analysis	57
3.3.5	Basins of attraction	60
3.3.6	Bifurcation Diagram and Lyapunov Exponent	63
3.4	Complex horseshoe chaos on a nonlinear oscillator with hysteretic Bouc- Wen force	66
3.4.1	General mathematical formalism	66
3.4.2	Complex behaviour versus fractal	71
3.4.3	Fractal basin boundaries	74
3.5	Conclusion	77
	General conclusion	79
	Bibliography	83
	List of publications	96
	Collection of the published papers	98

List of Figures

1.1	a) A Han dynasty magnetic compass [124]; b) Magnetite [125],	6
1.2	Coulomb model	10
1.3	Hysteresis loop of Dahl model ($i = 1$)	11
1.4	Hyde System [45]	14
1.5	Principle of Tendon System [46]	15
1.6	Isolator device [126]	15
1.7	Principle of pagoda System [126]	17
2.1	Physical model	24
2.2	Hysteretic loops generated by BW model	27
2.3	Hysteresis loops generated by variation of the parameters of BW model: a) A, b) β , c) γ , d) n	28
3.1	a) Real system; b) Physical model	39
3.2	Softening hysteresis loop generated by the model for $D = 1, n = 2, A =$ $1, \gamma = 0.05$ and $\beta = 0.95$	40
3.3	Hardening hysteresis loop generated by the model for $D = 1, n = 2, A =$ $1, \gamma = -0.65$ and $\beta = 0.35$	40
3.4	a) Potential curve, b) Energy diagram of system for $\varepsilon = 1$	42
3.5	Heteroclinic orbit of unbounded monostable potential	44
3.6	Evolution of the critical amplitude F_{CR} as a function of : Ω (a), (c) and (e) ; α (b) ; A (d) and $(\gamma + \varepsilon\beta)$ (f) with $\varepsilon = 1$	46
3.7	Basins of attraction showing the confirmation of the analytical prediction for $\varepsilon = 1; \alpha = -0.5; \beta = 0.95; \gamma = 0.05; \varsigma = 0.02$ and $A = 1$	48
3.8	Effect of parameters $(\gamma + \varepsilon\beta)$, A and α , on the basin of attraction for $\Omega = 1$; $\alpha = -0.4; \gamma + \varepsilon\beta = 0.9$ and $A = 0.7$	49

3.9	Response of BW model under cyclic excitation, with parameters used in Fig 3.7 without control and Fig 3.8 with control: – without control; ... with control	49
3.10	Stability curve of system: With hysteretic force at point P_1 class III and class IV	52
3.11	Energy diagram of system for P_1 : a) Stable $\alpha = 0.85$, b) Unstable $\alpha = 0.5$ with $A = -2$; $\gamma = 0.05$; $\beta = 0.95$ and $\epsilon = 1$ (class III)	53
3.12	Potentials curves of system: Without hysteretic force (a) , with hysteretic force class III (b) and class IV (c) for $\epsilon = 1$; $\alpha = 0.666$; $A = -2$	55
3.13	Potentials curves of system, separatrix and homoclinic orbit of unbounded monostable potential :(a) Original and approximated potential (b) Separatrix (solid line) and homoclinic orbit(dashed-dashed line): for $\epsilon = 1$; $\alpha = 0.666$; $A = -2$; $\beta = 0.95$ and $\gamma = 0.05$	56
3.14	Evolution of the critical amplitude F_{cr} for appearance or disappearance of horseshoes chaos as a function ω for different values of α (a), A (c) and $\gamma + \epsilon\beta$ (e), as a function of α (b), A (d) and $\gamma + \epsilon\beta$ (f) : With $\epsilon = 1$; $\beta = 0.95$; $\gamma = 0.05$; $\alpha = 0.5$; $A = -2$ and $\zeta = 0.02$	58
3.15	Basins of attraction showing the confirmation of the analytical prediction: $D = 1$; $n = 1$; $\epsilon = 1$; $\omega = 0.85$; $\beta = 0.95$; $\gamma = 0.05$; $\alpha = 0.5$; $A = -2$ and $\zeta = 0.02$	61
3.16	Basins of attraction showing the confirmation of the analytical prediction: $\epsilon = 1$; $\omega = 0.85$; $\beta = 0.95$; $\gamma = 0.05$; $\alpha = 0.5$ and $\zeta = 0.02$	62
3.17	Bifurcation diagram (a) and Lyapunov exponent (b) vs the amplitude F_0 with the parameters of system: $D = 1$; $n = 1$; $\epsilon = 1$; $\alpha = 0.666$; $A = -2$; $\beta = 0.55$ and $\gamma = -0.54$	64
3.18	Various phase portraits in some intermittency areas for different values of F_0 : $F_0 = 4.3$ (a); $F_0 = 5.5$ (b). With $D = 1$; $n = 1$; $\omega = 1$; $\omega_0 = 1$; $\epsilon = 1$; $\alpha = 0.666$; $A = -2$; $\beta = 0.55$ and $\gamma = -0.54$	65
3.19	Physical model	67

3.20 Phase space, Asymmetric potentials and separatrix due to the hysteretic force:(a) Phase space of double well, (b) Asymmetric potential of double well ,(c) Asymmetric separatrix of double well, (d) Phase space of single well, (e) Asymmetric potential of single well ,(f) Asymmetric separatrix of single well (Heteroclinic Blue and Homoclinic Red) . $A = 1, \lambda_1 = 1, a_1 = -1, \lambda_2 = -1, a_2 = 1, \alpha = 0.5, n = 1$ and $\varepsilon = 1$ 69

3.21 Pertubed potential due to hysteretic force for orginal and approximated potential: (a) Two wells, (b) Single well. for $A = 1; \lambda_1 = 1; a_1 = -1; \lambda_2 = -1; a_2 = 1 \beta = 0.65 ; \gamma = -0.35 ; \alpha = 0.5 ; n = 1$ and $\varepsilon = 1$ 70

3.22 Melnikov criteria for the appearance of chaos in the $\omega - F_{Cr}$ plane. (a) Case of a homoclinic orbit (potential of Figure 3.17(a)). (b) Case of a single well potential (Figure 3.17(b)). for $A = 1; \lambda_1 = 1; a_1 = -1; \lambda_2 = -1; a_2 = 1 \beta = 0.65 ; \gamma = -0.35 ; \alpha = 0.5 ; n = 1$ and $\varepsilon = 1$ 73

3.23 Basins of attraction showing the Melnikov predictions: Case of two wells at left well as f_0 increases for $\lambda_1 = 1, a_1 = -1 \alpha=0.5, \beta=0.65, \gamma=-0.35, \varsigma=0.02$ and $A=1$; a) $f_0 = 0$; b) $f_0 = 0.02$; c) $f_0 = 0.05$; d) $f_0 = 0.5$ 75

3.24 Basins of attraction showing the Melnikov predictions: case of single well as f_0 increases for $\lambda_2 = -1, a_2 = 1 \alpha=0.5, \beta=0.65, \gamma=-0.35, \varsigma=0.02$ and $A=1$; a) $f_0 = 0$; b) $f_0 = 0.027$; c) $f_0 = 0.05$; d) $f_0 = 0.15$ 76

3.25 Effect of BW parameters A and α on the basins of attraction a) Case of two wells At left, b)case of single well. for $\Omega = 1 ; \alpha = 0.9 ; A = 0.2$ and $f_0 = 0.05$ 77

List of Tables

1.1	Some hysteresis models and their properties	9
2.1	Classification of the BIBO-stable Bouc-Wen models [78]	25
2.2	Different Cases of Hysteresis [78]	26

Dedications

I dedicate this work to:

♠ **Almighty God:** *The Eternal of Hosts* all love, joy, prosperity, honor and glory be yours.

♠ My Lovely Parents Mr. and Mrs. **NGOUOKO**: your love and advice are a source of success.

♠ My Brothers and Sisters **Valentin, Josiane, Marion, Ghislaine, Adjani, Audrey** and **Béneski**: your encouragements are full of confidence.

♠ My Queen **Leila Sandra**: Your love and help are precious.

♠ And My Sons **Archange Brell** and **Ethan Raphael**: having them is a blessing.

Acknowledgements

The work described in this thesis was carried out in the Laboratory of Modelling and Simulation in Engineering, Biomimetics and Prototypes (LaMSEBP), at the University of Yaoundé I (UYI). Many people have contributed wonderfully to the glorious end of this thesis. I would like to address my very king gratitude:

- To Professor **Blaise Roméo NANA NBENDJO**, Director of this thesis, For having granted me his confidence, his encouragement, his life advice, his rigor in the work, our constructive exchanges, his material and financial support and his spirit of conviviality have stayed the course for the realization of this work. The freedom he grants in the choice of ideas for the realization of projects has allowed me to evolve rapidly. This expression « *YOUTH Never Capitulate* » was for me a flight, a lightning starting point for the success of this work. Professor, thank you very much.
- To **Prof. Dr.-Ing Uwe DORKA** of University of Kassel, in Germany for his fruitful collaboration with **Prof. NANA NBENDJO** which led to this thesis topic. For his warm hospitality, our fruitful discussions and his helpful suggestions during my stay in Germany for the writing of this thesis.
- To Professor **Paul WOAFO**, Head of LaMSEBP for the spirit of openness that he brought to us in his teachings so that we could innovate in new technologies.
- To Professor **Jean-Marie Bienvenu NDJAKA**, the Head of Department of Physics, for the teachings, advices and encouragements that He gave to me during the academic cycles of Master and Doctorate/PhD.
- I wish to express my acknowledgements to all the members of the public defence jury, for the time that they give to evaluate this work and for all their remarks to render it.

-Prof. **Paul WOAFO**

-Prof. **Blaise Roméo NANA NBENDJO**

-Prof. **Clément TCHAWOUA**

-Prof. **Cornelius LUKONG FAI**

-Prof. **Germaine DJUIDJE KENMOE**

-Prof. **Martin SIEWE SIEWE**

-Prof. **Serge Ibraïd FEWO**

- I wish to express my acknowledgements to all the members of the jury audition, for all their remarks.
-Prof. **Jean-Marie Bienvenu NDJAKA**
-Prof. **SAÏDOU**
-Prof. **Aurelien KENFACK-JIOTSA**
- To Professor **Timoléon Crépin KOFANE**, for the valuable advice he taught us during his lectures.
- To Professor **Clément TCHAWOUA** for my successful initiation into the field of structures through its teachings in Elasticity-Plasticity and Rupture Mechanics during the Master's courses and my Master's Defence.
- To All the teaching staff and personnel of the Department of Physics, Faculty of Science, University of Yaoundé I, for their teachings and help since my Master degree in this institution.
- To **Steel and composite structures team of University of Kassel, Germany**, for the opportunity that they give me to follow part of this research study in their laboratory through ERASMUS PROJECT PhD Programme for Foreign PhD Student, Scholarship Partner Universities.
- To my elders in the lab: **Dr. Armand NANHA, Dr. Peggy NDEMANOU, Dr. Jules METSEBO, Dr. Hervé SONFACK, Dr. Merveil ANAGUE, Dr. Gabin OUMBE, Dr. Cloriant MBA, Dr. Eliane FANKEM** for your fruitful exchanges during my stay; One more time thank you .
- To my pairs and labmates: **Thomas DJUITCHOU, Dr. Hilaire SEGNING, Dr. Alex PIEDJOU, Dr. Dorota YOUMBI, Dr. Armel NGOUNOU, Dalahai MOKOLA, Gaëlle YANKAM, Ashley FEULEFACK, Merlin GUEPSI, Paola POUOKAM** and all the others, thank for your trust.
- To **Mr. and Mrs. NNANG** thank you for your encouragement and love.
- To **Uncle Alfred NZEA** for his ongoing guidance and unwavering support.
- To **Uncle Thierry LEUKOUA, families NNANG, MFABO, AFRICA, NNA, MASSANGO, BITCHEKI, FODJO, MANDA, FEUBI** for their full love.

-
- To that particular group of special persons on which I am extremely happy to be a member of. I think of **School Training Group (STG): LA RELEVE, Alain AVOM, Emmanuel MBARGA, Yves ENGON, Janice TCHANGBA, Julioce TCHINDA**, thank for the supports.
 - To all my parents, uncles, aunts, brothers, sisters, nephews, nieces, friends those whose names have not been mentioned here, those reading this work for their active support.

Please, receive all of you moreover, my gratefulness for this achievement, your achievement for you guide me unconditionally with love and I will respond also with unconditional and pure love.

List of abbreviations

SDoF: Single Degree Of Freedom

BIBO: Bounded Input-Bounded Output

BW: Bouc-Wen

HyDe: Hysteretic-Device

MR: Magneto-Rheological

ODE(s): Ordinary Differential Equation(s)

PDE(s): Partial Differential Equation(s)

RK4: Fourth-Order Runge-Kutta

FORTTRAN: mathematical FORMula TRANslating system

MATLAB: MATRIX LABORATORY

Abstract

This thesis highlights the dynamic response of a mechanical structure whose model takes into account its history of solicitation, and whose non-linearity refers to the memory effect that represents the phenomenon so-called hysteresis. The Bouc-Wen hysteresis model approach based on partial differential equations is used to highlight this type of behaviour. The following main results were obtained:

The appearance of catastrophic φ^4 monostable potential due to the presence of hysteretic force in the system is obtained as well as the appearance of Smale horseshoe chaos using Melnikov's theory. In addition, the effectiveness of the adaptive control is proven when the negative stiffness of spring increases.

A second approach is to choose a negative value of the shape parameter \mathbf{A} of the hysteretic model in the instability zone established using the Routh-Hurwitz criterion. Thus, a homocline catastrophic separatrix appears; therefore, this separatrix describes well the behaviour of real structures. The Melnikov limits for the appearance of Smale's horseshoe chaos are found and verified by the representation of stability basins at fractal boundaries, bifurcation diagram, Lyapunov Exponent and phase portraits of system are also investigated by means of numerical simulation. A very important step forward for the world of control has thus been updated.

A final approach considers the Duffing oscillator in the presence of the hysteretic force: Several complex behaviors are observed. We show how the parameters of the Bouc-Wen model strongly affect the dynamics of the crossing well in the case of two-well potential, and the configuration of the catastrophic monostable potential. We obtain approximately the criterion of appearance or disappearance of Smale's horseshoe chaos in the adaptive controlled system and the effect of the parameters of gain of control is analyzed.

Keywords: Degree of freedom, Hysteresis force, Bouc-Wen model, Negative Stiffness, Separatrix, Melnikov's theory, Horseshoes Chaos, Adaptive control, Duffing oscillator.

Résumé

Cette thèse met en exergue la réponse dynamique d'une structure mécanique dont le modèle prend en compte son histoire de sollicitation, et dont la non-linéarité renvoie à l'effet de mémoire qui représente le phénomène dit d'hystérésis. L'approche du modèle d'hystérésis de Bouc-Wen basée sur des équations aux dérivées partielles est utilisée pour mettre en évidence ce type de comportement. Les principaux résultats suivants ont été obtenus:

L'apparition du potentiel φ^4 mono-stable catastrophique dû à la présence de la force d'hystérésis dans le système est obtenue de même que l'apparition du chaos de fer-à-cheval de Smale en utilisant la théorie de Melnikov. En outre, l'efficacité du contrôle adaptatif est prouvée lorsque la rigidité négative du ressort augmente.

Une deuxième approche consiste à choisir une valeur négative du paramètre \mathbf{A} du modèle d'hystérésis dans la zone d'instabilité établie à l'aide du critère de Routh-Hurwitz. Ainsi, une séparatrice homocline catastrophique apparaît; par conséquent, cette séparatrice décrit bien le comportement des structures réelles. Les frontières de Melnikov pour l'apparition du chaos sont trouvées et vérifiées par la représentation des bassins de stabilité aux frontières fractales, le diagramme de Bifurcation, l'Exposant de Lyapunov et les portraits de phase du système sont aussi analysés au moyen des simulations numériques. Une avancée très importante pour le monde du contrôle a ainsi été mise à jour.

Une dernière approche considère l'oscillateur de Duffing en présence de la force d'hystérésis: Plusieurs comportements complexes sont observés. Nous montrons comment les paramètres du modèle Bouc-Wen affectent fortement la dynamique des puits de croisement dans le cas du potentiel à deux puits, et la configuration du potentiel mono-stable catastrophique. Nous obtenons approximativement le critère d'apparition du chaos dans le système adaptatif contrôlé et l'effet des paramètres de gain de contrôle est analysé.

Mots-clés: Degré de liberté, Force d'hysteresis, Modèle Bouc-Wen, Rigidité négative, Séparatrice, Théorie de Melnikov, Chaos de fer-à-cheval, Contrôle adaptatif, Oscillateur de Duffing.

General introduction

Structural systems often show nonlinear behavior under severe excitations generated by natural hazards. In that condition, the restoring force becomes highly nonlinear showing significant hysteresis. The hereditary nature of this nonlinear restoring force indicates that the force cannot be described as a function of the instantaneous displacement and velocity. Nowadays, one of the constant challenges of mechanical systems is to design new reinforcement techniques for existing structures so that they offer a real comfort of safety for their occupant while ensuring the lifespan of the structure. Accordingly, many hysteretic restoring force models were developed to include the time dependent nature using a set of differential equations [1]. This nonlinear behavior is encountered in a wide variety of processes in which the input-output dynamic relations between variables involve memory effects. Examples are found in biology, optics, electronics, ferroelectricity, magnetism, mechanics, structures, among other areas. In mechanical and structural systems, hysteresis appears as a natural mechanism of materials to supply restoring forces against movements and dissipate energy. In these systems, hysteresis refers to the memory nature of inelastic behavior where the restoring force depends not only on the instantaneous deformation, but also on the history of the deformation.

In general, hysteresis describes a situation where entry into a system results in a delayed result, and the system changed significantly during the delay. Delays caused by these situations, called mechanical hysteresis, can cause unexpected behavior in a mechanical system. This unexpected behavior can range from slight friction to severe vibration problems that could threaten the structural integrity of a project. Mechanical hysteresis is notoriously difficult to predict and minimize in many areas of engineering. This limitation in modelling makes it difficult to anticipate the stability and control of mechanical systems. Indeed, in nature, internal factors: type of materials, chemical composition, crystalline or amorphous structure, etc. External factors: temperature, initial load, initial stress, etc. And the factors related to motion: amplitude and frequency of deformation, state of the

stress can generate a variation of dissipative and elastic forces, accompanied by a dissipation of energy [2] which in most cases lead to explosions, fires, destruction of rooms, collapses of buildings.

In order to characterize the presence of hysteresis in a physical system, several researchers, in this case engineer Bouc in 1966 [3], initiated the mathematical study of hysteresis. This study was extended by Wen in 1976 [4], Mayergoyz [5], Visintin [6], Brokate and Sprekels [7], and Krejci [8] in the 1980s led to an understanding of general scalar hysteresis operators, including, in particular, the Preisach operator [9]. These authors also studied the existence and uniqueness of solutions of ordinary differential equations (ODEs) and partial differential equations (PDEs) coupled with hysteresis operators. A renewed interest in smart materials and their control took place in the 1990s stimulated by the development of new materials that showed significant magnetostrictive and electrostrictive properties. Numerical and experimental analyses as well as theories have been developed, in particular in the modelling of the behavior of rheological magneto dampers, basic insulation devices for buildings and other types of damping devices [10]. In these contexts, a certain type of structural protection system must be implemented to mitigate the effects of environmental damage. From this, many unresolved problems of vibration analysis with contact, play or friction still remain.

Therefore, health control technologies and their overall integration offer a new approach to manage the life cycle of structures. They allow designers to hope for smaller design margins and lighter structures: this is the case of the BW [4, 11] model, which is undergoing a meteoric evolution, including the latest techniques for modelling intelligent structures and materials and is formulated according to the problem posed. The precise prediction of mechanical hysteresis and the limitations on the consideration of hysteretic behavior when designing mechanical structures subject to external actions are complex and continuous problems encountered in structural dynamics.

To understand the stakes of this phenomenon of hysteresis in mechanical structures, the case of interest in the thesis is to characterize the vibrational behavior of a mechanical structure by using hysteresis type BW and to propose adequate adaptive control techniques to reduce vibration within the said structure. We are focused on the following problems:

1- Mathematical modelling of the hysteresis phenomenon and its insertion into the simulation of mechanical systems.

2- The use of mathematical and numerical tools to access the behavior of the

structural system and analyze the influence of hysteresis on each type of system.

3- The design and optimization of a new control strategy (Find the best control parameters for which the system is adaptive while ensuring the safety and stability of the structures)

Following this introduction, the thesis is organized as follows:

- In the first chapter, Literature review on hysteresis, some mechanical hysteresis models and general formalism in vibration control are presented.
- Chapter two presents Bouc-Wen hysteresis model : analytical and numerical formalisms. The mathematical and numerical tools used to characterize the dynamic responses of the studied structural system are also illustrated in this chapter.
- Chapter three presents and discusses our main results. The mathematical model describing the dynamic behavior of the structural system with Bouc-Wen hysteretic force under the periodic excitation is presented. Afterwards, a adaptive control law is defined and used to suppress the chaotic behavior in the structural system.
- We end by a general conclusion which gives the main results obtained and perspectives for future investigations.

CHAPTER I

LITERATURE REVIEW

1.1 Introduction

Hysteresis is a phenomenon observed across many scientific fields ranging from physics, chemistry, and engineering to biology, materials and economics. It is incorporated in many artificial systems [12, 13]. In addition, hysteresis is ubiquitous in smart materials, such as piezoelectric, magnetostrictive, shape memory alloys, and active electro polymers as well as in many other natural phenomena. In natural systems, it is often associated with irreversible thermodynamic changes such as phase transitions and internal friction; and dissipation is a common side effect.

Hysteresis also occurs in mechanical systems (in the form of backlash and friction) and geophysical systems. Mechanical hysteresis is a common engineering problem that can lead to unexpected results in mechanical systems, it affects many materials and industries in various ways, including through friction and wear of components. Therefore, consideration of this nonlinearity in the design of mechanical structures would be of great interest to the control community in order to better predict the dynamic behavior of future structures.

The purpose of this chapter is to provide background information on some mechanical hysteresis models, their mathematical modelling, and some additional details on control mechanisms. The chapter is organized as follows: Section 1.2 provides general information on hysteresis and its applications. In Section 1.3, we briefly describe some models of mechanical hysteresis and the equations modeling their behavior. In Section 1.4, an overview of the control mechanisms used in the literature will be presented, Finally Section 1.5 concludes the chapter.

1.2 Generality on mechanical hysteresis and its applications

Hysteresis is a phenomenon observed across many scientific fields such as physics, chemistry, engineering, biology and economics. In general Hysteresis is the dependence of the state of a system on its history.

1.2.1 History of hysteresis

The term “hysteresis” is derived from the Greek hysteros word meaning “delay”. The study of hysteresis has a long history (see [6]). Although James A. Ewing [14] coined the word

hysteresis during his study of ferromagnetism in 1881, the special properties of magnetite, that is, loadstone, seem to have been known and utilized by ancient Greek and Chinese civilizations at least in first and second millennia B.C. respectively (see [15]). The ancients constructed compasses (fig.1.1(a)) that take advantage of the remanance property of magnetite (fig.1.1(b)), which is a consequence of hysteresis in the magnetic–field input versus the magnetization output. Contributions to the study of hysteresis were made by Madelung (1905) [16], who discovered the rules for scalar hysteresis; Weiss (1907) [17], who introduced the concept of a magnetic domain based on spontaneous magnetization; By the 1920s, researchers in plasticity and soil mechanics had discovered the hysteresis phenomenon as well. and the rate at which these maxima or minima are achieved does not matter. Prandtl (1924) considered a scalar model of elastoplasticity, which was later rediscovered by Ishlinskii (1944). Heisenberg (1928), who explained spontaneous magnetization in terms of quantum mechanics; Haines (1930) [19] discovered a hysteretic relationship between moisture content in the soil and capillary pressure. Preisach (1935) [9] who introduced a model for scalar hysteresis; and Landau (1937) [20], who developed a qualitative theory of phase transitions, which explains various kinds of hysteretic phenomena. The mathematical study of hysteresis was initiated not by a mathematician, but by an engineer Bouc (1966) [3], who studied scalar hysteresis as a map between function spaces, This study is extended by Wen in (1976) [4]. Starting in 1970, systematic study was undertaken by Krasnoselskii, Pokrovskii, and others, who constructed rate–independent hysteresis operators from elementary units called hysterons [21]. Further work by Mayergoyz [5], Visintin [6], Brokate and Sprekels [7], and Krejci [8] in the 1980s led to an understanding of general scalar hysteresis operators. Hysteresis due to sunk–costs was studied as a fundamental economic phenomenon in the 1980s [22].

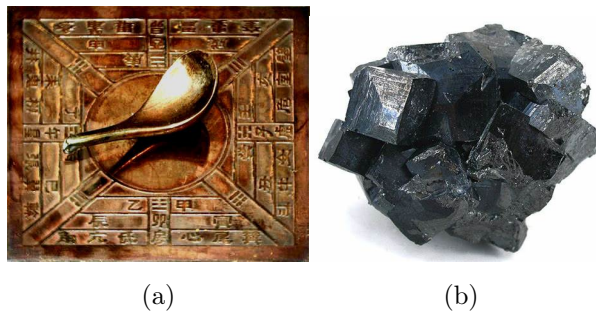


Figure 1.1: a) A Han dynasty magnetic compass [124]; b) Magnetite [125],

1.2.2 Mechanical hysteresis

Mechanical hysteresis can come from many sources and can have a broad effect on mechanical and electrical systems. Two of the most easily recognizable are deformation and friction. Deformation can be the product of many forms of hysteresis, including mechanical and voltage hysteresis. Mechanical hysteresis promotes deformation once it starts. Once a component is deformed, it dissipates energy at an increasing pace as its deformation continues, rather than converting energy into work as intended. This is partially due to friction but can be affected by many other factors, including the integrity of materials and the environment in which energy dissipation happens. Engineers and designers can calculate how much energy is being lost by estimating the amount of mechanical hysteresis in a system.

There are two different types of mechanical hysteresis: rate-independent and rate-dependent. Rate-independent hysteresis has the potential to permanently change the properties of a mechanical system. Rate-dependent hysteresis, by contrast, depends on how long unexpected inputs continue and eventually levels off to zero when unexpected inputs end. The effects of rate-independent hysteresis can persist after unexpected inputs end. Both types of mechanical hysteresis can cause physical changes to a system, but those created by rate-dependent hysteresis may take much longer to alter the system's functionality in a significant way.

- **Rate-dependent** hysteresis usually occurs as a simple lag between input and output. If the input is reduced to zero, the output continues to respond for a finite time. When rate-dependent hysteresis is due to dissipative effects like friction, it is associated with power loss.

- **Rate-independent** hysteresis indicates a persistent memory of the system to its past (loading history/response) that remains after the transients have died out.

Mechanical hysteresis is usually characterized as an engineering problem, which is how the rest of this thesis will describe it. However, it is important to note that there are also specific instances where mechanical hysteresis can be helpful to engineers.

1.2.3 Some applications of hysteresis

Hysteresis can be exploited in a positive ways both in nature and in engineering applications.

1- In Nature:

- Biological systems

- In biology, hysteresis provides a mechanism that enhances the robustness of cell functions against random perturbations.

2- In Engineering:

- Electronic circuits

- Often, some amount of hysteresis is intentionally added to an electronic circuit to prevent unwanted rapid switching. Example a Schmitt trigger is a simple electronic circuit that exhibits this property.

- Hysteresis is essential to the workings of some memristors (circuit components which *remember* changes in the current passing through them by changing their resistance) [23].

- As another example, hysteretic switching prevents chattering and the associated consequences in switched systems, such as thermostats, digital circuits, and power electronics.

- User interface design

- A hysteresis is sometimes intentionally added to computer algorithms. The field of user interface design has borrowed the term hysteresis to refer to times when the state of the user interface intentionally lags behind the apparent user input.

- Control systems

- In control systems, hysteresis can be used to filter signals so that the output reacts less rapidly than it otherwise would by taking recent system history into account. For example, a thermostat controlling a heater may switch the heater on when the temperature drops below A, but not turn it off until the temperature rises above B.

- Magnetorheological (MR) fluids are a class of new smart materials whose rheological characteristics change rapidly and can be controlled easily in the presence of an applied magnetic field. The devices based on MR fluids, including dampers, brakes, clutches, polishing devices and hydraulic valves, etc., have a very promising potential future; some of them have been used commercially in engineering applications such as automobiles, polishing machines, exercise equipment, etc.

- Hysteresis is the fundamental mechanism in magnetic data storage and emerging computer memory technologies, such as ferroelectric nonvolatile thin-film memories, which

are major enablers of the information technology industry.

1.3 Some mechanical hysteresis models

Hysteresis models are linear or nonlinear and can be mathematically difficult to model. A fundamental theory allowing a general mathematical framework for modelling hysteresis has not been developed up to now. For specific problems, models describing hysteretic systems can be derived from an understanding of physical laws. Usually this is an arduous task and the resulting models are too complex to be used in practical applications. In general, engineering practice seeks for alternative more simple models which, although not giving the best description of the physical behavior of the system, do keep relevant input-output features and are useful for characterization, design and control purposes. These models are referred to as phenomenological or semi-physical models. The mathematical formulations used to model hysteretic phenomena lead to both finite and infinite dimensional models, in which the state is the system memory.

In the literature on hysteresis, there are some types of commonly used hysteresis models, namely, Coulomb model, the Preisach model, the Dahl model, the Duhem model, and the Bouc-Wen model. A brief overview of these models and their properties is given in Table 1.1.

Table 1.1: Some hysteresis models and their properties

Hysteresis models	Rate-dependence	Type of Memory	continuity
Coulomb	Rate-independent	nonlocal	discontinuous
Preisach	Rate-independent	nonlocal	discontinuous
$\gamma = 0$	Rate-independent	local	discontinuous
Dahl $0 < \gamma < 1$	Rate-independent	local	continuous
$\gamma \geq 1$	Rate-independent	local	Lipschitz
Duhem	Rate-dependent or independent	local or nonlocal	Lipschitz
Bouc-Wen	Rate-independent	nonlocal	Lipschitz

1.3.1 Coulomb model

From the macroscopic point of view, the contact between two surfaces creates a contact force whose tangential component defines the friction force. The magnitude of the Coulomb model friction force is proportional to the normal load [34], that is:

$$F_C = \mu F_N \quad (1.1)$$

where μ is commonly referred to as the friction coefficient and F_N is the normal force. The magnitude of the Coulomb model friction force is independent of the magnitude of the velocity and the contact area and the friction force opposes the motion of the body. The friction force can be expressed as:

$$F_f = \text{sign}(v) F_C \quad (1.2)$$

where v is the velocity of the body relative to the surface [34–36].

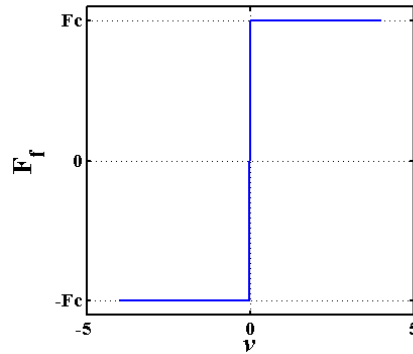


Figure 1.2: Coulomb model

1.3.2 Preisach model

The Preisach model [24] is an integral operator, that operates on an infinite number of elementary hysteresis operators called hysterons. The hysterons are turned *on* or *off* depending on the direction and value of the input. The hysterons that are on contribute to the output, while the hysterons that are *off* do not. The Preisach model has the form:

$$y(t) = \int \int_{\alpha \geq \beta} \mu(\alpha, \beta) \hat{\gamma}_{\alpha\beta} u(t) d\alpha d\beta \quad (1.3)$$

where $u(\alpha, \beta)$ is a weight function, $u(t)$ is the input, the hysteresis operator $\hat{\gamma}_{\alpha\beta}$ is called a hysteron, and α and β are the values at which the output of the hysteron, is switched on

and off, respectively. Preisach models are rate-independent and have nonlocal memory. They are often used to model hysteresis in piezoceramic actuators, shape memory alloys, and magnetism [25–27]. The Prandtl-Ishlinskii model, which is a special type of Preisach model, replaces the hysterons by the play operators weighted by a density function [6, 7, 28, 29].

1.3.3 Dahl model

One of the first models proposed to improve system control in the presence of dry friction is the Dahl model. This model [37–39] has the form :

$$\dot{F}_f(t) = \sigma \left| 1 - \frac{F_f(t)}{F_c} \operatorname{sgn}(\dot{u}) \right|^i \operatorname{sgn} \left(1 - \frac{F_f(t)}{F_c} \operatorname{sgn}(\dot{u}) \right) \dot{u}(t) \quad (1.4)$$

where F_f is the friction force, u is the relative displacement between the two surfaces in contact, $F_c > 0$ is the Coulomb friction force, $i \geq 0$ is a parameter that determines the shape of the force- displacement curve, and $\sigma > 0$ is the rest stiffness, that is, the slope of the force-deflection curve when $F_f = 0$. The right-hand side of Eq(1.4) is Lipschitz continuous in F_f for $i \leq 1$. but not Lipschitz continuous in F_f for $0 \leq i \leq 1$.

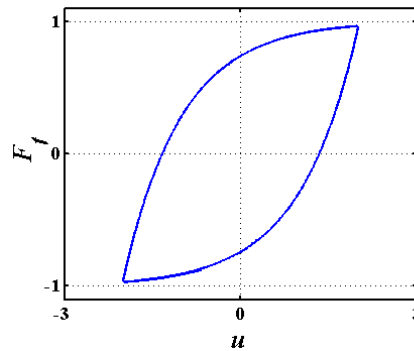


Figure 1.3: Hysteresis loop of Dahl model ($i = 1$)

1.3.4 Duhem model

The Duhem model has been used to represent friction [55], electromagnetic behavior [53, 54], or hysteresis in magnetorheological dampers [56]. The state of the Duhem model depends on the derivative of the input and thus the output changes its character when the input changes direction [30–33] The general form of the Duhem model is:

$$\dot{x} = f(x(t), u(t)) g(\dot{u}(t)) \quad (1.5)$$

$$y(t) = h(x(t), u(t)) \quad (1.6)$$

where g is a function that determines how the output changes as the input changes direction [50]. The function g satisfies $g(0) = 0$ and thus, for a constant input $u(t) = \bar{u}$, there is an infinite number of equilibria. Duhem models can be rate-dependent or rate-independent and can exhibit local or nonlocal memory [30].

1.3.5 Bouc-Wen model

This model was proposed for application to vibratory systems. The Bouc-Wen [5] model has the form:

$$\dot{z}(t) = A\dot{u}(t) - \beta |\dot{u}(t)| |z(t)|^{n-1} z(t) - \gamma \dot{u}(t) |z(t)|^n \quad (1.7)$$

or simply as:

$$\dot{z}(t) = (A - [\beta \text{sgn}(z(t) \dot{u}(t)) + \gamma] |z(t)|^n) \dot{u}(t) \quad (1.8)$$

$z(t)$ is a non-observable hysteretic parameter (usually called the hysteretic displacement) that obeys the following nonlinear differential equation with zero initial condition ($z(0) = 0$), and that has dimensions of length: where sgn denotes the signum function, and $A, \beta > 0$, γ and n are dimensionless quantities controlling the behaviour of the model ($n = \infty$ retrieves the elastoplastic hysteresis).

1.4 General formalism of vibration control

Engineers are becoming increasingly aware of the problems caused by vibration in engineering design, particularly in the areas of structural health monitoring and smart structures. Vibration is a constant problem as it can impair performance and lead to fatigue, damage and the failure of a structure. Control of vibration is a key factor in preventing such detrimental results. The structural control presents a homogenous treatment of vibration by including those factors from control that are relevant to modern vibration analysis, design and measurement . Mechanisms for control of structural response can be classified into four main groups: passive, active, semi-active and hybrid [40].

1.4.1 Structural control systems

For several years, always with the aim of improving the performance of controllers and having stronger structures, Structural control system has emerged and is now more and more widespread in the world. It can be passive, active, semi-active or hybrid; it depends on how it is modeled. Structural control is the control of selected response variable of a structure subjected to dynamics loading [41].

- Such variables may be displacements or their time derivatives (velocities, accelerations) and/or forces
- Full controllability can be achieved in mode control and the control of rigid body mechanism
- For mode control, a structural system is needed that has clearly defined modes
- For rigid body control, a structural system must consist of an assemblage of rigid bodies

Therefore, Structural Control is **NOT**:

- Added damping
- Added damping and stiffness
- Or any conventional structural system with additional devices: **No system variable is controlled in such structures!**

The first step in structural control is to select a structural concept that is controllable! [42]

1.4.1.1 Control system with hysteretic devices

1.4.1.1.1 Hysteretic device (HyDe) system

Hysteretic-Device or Hyde-systems are a kind of structural control system that introduces a stiff-ductile mechanism into the structure [43, 44]. By doing so, the structure becomes an assembly of rigid bodies moving in a defined pattern with internal forces limited by the yield level of the devices that are placed in the joints between the rigid bodies (fig.1.4). Such an assembly dissipates almost all the input energy due to an earthquake in these devices through plastic yielding or friction. This characteristic leads to very small stresses in the structure and at the same time limits the motion of the mechanism. It is a system that can be applied to new structures but is most suitable for retrofitting, especially when it comes to the so-called soft storey structures. Such structures are abundant in modern cities due to the presence of open spaces in the ground floor and apartment floors above stiffened by “non-structural” partition walls usually made of bricks. The upper storeys thus form a rigid block on top of a horizontal seismic joint: The natural place for stiff-ductile devices to make it a HyDe-system [45].

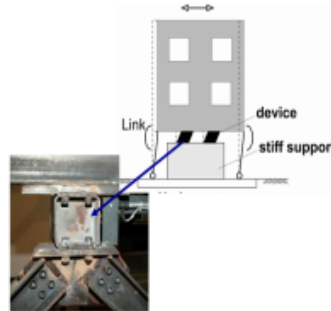


Figure 1.4: Hyde System [45]

1.4.1.1.2 Tendon system

Tendon Systems are one of the structural control systems for earthquake protection. In this system, rigid bodies are connected through single cables or through a cable network as shown in fig.1.5 below [46]. Systems of this type generally consist of a set of prestressed tendons connected to a structure with their tensions being controlled by servomechanisms. One of the reasons for favoring such a control mechanism has to do with the fact that tendons are already existing members of many structures. This is attractive, for example in the case of retrofitting or strengthening an existing structure [47]. The pre-stressing

forces of the cables are regulated strategically at given locations. Therefore, a suitable dynamic mechanism can be established [48].

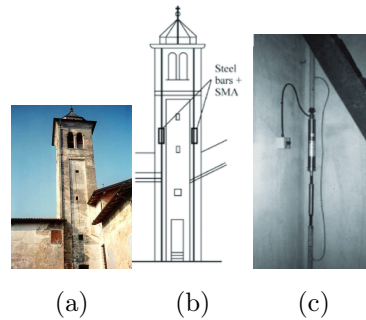


Figure 1.5: Principle of Tendon System [46]

1.4.1.1.3 Base isolation system

These systems consist of placing, between the foundations and the superstructure, devices that have a very high horizontal deformability and a very high vertical stiffness. These devices make the decouple of the movement of the ground from the structure possible in order to reduce the forces transmitted to it. The isolator captures deformations (inelastic) and filters the accelerations (high frequencies) so that the isolated superstructure moves essentially in a rigid mode undergoing low accelerations and almost no deformation. As a result, the inertial forces transmitted to the foundation elements are limited and remain below the elastic capacity of such elements. Base isolation is based on the principle that if the vibration period is increased sufficiently to move away from the predominant earthquake excitation period, the accelerations transmitted to the structure (and consequently the inertial forces) are considerably reduced. On the other hand, the increase of the period generates larger displacements concentrated at the level of the isolator [131] (fig.1.6).

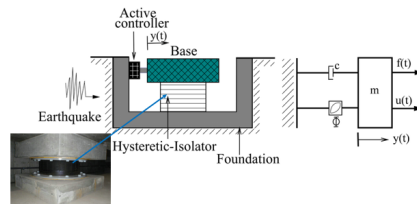


Figure 1.6: Isolator device [126]

1.4.2 The Self-vibration control

- A self-controlled system is a system which has the ability to maintain or turn back itself in a suitable stage whatever what disturb it and put it away from that stage

- Self-controlled is also known as maintained self-oscillation, self-excited, self-induced, spontaneous, autonomous.

- These structures do not need any external help or internal system (structural control system, etc) to be controlled

- This new system is suitable for high-rise buildings because there generally have flexible and low damping characteristics

This fact is already scientifically explained, but no modern structure has been built with this robust structural system, which belongs to a class of seismic control concepts. These concepts rely on the control of rigid body motions allowing for a drastic reduction in kinetic and potential energy in the structure, thus leading to a very robust behaviour. In this field, two first models were already proposed and is shown in the following paragraphs.

1.4.2.1 Control system with hysteretic behaviour

1.4.2.1.1 Pagoda system

Pagoda system, inspired by high seismic performance of old built Pagoda structures (fig.1.7), is one of the most powerful design structure which react positively when they face earthquake [49–51]. The traditional Pagoda already was built by a highly flexible kit system allowing the building to move and shake in a controlled way thus absorbing the vibrations. The Pagoda performs a so-called **snake dance** during an earthquake, which has protected it from failure for over 1300 years. Therefore, the beams and columns of such a house were only plugged together (interlocking technology) and not joined in a fixed way or nailed. These joints allowed the joined elements to move within a certain scope [52]. In the literature, according to dear configuration, it is two different kinds of Pagoda structures:

- The first one is most build with wood, we usually see that kind of building in China and all the pieces of wood are assembled without the least nail! All is indeed fitted one in another thanks to sets of tenons, mortises.

- The second one is characterized by his central mast called **”Shin-bashira”** which can be useful for repositioning of one story if it is deviated, we can also notice that Load at different levels can help to stabilize the building after a disturbance.

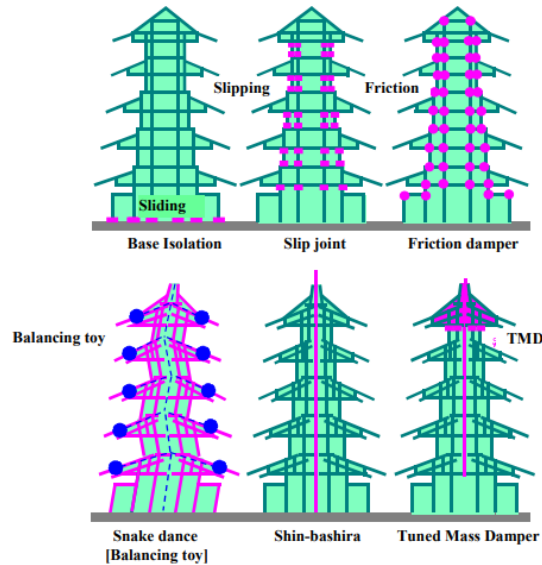


Figure 1.7: Principle of pagoda System [126]

1.5 Problematic of the thesis

As mentioned earlier, hysteresis describes a situation where entry into a system results in a delayed result, and the system changed significantly during the delay. Delays caused by these situations, called mechanical hysteresis, can cause unexpected behavior in a mechanical system. This unexpected behavior can range from slight friction to severe vibration problems that could threaten the structural integrity of a project. Mechanical hysteresis is notoriously difficult to predict and minimize in many areas of engineering. This limitation in modelling makes it difficult to anticipate the stability and control of mechanical systems. The Bouc-Wen model is a common equation for measuring mechanical hysteresis in engineering and electronics. It was directly inspired by vibrations caused in physical systems, a problem that is common in electrical engineering.

Our model is based on the behavior of pagoda systems which have great deformity and resistance to extreme excitations. Thus, the attention of this thesis work is to evaluate the total energy dissipated by the structure by means of the Bouc-Wen model in order to analyse the response of the structural system and finally to evaluate the performance of the self-contained system by playing with the parameters of the model.

1.6 Conclusion

In this chapter, the generalities on mechanical hysteresis and its applications were provided. Some hysteresis models and general formalism of vibration control are too presented. The Bouc-Wen model, which takes into account memory effects, depending on the rate and which can account for elasto-plastic behavior, was adopted to model the structures used in this work. The next chapter will be devoted to the mathematical modelling of Bouc-Wen model in mechanical structures, the analytical and numerical formalism used to solve the problem of the thesis.

CHAPTER II

MATERIAL AND METHODS

2.1 Introduction

This chapter deals a general background on the BW model and focuses on the different methods used to solve the problems statement of the thesis. Section 2.2 presents the conception of BW model and theirs dynamics properties. Section 2.3 is devoted to the mathematical formalisms and the numerical methods used to solve the differential equations as well as the hardware and software used. In section 2.4, the computational tools for the characterization of the dynamical states are given. The conclusion of the chapter appears in section 2.5.

2.2 Bouc-Wen model: Considerations

A popular and versatile hysteretic model is the BW model [4, 57]. It has been applied in many problems, including the response of beam members [58, 59], concrete walls [60], masonry walls [61], seismic isolation devices [62, 63], wood joints [64], caisson foundations [65], magnetorheological fluid dampers [66, 67], as well as more specific applications such as the stick-slip phenomena in elevator guide rails [68], or the restoring force in seat suspension systems [69], to name a few. A survey on the implementations of the BW model can be found in the work of Ismail et al. [70]. Being phenomenological, the BW model is able to describe complex responses using even single degree-of-freedom (SDoF) systems. These can be embedded into large-scale models or used in finite element analysis [71–73]. The complex internal mechanism producing the overall hysteresis is not examined at all. Obviously, the response and dissipated energy of such a system is of great interest.

Within this context, a hysteretic semi-physical model was proposed initially by Bouc early in 1971 and subsequently generalized by Wen in 1976. Since then, it was known as the BW model and has been extensively used in the current literature to describe mathematically components and devices with hysteretic behaviors, particularly within the areas of civil and mechanical engineering. The model essentially consists in a first-order nonlinear differential equation that relates the input displacement to the output restoring force in a hysteretic way. By choosing a set of parameters appropriately, it is possible to accommodate the response of the model to the real hysteresis loops.

2.2.1 The memory operators

The hysteresis phenomena due to a (temporal) memory of the system can be noted in a very general way [74–76]:

$$r(t) = H(u(\cdot), t, r(0)), \quad (2.1)$$

where H is a causal operator: the value $r(t)$ is the function of both the initial value $r(0)$ and the history $u(\tau)$, $0 \leq \tau \leq t$ of the input signal. H is for example a convolution operator:

$$r(t) = \int_0^t K(t-s, t) \cdot G(u(s)) \cdot ds + r_0 \quad (2.2)$$

The definition given here of H : a causal operator, or even more specifically a causal convolution operator - is very broad: in particular, it includes linear operators, the behavior of which is not usually considered hysteretic. This is the reason why it must be restricted.

According to Visintin [6], *hysteresis = rate-independent* memory effect. Thus, the future state of a hysteretic system depends not only on its current state but also on its past history.

$$r(t) = \mu^2 u(t) + f(u(t)) + \psi(t), \quad (2.3)$$

where $\mu^2 u$, $f(u)$ and ψ represent linear, nonlinear, and hysteresis instantaneous terms, respectively. ψ takes into account the memory of the material studied, its "**heredity**". We first choose to write:

$$\psi(t) = \int_{t_0}^t F(t, s) du(s) \quad (2.4)$$

$F(t, s)$ is the forgetting function; it generally only depends on the quantity $(t-s)$ and ψ then appears as a convolution; hereditary actions being forgotten as time passes, $F(s)$ is chosen as a finite, continuous, positive, decreasing function for $s \geq 0$, zero for $s \leq 0$. But it is also required that the trajectories remain identical by compression or dilation of time (rate-independence); this means that, for the physical systems described, the rate of the observed hysteresis cycles does not depend on the frequency of the operator input signal. The expression of ψ above is not suitable, but we keep the idea of such an integral expression, the argument of the function F then being an interval function; positive, increasing as s moves away from t .

2.2.2 Presentation of the model

The starting point of the so called **Bouc-Wen** model is the early paper by [11], where a functional that describes the hysteresis phenomenon was proposed. Among the different

models of hysteresis proposed by Bouc (1971) [11], the simplest one can be formulated by a Stieltjes integral as follows:

$$\begin{cases} F(t) = \alpha x(t) + z(t) \\ z(t) = \int_0^{\xi_s} \mu(\xi_s(t) - \tau) dx(\tau) \end{cases} \quad (2.5)$$

where α is a non-negative constant; x and F are two time-dependent functions, which are considered as input and output functions, respectively. In structural engineering applications the input usually has the meaning of a generalized displacement, while the output F plays the role of a generalized force, defined as the sum of a linear term $\alpha x(t)$ and a hysteretic term $z(t)$.

The integral in Eq(2.5)₂ depends on the time-function $\xi_s(t)$, which is named internal time and is assumed to be positive and non-decreasing. The function μ , called the hereditary kernel, takes into account hysteretic phenomena. One of the definitions of ξ_s proposed by Bouc is the total variation of x :

$$\xi_s(t) = \int_0^t \left| \frac{dx}{d\tau} \right| d\tau \quad \text{or, equivalently} \quad \dot{\xi}_s = |\dot{x}|, \quad \text{with} \quad \xi_s(0) = 0 \quad (2.6)$$

where the superposed dot indicates time-differentiation. (2.6) implies the rate-independence of ξ_s and as a result, z and F are in turn rate-independent. Bouc (1971) [11] defined μ as a continuous, bounded, positive and non-increasing function on the interval $\xi_s \geq 0$, having a bounded integral. In the special case of an exponential kernel.

$$\mu(\xi_s) = A e^{-\beta \xi_s} \quad \text{with} \quad A, \beta > 0 \quad (2.7)$$

a differential formulation of (2.5) can be easily deduced. Then, (2.6) and (2.7) imply:

$$\begin{cases} F(t) = \alpha x(t) + z(t) \\ \dot{z} = A\dot{x} - \beta z \dot{\xi}_s \quad \text{with} \quad \dot{\xi}_s = |\dot{x}| \end{cases} \quad (2.8)$$

One can observe that for an initial value in the interval $(-z_x, z_x)$, with $z_x = A/\beta$, the hysteretic force z remains in the same interval. Bouc (1967) [57] proposed a more general formulation of (2.8):

$$\begin{cases} F(t) = \alpha x(t) + z(t) \\ \dot{z} = A\dot{x} - \beta z |\dot{x}| - \gamma |z| \dot{x} \quad \text{with} \quad \gamma < \beta \end{cases} \quad (2.9)$$

While Wen (1976) [4] suggested a further modification by introducing a positive exponent n :

$$\begin{cases} F(t) = \alpha x(t) + z(t) \\ \dot{z} = A\dot{x} - (\beta \text{sgn}(z\dot{x}) + \gamma) |z|^n \dot{x}, \end{cases} \quad (2.10)$$

where $\text{sgn}(\bullet)$ is the signum function. Wen did not impose any condition on the value of γ and assumed integer values for n ; however, all real positive values of n are admissible. When n is large enough, force-displacement curves similar to those of an elastic-perfectly-plastic model with the additional linear term αx are obtained. Provided that $\beta + \gamma > 0$, the limit strength value z of (2.10) becomes:

$$z_{max} = \pm \left(\frac{A}{(\beta + \gamma)} \right)^{\frac{1}{n}} \quad (2.11)$$

The parameter β is positive by assumption, while the admissible values for γ can be derived from the condition $\dot{\xi}_s \geq 0$ [77].

2.2.3 Physical and mathematical consistency of the Bouc-Wen model

In the current literature, the BW model is mostly used within the following black-box approach: given a set of experimental input-output data, how to adjust the BW model parameters so that the output of the model matches the experimental data. The use of system identification techniques is one practical way to perform this task. Once an identification method has been applied to tune the BW model parameters, the resulting model is considered as a good approximation of the true hysteresis when the error between the experimental data and the output of the model is small enough. Then this model is used to study the behavior of the true hysteresis under different excitations. On the other hand, the BW model is a nonlinear differential equation, and has to have some general mathematic properties to be used properly. The following properties have been considered in the literature:

- Bounded input-bounded output (BIBO) stability
- Consistency with the asymptotic motion of physical systems
- Passivity
- Thermodynamic admissibility
- Accordance with Drucker and Il'iushin stability postulates
- Consistency with the hysteresis property

a) Bounded input-bounded output (BIBO) stability

For any bounded input x , the output of the true hysteresis $\phi_{BW}(x)$ is bounded : This BIBO stability property stems from the fact that we are dealing with mechanical and

structural systems that are stable in open loop [78]. We consider a system with the rate-independence property (see equation (2.6)). It is assumed that the force ϕ_{BW} delivered by the system can be broken down into an elastic force F_e and a hysteretic force F_h , operating in parallel (Figure 2.1). The force F_e is related to the elastic deformation of the elements ($F_e(0) = 0$) while F_h corresponds to plastic phenomena. The BW model that approximates the true hysteresis $\phi_{BW}(x)$ is :

$$\phi_{BW}(x)(t) = \alpha kx(t) + (1 - \alpha)z(t) \quad (2.12)$$

$$\dot{z} = D^{-1} (Ax - \beta |\dot{x}| |z|^{n-1} - \gamma \dot{x} |z|^n) \quad (2.13)$$

Generally for the sake of simplicity we take $D = 1$.

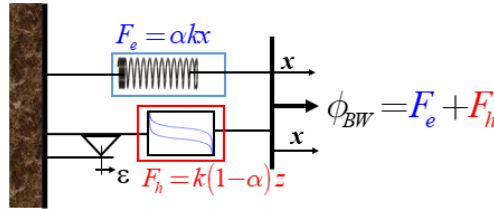


Figure 2.1: Physical model

b) Consistency with the Asymptotic Motion of Physical Systems

Accordingly, **Theorem 2** [70] shows that, for the *classes I* and *II*, the displacement x goes to a constant value asymptotically and that the velocity \dot{x} goes to zero. This is compatible with experimental observations for base-isolation devices which means that both classes are good candidates for the description of the real physical behavior of a base-isolation system. Based on numerical simulations, *classes III* and *IV* are shown not to behave in accordance with experimental observations.

c) Passivity

Passivity is related to the energy dissipation and means that the system does not generate energy. In [78], the model (2.12)-(2.13) is written as:

$$\begin{cases} \dot{x} = u \\ \dot{z} = D^{-1} (Au - \beta |u| |z|^{n-1} - \gamma u |z|^n) \\ y = \alpha kx + (1 - \alpha)z \end{cases} \quad (2.14)$$

where u is the input of the model and y is its output.

d) The thermodynamic admissibility

The thermodynamic admissibility is investigated in [77] using the endochronic theory (a

Table 2.1: Classification of the BIBO-stable Bouc-Wen models [78]

Case		Ω	Upper bound on $ z(t) $	Class
$A > 0$	$\beta + \gamma > 0$ and $\beta - \gamma \geq 0$	\mathbb{R}	$\max(z(0), z_0)$	I
	$\beta - \gamma < 0$ and $\beta \geq 0$	$[-z_1, z_1]$	$\max(z(0), z_0)$	II
$A < 0$	$\beta - \gamma > 0$ and $\beta + \gamma \geq 0$	\mathbb{R}	$\max(z(0), z_0)$	III
	$\beta + \gamma < 0$ and $\beta \geq 0$	$[-z_0, z_0]$	$\max(z(0), z_0)$	IV
$A = 0$	$\beta + \gamma > 0$ and $\beta - \gamma \geq 0$	\mathbb{R}	$ z(0) $	V
	All other cases	\emptyset		

theory of viscoplasticity without a yield surface, proposed in [79]). The BW type models that are considered are univariate and tensorial. **Theorem 3** [70] The BW models of (23)-(31) fulfill the second principle of Thermodynamics if and only if the following holds:

$$\begin{aligned}
 n &> 0 \\
 \beta &> 0 \\
 -\beta &\leq \gamma \leq \beta
 \end{aligned} \tag{2.15}$$

e) Accordance with Drucker and Il'iushin Stability Postulates

Drucker's postulate [80] implies that the hysteresis system should not produce a negative energy dissipation when the unloading-reloading process occurs without load reversal. For the BW model, it has been noted in many references that this may not be the case, although the effect of this violation on the expected results may be minor [81–85]. An attempt to reduce the violation is presented in [86] by modifying the BW model. On the other hand, [87, 88] show that for $n = 1$, $\beta + \gamma > 0$ and $\gamma - \beta \leq 0$ (β being positive by assumption), the BW model verifies Drucker's postulate. The more general result for n arbitrary is obtained in **Theorem 3** of [77], as the thermodynamic consistency for the BW model implies that it verifies Drucker's postulate.

f) Consistency with the Hysteresis Property

The hysteresis property means that the output depends on the sign of the derivative of the input.

Table 2.2: Different Cases of Hysteresis [78]

Case No	Nature of Hysteresis loop	Condition
1	Weak Softening	$\left. \begin{array}{l} \beta + \gamma > 0 \\ \gamma - \beta < 0 \end{array} \right\}$
2	Weak Softening on loading, mostly linear unloading	$\left. \begin{array}{l} \beta + \gamma > 0 \\ \gamma - \beta = 0 \end{array} \right\}$
3	Strong softening on loading and unloading, narrow loop	$\left. \begin{array}{l} \beta + \gamma > \gamma - \beta \\ \gamma - \beta > 0 \end{array} \right\}$
4	Weak Hardening	$\left. \begin{array}{l} \beta + \gamma = 0 \\ \gamma - \beta < 0 \end{array} \right\}$
5	Strong Hardening	$\left. \begin{array}{l} 0 > \beta + \gamma \\ \beta + \gamma > \gamma - \beta \end{array} \right\}$

2.2.4 Characteristic of Bouc-Wen parameters model

Using this simple differential model proposed by Bouc(1967) and generalized in (1976) by Wen, a variety of hysteretic loops are obtained. In this model, the hysteretic force z is obtained for an imposed cyclic displacement x and is described by a nonlinear differential equation [3]- [4]:

Typical shapes of hysteretic loops are obtained using BW model for different values of loop parameters and a imposed displacement $x(t) = x_0 \sin(2\pi ft)$ and $n = 1$ where the frequency $f = 1Hz$ and the amplitude $x_0 = 1mm$ [89].(see Fig.(2.1))

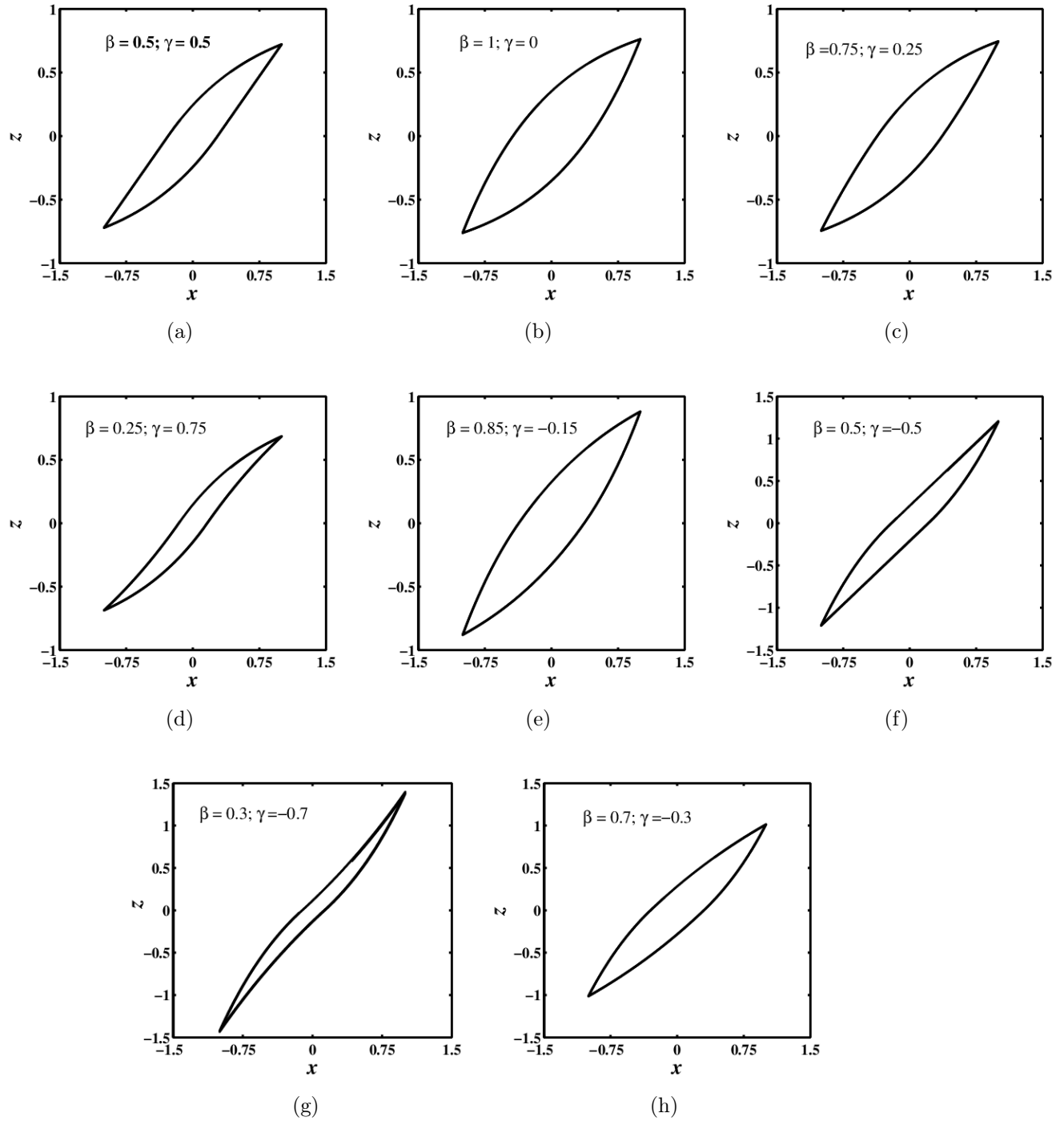


Figure 2.2: Hysteretic loops generated by BW model

Parameter A (fig.2.2(a)) controls the scale and the amplitude of the hysteretic curved controls and the slope variation of the stiffness characteristic. The BW model must reproduce the property of energy dissipation for an adequately representation of physical behavior of the real systems.

The variation of parameter β (fig.2.2(b)) has the effect of turning the hysteresis loop in clockwise, increasing the area of the hysteresis loop and curved of backbone.

The variation of parameter γ (fig.2.2(c)) has the effect of turning the backbone of hysteresis loop in clockwise simultaneously with its curving clockwise for negative values of the parameter and clockwise for positive values of the same parameter.

The parameter n (fig.2.2(d)) governs the smoothness of the transition from linear to nonlinear range and controls the shape of the hysteretic curve. The effect is important between 1 and 2 values. For $n > 2$ the differences are less important.

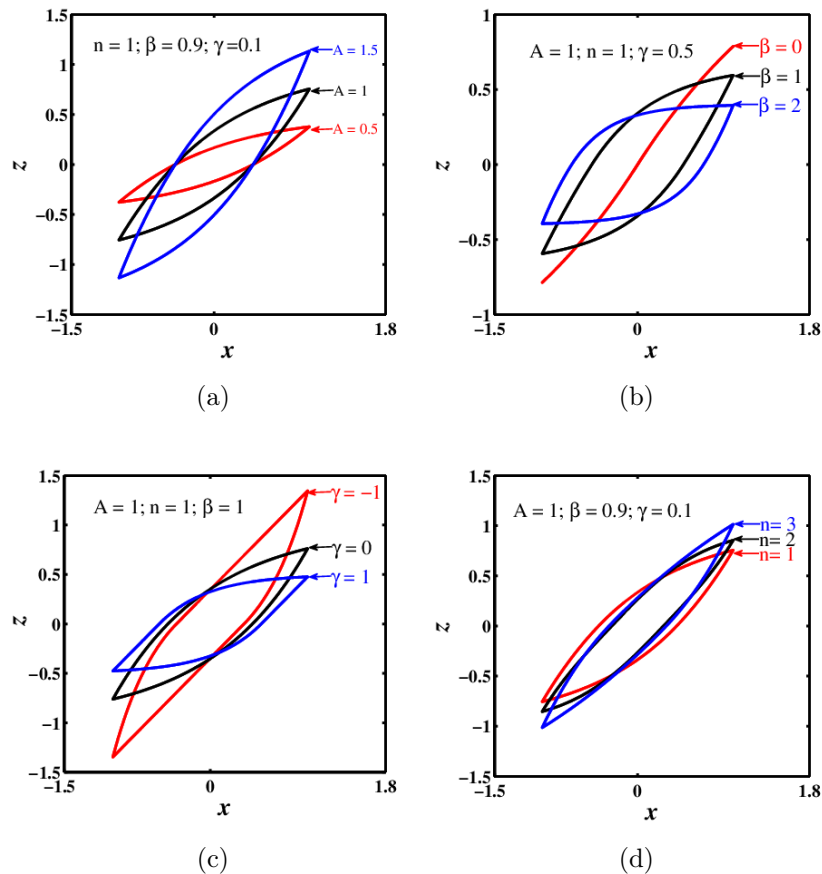


Figure 2.3: Hysteresis loops generated by variation of the parameters of BW model: a) A , b) β , c) γ , d) n

2.3 Mathematical formalisms and numerical methods

2.3.1 Mathematical formalisms

To predict the response and to give the decision on its stability, three analytical techniques [90–94] are used to approach our reduced mathematical models (nonlinear ODEs, PDEs and linear equations) and will present in the following subsection.

2.3.1.1 Taylor expansion serie

Taylor's theorem, [90] is taught in introductory-level calculus courses and is one of the central elementary tools in mathematical analysis. It gives simple arithmetic formulas to accurately compute values of many transcendental functions such as the exponential function and trigonometric functions. It is the starting point of the study of analytic functions, and is fundamental in various areas of mathematics, as well as in numerical analysis and mathematical physics. Taylor's theorem also generalizes to multivariate and vector valued functions. if $f : R \rightarrow R$ infinitely differentiable at $x = x_0$ then the Taylor series for f at x is the following power series.

$$f(x) = f(x_0) + f'(x_0) \Delta x + f''(x_0) \frac{(\Delta x)^2}{2!} + \dots + f^{(k)}(x_0) \frac{(\Delta x)^k}{k!} + \dots \quad (2.16)$$

Truncating this power series at some power results in a polynomial that approximates f around the point x . In particular, for small ,

$$f(x + \Delta x) \simeq f(x) + f'(x) \Delta x + f''(x) \frac{(\Delta x)^2}{2!} + \dots + f^{(k)}(x) \frac{(\Delta x)^k}{k!} \quad (2.17)$$

Here the error of the approximation goes to zero at least as fast as $(\Delta x)^k$ as $\Delta x \rightarrow 0$. Thus, the larger the k the better is the approximation. This is called the k th-order Taylor approximation of f at x . This can be generalized to the multivariate case

2.3.1.2 Routh-Hurwitz stability criterion

Routh-Hurwitz stability criterion is a method for stability analysis of linear systems. This approach is a necessary and sufficient condition for the stability of a system, since it has bounded output for bounded inputs, if the roots of its characteristic equation have negative real parts only. The characteristic equations is given by:

$$f(\lambda) = a_0 \lambda^n + a_1 \lambda^{n-1} + \dots + a_{n-1} \lambda + a_0 = 0 \quad (2.18)$$

where the coefficients a_i are real constants. The main diagonal of the Hurwitz's matrix are the form:

$$\Delta_1 = a_1, \quad \Delta_2 = \begin{vmatrix} a_1 & a_0 \\ a_3 & a_2 \end{vmatrix}$$

$$\Delta_3 = \begin{vmatrix} a_1 & a_0 & 0 \\ a_3 & a_2 & a_1 \\ a_5 & a_4 & a_3 \end{vmatrix}, \quad \dots, \quad \Delta_n = \begin{vmatrix} a_1 & a_0 & 0 & \dots & 0 \\ a_3 & a_2 & a_1 & \dots & 0 \\ a_5 & a_4 & a_3 & \dots & 0 \\ \dots & \dots & \dots & \dots & \dots \\ 0 & 0 & 0 & \dots & a_n \end{vmatrix} \quad (2.19)$$

In general, Hurwitz condition states: all of the roots of the polynomial have negative real part if the determinant of all Hurwitz matrix are positive. That is, none of them are zero or negative.

$$\Delta_1 > 0, \quad \Delta_2 > 0, \quad \dots, \quad \Delta_n > 0 \quad (2.20)$$

Since, $\Delta_n = a_n \Delta_n$ the condition $\Delta_n > 0$ can be changed by a_n

$$n = 2; \quad a_1 > 0 \quad \text{and} \quad a_2 > 0 \quad (2.21)$$

$$n = 3; \quad a_1 > 0, \quad a_3 > 0 \quad \text{and} \quad a_1 a_2 > a_3 \quad (2.22)$$

$$n = 4; \quad a_1 > 0, \quad a_3 > 0, \quad a_4 > 0 \quad \text{and} \quad a_1 a_2 a_3 > a_3^2 + a_1^2 a_4 \quad (2.23)$$

2.3.1.3 Melnikov's method to predict Smale horseshoe chaos

Melnikov's method [96] is one of relatively few analytical methods used to predict the onset of chaotic motion in dynamical systems with deterministic or random perturbation. It gives a bound on the parameters of a system such that chaos is predicted not to occur. It is applicable to conservative one DOF systems which include a separatrix loop, and which are perturbed by small forcing and damping. The idea is to show by perturbation expansions that there exists an intersection of the stable and unstable manifolds of an equilibrium point in a two-dimensional Poincare map M . This implies that there is a horseshoe in the map M , which in turn implies that there exist periodic motions of all periods, as well as motions which are not periodic. The horseshoe map also exhibits sensitive dependence on initial conditions. The method was first applied by Holmes [97] to study a periodically

forced Duffing oscillator with negative linear stiffness. To perform the general Melnikov technique for horseshoe chaos analysis, let's Consider a SDoF Hamiltonian system subject to light damping and external or parametric excitation. This system has the following form:

$$\begin{cases} \dot{x} = \frac{\partial H}{\partial y} \\ \dot{y} = -\frac{\partial H}{\partial x} - \varepsilon \lambda(x, y) \frac{\partial H}{\partial y} + \varepsilon f(x, y) \eta(t), \end{cases} \quad (2.24)$$

where x and y are generalized displacement and velocity respectively; $H = H(x, y)$ is the Hamiltonian with continuous first-order derivatives; ε is a small positive parameter; $\eta(t)$ is the external perturbation which can be purely periodic excitation or random noise excitation. $\lambda = \lambda(x, y)$ represents the coefficient of damping; $f(x, y)$ represents the amplitude of excitation. We assume that $(x_0(t), y_0(t))$ is a solution on the separatrix loop in the $\varepsilon = 0$ system. The separatrix loop in the $\varepsilon = 0$ system will generally be "broken" when the perturbation is applied. The question of whether or not chaos can occur in a particular system depends upon what happens to the broken pieces of the separatrix loop (the stable and unstable manifolds of the saddle), that is, whether they intersect or not. In the case of 2.24 and based on a formula given by Wiggins [98], Melnikov's method involves the following integral:

$$M(t_0) = \int_{-\infty}^{+\infty} \frac{\partial H}{\partial y} \left[-\lambda(x, y) \frac{\partial H}{\partial y} + f(x, y) \eta(t + t_0) \right] dt \quad (2.25)$$

where before integrate the previous (2.25), the couple (x, y) is substituted by the orbit $(x_0(t), y_0(t))$ - Melnikov method for chaos analysis: Deterministic state of the system when a system (2.24) is under purely periodic excitation (case where $\eta(t)$ is periodic function of time), the system is said to respond in a deterministic state. In this case, the deterministic Melnikov method need to be adopt in other to define the condition for the appearance of the so-called transverse intersection points between the perturbed and the unperturbed separatrix, thus identifying possible chaotic response by the Smale Birkhoff theorem, in a two dimensional vector field [98, 99]. This transverse intersection manifests itself by the fractality on the basin of attraction of the system. According to the assumption made in this section, $M(t_0)$ in (2.25) is a deterministic function which characterizes the size of the gap between the stable and unstable manifolds of the saddle. If $M(t_0)$ vanishes for some t_0 , then the stable and unstable manifolds intersect and system (2.24) is predicted to contain a horseshoe. If $M(t_0)$ does not vanish for any t_0 , then Melnikov's method predicts that there is no intersection of the stable and unstable manifolds, and

hence no associated horseshoe or chaos in system (2.24). All these results assume that ε is a small quantity.

2.3.2 Numerical methods

When analytic solutions are not apparent, numerical integration is the only way to obtain information about the trajectory. Many different methods were proposed and used in an attempt to solve accurately various types of the ODEs. Unfortunately it is seldom that these equations have solutions that can be expressed in closed form, so it is common to seek approximate solutions by means of numerical methods; nowadays this can usually be achieved very inexpensively to high accuracy and with a reliable bound on the error between the analytical solution and its numerical approximation. In this thesis, two numerical methods including a classical RK4 to integrate the ODEs, Newton-Raphson to integrate the PDEs and to solve a complex or non-trivial polynomial equations are presented.

2.3.2.1 Fourth-order Runge-Kutta method for ordinary differential equations

Runge-Kutta methods are among the most popular ODEs solver. It has been elaborated for the first time in 1894 by Carle Runge and has been improved by Martin W. Kutta in 1901. Their modern developments are mostly due to John Butcher in the 1960s, it is widely used since it is most stable [94]. Generally, we distinguish 04 important families of Runge-Kutta methods: Second-order, Fourth-order, Five-order and Six-order Runge Kutta Methods. But the most used method is the Fourth-order one since that it is easy to use and no equations need to be solved at each stage, highly accurate for moderate values of the normalization integration time step and easy to code. Let us consider the ordinary first order. differential equation:

$$\frac{dX(t)}{dt} = F(t, X(t)) \quad (2.26)$$

with $X(t_0) = X_0$; this equation can also be under a vectorial form (X and F being vectors). One define h as the time step size and $t_i = t_0 + ih$. The aim of the RK4 method is to find solutions after each time step, the next solution as a function of the previous one. The classical RK4 flow for this problem is given by:

$$\begin{aligned}
x_{0,j} &= X_0 \\
L_{1,j} &= hf_j(t_i, x_{i,j}) \\
L_{2,j} &= hf_j\left(t_i + \frac{h}{2}, x_{i,j} + \frac{L_{1,j}}{2}\right) \\
L_{3,j} &= hf_j\left(t_i + \frac{h}{2}, x_{i,j} + \frac{L_{2,j}}{2}\right) \\
L_{4,j} &= hf_j(t_i + h, x_{i,j} + L_{3,j}) \\
x_{i+1,j} &= x_{i,j} + \frac{1}{6}(L_{1,j} + 2L_{2,j} + 2L_{3,j} + L_{4,j})
\end{aligned} \tag{2.27}$$

where i runs for time incrementation and j labels the variables related to x_j . $L_{1,j}$, $L_{2,j}$, $L_{3,j}$ and $L_{4,j}$ are intermediate coefficients. This procedure needs in its iteration only the initial value X_0 , to calculate all the other values taken by the function X at other times separated by the time step h .

2.3.2.2 Newton-Raphson method for system of equations

Newton-Raphson method for system of equations. Due to the encountered difficulties for solving the nonlinear system of equations. Many iterative methods are employed in the literature to remedy to this problem. The Newton-Raphson method is defined as an iterative procedure for finding zeros of an equation or the system of nonlinear equations. To illustrate this principle, the system of equations is defined as follows.

$$\begin{cases} f(x, y) = 0 \\ g(x, y) = 0 \end{cases} \tag{2.28}$$

The functions $f(x, y)$ and $g(x, y)$ are two arbitrary functions

$$f(x, y) = f(x_0, y_0) + \frac{\partial f}{\partial x}(x - x_0) + \frac{\partial f}{\partial y}(y - y_0) + 0(x, y) \tag{2.29}$$

$$g(x, y) = g(x_0, y_0) + \frac{\partial g}{\partial x}(x - x_0) + \frac{\partial g}{\partial y}(y - y_0) + 0(x, y) \tag{2.30}$$

The Jacobian matrix associated with above equations is found as follows:

$$J(x, y) = \begin{pmatrix} \frac{\partial f}{\partial x} & \frac{\partial f}{\partial y} \\ \frac{\partial g}{\partial x} & \frac{\partial g}{\partial y} \end{pmatrix} \tag{2.31}$$

If $\det(J) \neq 0$, the iterative method is written as

$$X_{n-1} = X_n - J^{-1}(X_n) F(X_n) \tag{2.32}$$

A convergence criterion for the solution of a system of nonlinear equation could be, for example, the magnitude of the absolute values of the functions $F(X_n)$ is smaller than a certain tolerance

$$|F(X_n)| < 0 \quad (2.33)$$

2.3.3 Hardware and software

During the course of this work, we used a Laptop computer having the following performances (Operating system: Windows 10 single language 64-bit, Processor: Intel(R)Core(TM)i5-3230M CPU @2.60GHz(4CPUs), 2.6GHz, Memory: 8 Go RAM) and five major softwares: Fortran and Python for differential equations, Matlab for data analysis, Mapple and Mathematica for integral calculus.

2.4 Computational tools for the characterization of the dynamical states of non-linear systems

Dynamical states of the nonlinear systems are usually investigated with a number of numerical tools such as the time histories diagram, phase portraits diagrams, bifurcation diagrams and Lyapunov exponent. In this section, we give a brief account of the computational techniques which are used for characterizing different dynamical states of new chaotic Bouc-Wen model.

2.4.1 Phase portraits diagrams

A phase portrait of a dynamical system is a mathematical space having orthogonal coordinate directions which represent each of the variables needed to specify the instantaneous state of the system. The state of a particle moving in one dimension is specified by its position and velocity. The phase space variables need not be mechanical coordinates like position and velocity. The state of a dynamical system is represented by a point in the phase space. As the system evolves in time, it constitutes a trajectory in the phase space. Phase portraits are an invaluable tool in studying dynamical systems. They consist of a plot of typical trajectories in the state space. This reveals information such as whether an attractor, a repeller or limit cycle is present for the chosen parameter value. However the drawback of this computational tool is that it can be hard to distinguish the quasi-

periodicity and chaos phenomena by using the phase portrait diagram. The most reliable numerical tools used to know if a dynamical system exhibited a chaotic phenomenon for a given parameter values is the Poincaré section.

2.4.2 Bifurcation Diagrams

A bifurcation is the event in which one of the properties of a dynamical system changes qualitatively when a control parameter of the system is varied. For plotting the bifurcation diagram of continuous dynamical systems, a set of values of a single variable representing the attractor must be obtained. This is usually done by the return map obtained from the Poincaré section [129]. There is another method for obtaining discrete mappings from the flows. In the bifurcation phenomena, attractors may appear, disappear or be replaced by another one. Bifurcation diagrams help us to visualize these transitions. We can identify various routes to chaos taken by dynamical systems. The most common are: the period doubling route, the quasi-periodic route and intermittency route.

2.4.3 Lyapunov exponents

Named after Lyapunov, a Russian mathematician, Lyapunov exponents are the widely accepted tools for characterizing chaotic and periodic states of a dynamical system. Lyapunov exponents describe the rate of divergence or convergence of nearby trajectories onto the attractor in different directions in phase space. It gives a measure of the sensitive dependence upon initial conditions which is a characteristic of chaotic system. In this subsection, we discuss briefly the definition and computational aspects of the Lyapunov exponents of the continuous and discrete dynamical systems. In the case of ODEs ,if you consider two initially nearby state variables $x(t_0)$ and $x(t_0) + \delta x(t_0)$, the derivation $\delta x(t)$ further evolves as :

$$\frac{d\delta x(t)}{dt} = \left[\frac{\delta F}{\delta x} \right]_x \cdot \delta x \quad (2.34)$$

with $\delta x(t_0) = \delta x_0$ and $[\delta F = \delta x]$ is the jacobian of the flow F evaluated on X . The n eigenvalues of this jacobian are referred to as Lyapunov exponents, and they can numerically be determined through [130].

$$\lambda_k = \lim_{t \rightarrow +\infty} \frac{1}{t} \ln \left[\frac{|\delta x_k(t)|}{|\delta x_k(0)|} \right] \quad (2.35)$$

with $k = 1, \dots, n$

The n eigenvalues λ_k constitute the Lyapunov spectrum of the flow F for the initial

condition $x(t_0)$. The average Lyapunov spectrum of an attractor is defined as the space average of the Lyapunov spectrum over its corresponding basin of attraction. Depending on its sign, an average Lyapunov exponent $\overline{\lambda}_k$ expresses convergence (when negative) or divergence (when positive) of nearby trajectories along the corresponding eigendirection in the attractor. Therefore, a dynamical system is said to be chaotic if at least one average Lyapunov exponent $\overline{\lambda}_k$ is positive. The system is said to be hyperchaotic if more than one average Lyapunov exponent is positive. Moreover, a greater number of positive $\overline{\lambda}_k$, as well as greater absolute values for each of them when positive indicate a higher complexity in the state space and a higher unpredictability in the time domain. Generally, if the initial value x_0 is properly chosen, the resulting Lyapunov spectrum does not differ substantially from the average Lyapunov spectrum.

2.5 Conclusion

In this chapter, the mathematical modelling of BW model and a brief description of parameters model were presented. A physical structure model was presented to highlight the applicability of the model. Afterwards, the mathematical and numerical simulation methods used to solve the equations subject to external perturbations such as external periodic force were also detailed in this chapter, as well as the hardware and software employed. The next chapter focuses on results and discussions.

CHAPTER III

RESULTS AND DISCUSSION

3.1 Introduction

This chapter is devoted to the results and discussions of the work carried out in this thesis. It is organized as follows. Section 3.2 deals the dynamic analysis of a SDOF hysteretic system with negative stiffness, and the effect of the BW parameters model on the dynamics responses. Here, we show that by playing only on the shape parameters of the BW hysteresis one can predict and suppress the appearance of chaotic motion Section 3.3 deals with the conditions for which homoclinic chaos appears in a class of systems with BW hysteresis. In this sense, Mathematical formalism and dynamics explanation are detailed. Section 3.4 presents the complex dynamic behavior of nonlinear mechanical structure modelled with asymmetric potential generated by the hysteretic force of BW type and the key role of BW parameters model on the dynamics response. The last section concludes the chapter.

3.2 On the appearance of horseshoe chaos in a nonlinear hysteretic systems with negative stiffness

3.2.1 Bouc-Wen model: Description

We consider a bridge on which periodic service loads are performed (see fig.3.1a). Under the action of these loads, the vertical beams deform and thus constitute a stiffness. This rigidity is highlighted by the so-called Bouc-Wen restoration force. During the movement, the system loses energy due to the viscous damping of the shape memory material that constitutes the structure.

Assume an SDOF system, e.g. a cantilever (see fig.3.1b), the equation of motion for SDOF system consisting of a mass ($m > 0$) connected in parallel to a viscous damper ($c > 0$) with BW hysteretic spring is described by:

$$m\ddot{x}(t) + c\dot{x}(t) + H(x, z, t) = F(t), \quad (3.1)$$

where x, \dot{x} and \ddot{x} are displacement, velocity and acceleration respectively, the non damping restoring force H , is composed of both linear and hysteretic restoring forces.

H is given by:

$$H(x, z, t) = \alpha kx(t) + k(1 - \alpha)z(t) \quad (3.2)$$

k is a stiffness, α the rigidity ratio of post-yield to pre-yield and z the hysteretic displacement. The relative input of the hysteretic part is therefore controlled by the parameter α . The non-linear restoring force is thus a function of the fictitious hysteretic displacement z rather than the total displacement x . At larger displacements, for a non-pinching, non-degrading system the so-called BW model represents the true hysteresis in the form [78, 101, 102]:

$$\dot{z} = D^{-1}(A\dot{x} - \beta|\dot{x}||z|^{n-1}z - \gamma\dot{x}|z|^n), \quad (3.3)$$

where \dot{z} denotes the time derivative, $n > 1$, $D > 0$, $k > 0$ and $A > 0$. A is the parameter controlling hysteresis amplitude β , γ and n are parameters describing shape and amplitude of hysteresis.

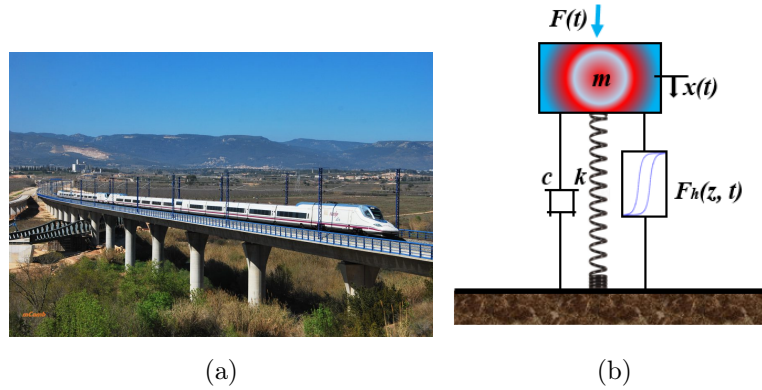


Figure 3.1: a) Real system; b) Physical model

In this study, thermodynamic admissibility issues impose the following inequality [77, 103, 104]:

$$\beta \geq \gamma \quad (3.4)$$

Based on (3.4), the hysteretic loop assumes a bulge shape (see Figure 3.2) as opposed to a slim-S one (see Figure 3.3).

$$\beta + \gamma \geq 0 \quad (3.5)$$

Equation (3.5) is a sufficient and necessary condition for strain-softening behaviour. The combination of β and γ dictates whether the model describes a softening (see Figure 3.2) or hardening (see Figure 3.3) load-slip relation.

This results are obtained assuming that the external excitation is harmonic i.e $F(t) = F_0 \sin(\Omega t)$, where F_0 and Ω are respectively the amplitude and frequency of the

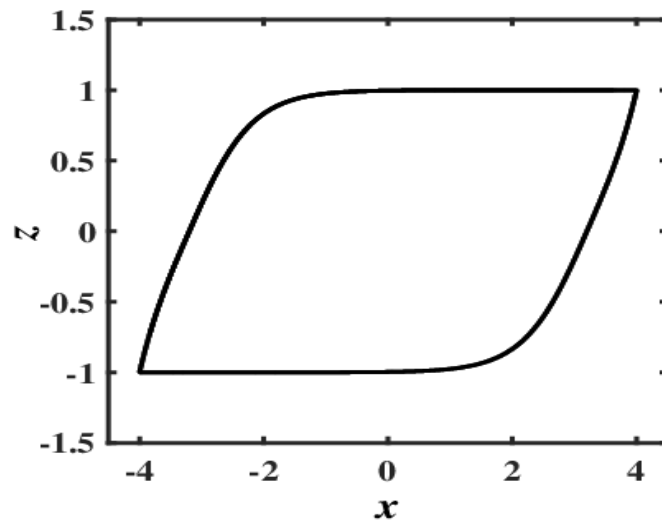


Figure 3.2: Softening hysteresis loop generated by the model for $D = 1$, $n = 2$, $A = 1$, $\gamma = 0.05$ and $\beta = 0.95$.

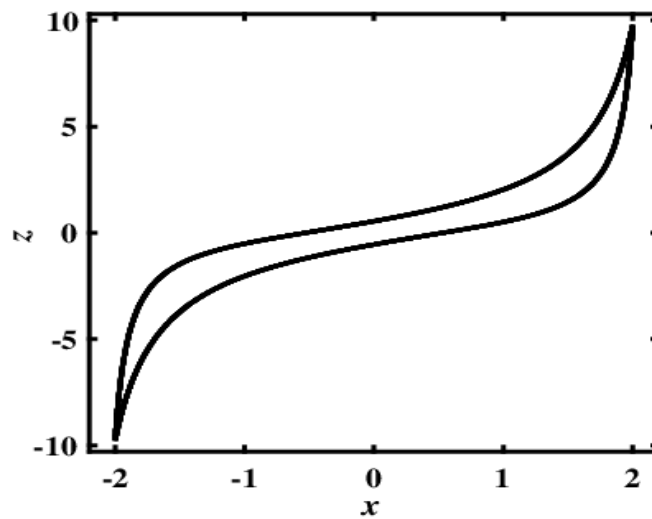


Figure 3.3: Hardening hysteresis loop generated by the model for $D = 1$, $n = 2$, $A = 1$, $\gamma = -0.65$ and $\beta = 0.35$.

excitation. To derive the total energy of the system, it is convenient to rewrite the system equation in the form [105]:

$$\begin{aligned} \ddot{x}(t) + 2\zeta\omega\dot{x}(t) + \alpha\omega^2x(t) + \omega^2(1-\alpha)z(t) &= F(t) \\ \omega = \sqrt{\frac{k}{m}}, \quad \zeta &= \frac{c}{2m\omega}, \end{aligned} \quad (3.6)$$

where ω is a pre-yield natural frequency of the system and ζ a linear viscous damping ratio. The evolution of the hysteretic displacement z given by the following constitutive differential equation:

$$\dot{z} = D^{-1} [A - (\gamma + \text{sgn}(\dot{x}) \text{sgn}(z) \beta) |z|^n] \dot{x} \quad (3.7)$$

We note that the phase space of the Bouc-Wen oscillator is three dimensional and is spanned by (x, \dot{x}, z) . Setting $\varepsilon = \text{sgn}(\dot{x}) \text{sgn}(z) = \pm 1$ with sgn denotes the signum function, in order to integrate z , (3.7) can be rewritten in the following form:

$$dz = D^{-1} [A - (\gamma + \varepsilon\beta) |z|^n] dx \quad (3.8)$$

3.2.2 Appearance of separatrix

The equations (3.6) and (3.8) can be recasted in state space form as:

$$\begin{aligned} \dot{x} &= y \\ \dot{y} &= -2\zeta\omega y - \alpha\omega^2x - (1-\alpha)\omega^2z \\ \dot{z} &= D^{-1} [A - (\gamma + \varepsilon\beta) |z|^n] y \end{aligned} \quad (3.9)$$

For $D = 1$ and $n = 2$, one obtains three fixed points $(0, 0, 0)$;

$$\left(-\frac{(1-\alpha)}{\alpha} \sqrt{\frac{A}{\gamma+\varepsilon\beta}}; 0; \sqrt{\frac{A}{\gamma+\varepsilon\beta}}\right) \text{ and } \left(\frac{(1-\alpha)}{\alpha} \sqrt{\frac{A}{\gamma+\varepsilon\beta}}; 0; -\sqrt{\frac{A}{\gamma+\varepsilon\beta}}\right)$$

Taking into account the influence of the hysteretic force, the potential energy of the system is given by:

$$V(x) = \frac{1}{2}\alpha\omega^2x^2 + \omega^2(1-\alpha) \int_{x(0)}^{x(t)} z dx \quad (3.10)$$

The energy absorbed by the hysteretic element is thus the continuous integral of the hysteretic force and the total energy displacement.

Equation (3.8) is integrated for $D = 1$ and $n = 2$. The initial conditions $x(0)$, $\dot{x}(0)$, $z(0)$ are known. For the sake of simplicity, it is assumed that $x(0) = \dot{x}(0) = z(0) = 0$. It is claimed that the hysteretic displacement z can thus be derived explicitly and given by:

$$z = \frac{\sqrt{A}}{\sqrt{(\gamma + \varepsilon\beta)}} \tanh\left(\sqrt{A(\gamma + \varepsilon\beta)}x\right) \quad (3.11)$$

Then complete potential of the system, taking into account the hysteresis component (see Figure 3.4(a)) is given by:

$$V(x) = \frac{1}{2}\alpha\omega^2x^2 + \omega^2\frac{(1-\alpha)\sqrt{A}}{\sqrt{(\gamma+\varepsilon\beta)}} \ln \cosh\left(\sqrt{A(\gamma+\varepsilon\beta)}x\right) \quad (3.12)$$

The critical amplitude x_u is obtained when the following conditions are satisfied:

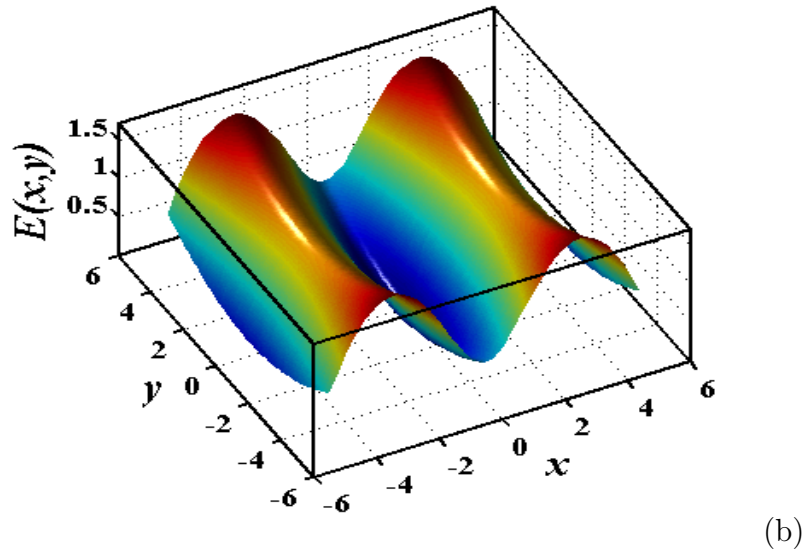
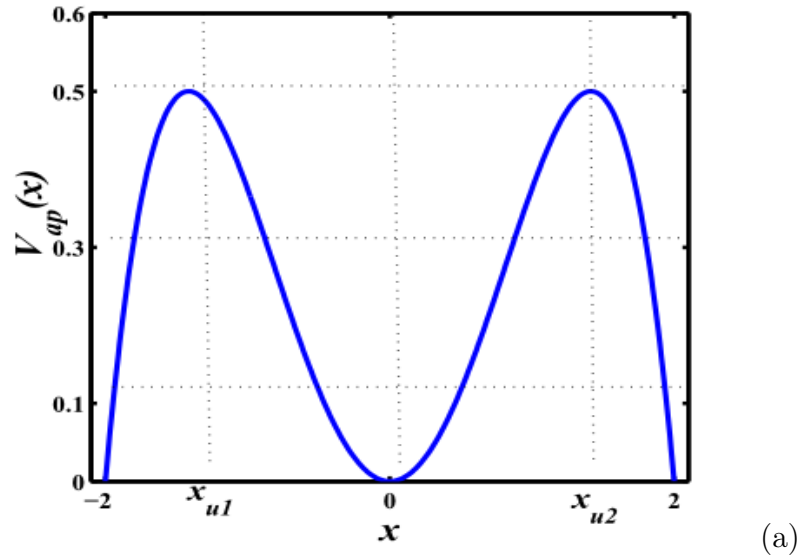


Figure 3.4: a) Potential curve, b) Energy diagram of system for $\varepsilon = 1$.

$$V'(x) = 0 \text{ and } V''(x) \geq 0 \quad (3.13)$$

But obtaining the analytical expression using the form given by (3.11) is quite impossible. To find an approximation solution, we carry out the expansion of $\tanh\left(\sqrt{A(\gamma+\varepsilon\beta)}x\right)$,

assume that $\beta = \xi\bar{\beta}$ and $\gamma = \xi\bar{\gamma}$, where ξ is a small positive constant. An expansion in power series of ξ allows to obtain an approximate description of the hysteresis loop by neglecting the ξ^3 and higher powers, and by integration of (3.10), one obtains:

$$V_{ap}(x) = \frac{1}{2}(\omega^2(\alpha + (1 - \alpha)A))x^2 - \frac{1}{12}(\omega^2 A^2(1 - \alpha)(\gamma + \varepsilon\beta))x^4 \quad (3.14)$$

The representation of this potential shows that the presence of hysteretic force describes the unbounded monostable potential (see Figure 3.4(b)). Equation of the dynamics of this system is given by :

$$\ddot{x}(t) + 2\zeta\omega\dot{x}(t) + (\alpha\omega^2(t) + \omega^2(1 - \alpha)A)x(t) - \frac{1}{3}\omega^2 A^2(1 - \alpha)(\gamma + \varepsilon\beta)x^3(t) = F_0 \sin(\Omega t) \quad (3.15)$$

Figure 3.4 also shows that we have three fixed points: one stable $(0; 0)$ and the other two unstable $\left(\pm\sqrt{\frac{3(\alpha+(1-\alpha)A)}{(1-\alpha)(\gamma+\varepsilon\beta)A^2}}; 0\right)$ leading to the appearance of heteroclinic orbit (see Figure 3.5). In this case, the separatrix appears leading to the possible transverse intersection between perturbed and unperturbed heteroclinic orbit. This means that the shape parameters of the hysteresis force have a direct link with the appearance of horseshoe chaos in the system. The presence of horseshoe chaos means that the existence of a starting point for successive route to chaotic dynamics. This can be detected analytically using Melnikov theory.

3.2.3 Melnikov analysis

In the present section, we apply the Melnikov method [96,98,106,107] to detect analytically the effects of Bouc Wen model parameters on the threshold condition for the inhibition of horseshoe chaos in the system and on the fractal basin boundaries. To apply this method, we introduce a small parameter μ in (3.15) and rewrite the governing system as the following set of first order differential equations :

$$\begin{cases} \dot{x}(\tau) = y(\tau) \\ \dot{y}(\tau) = -\omega^2(\alpha + (1 - \alpha)A)x(\tau) + \frac{1}{3}A^2\omega^2(\gamma + \varepsilon\beta)(1 - \alpha)x^3(\tau) + \mu\Gamma(t), \end{cases} \quad (3.16)$$

with $\Gamma(\tau) = -2\zeta\omega y(\tau) + F_0 \cos(\Omega\tau)$. For $\mu = 0$ and after assuming that : $x = x(\tau)$, $y = y(\tau)$ the system of (3.16) is the Hamiltonian system with Hamiltonian function.

$$H(x, y) = \frac{1}{2}y^2 + \frac{1}{2}\omega^2(\alpha + (1 - \alpha)A)x^2 - \frac{1}{4}\left(\frac{1}{3}(1 - \alpha)(\gamma + \varepsilon\beta)\omega^2 A^2\right)x^4 \quad (3.17)$$

The saddle points (see Figure 3.4) x_{u1} and x_{u2} are connected by heteroclinic orbits (see Figure 3.5) that satisfied the following equation:

$$\begin{aligned} x_{het} &= \pm \sqrt{\frac{3(\alpha+(1-\alpha)A)}{(1-\alpha)(\gamma+\varepsilon\beta)A^2}} \tanh\left(\omega \sqrt{\frac{\alpha+(1-\alpha)A}{2}} \tau\right) \\ y_{het} &= \pm \frac{3(\alpha+(1-\alpha)A)\omega}{(1-\alpha)(\gamma+\varepsilon\beta)A^2} \sqrt{\frac{\alpha+(1-\alpha)A}{2}} \operatorname{sech}^2\left(\omega \sqrt{\frac{\alpha+(1-\alpha)A}{2}} \tau\right) \end{aligned} \quad (3.18)$$

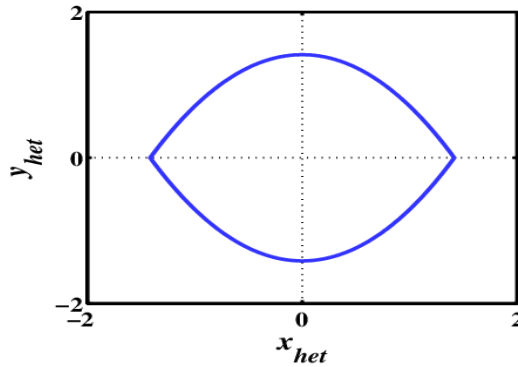


Figure 3.5: Heteroclinic orbit of unbounded monostable potential

The Melnikov theory defines the condition for the appearance of the so called transverse intersection points between the perturbed and the unperturbed separatrix or the appearance of the fractality on the basin of attraction. This theory can be applied in the case of (3.15) by using the formula given by Wiggins [98] as follows:

$$\begin{aligned} M_Y(\tau_0) &= \int_{-\infty}^{+\infty} g_0(u_{het}(\tau)) \times g_p(u_{het}(\tau), \tau + \tau_0) d\tau \\ &= -2\zeta\omega \int_{-\infty}^{+\infty} y_{het}^2(\tau) d\tau + F_0 \int_{-\infty}^{+\infty} y_{het}(\tau) \sin(\Omega(\tau + \tau_0)) d\tau \\ &= I \pm Z(\tau_0) \end{aligned} \quad (3.19)$$

where

$$I = -24\zeta\omega^2 \sqrt{\frac{\alpha+(1-\alpha)A}{2}} \left(\frac{\alpha+(1-\alpha)A}{(1-\alpha)(\gamma+\varepsilon\beta)A^2} \right)^2$$

and

$$Z(\tau_0) = \frac{3F_0\Omega\pi(\alpha+(1-\alpha)A) \sin(\Omega\tau_0)}{\omega(1-\alpha)(\gamma+\varepsilon\beta)A^2 \sqrt{\frac{\alpha+(1-\alpha)A}{2}} \sinh\left(\frac{\Omega\pi}{2\omega \sqrt{\frac{\alpha+(1-\alpha)A}{2}}}\right)}$$

When the Melnikov function has a simple zero point, the stable manifold and the unstable manifold intersect transversally, chaos in the sense of Smale horseshoe transform

occurs. So let $M_Y(\tau_0) = 0$, one concludes that Melnikov chaos appears when:

$$F_0 \geq F_{CR} = \left| \frac{4\zeta\omega^3(\alpha+(1-\alpha)A)^2}{((\gamma+\varepsilon\beta)(1-\alpha)A^2)\Omega\pi\sin(\Omega\tau_0)} \sinh\left(\frac{\Omega\pi}{2\omega\sqrt{\frac{\alpha+(1-\alpha)A}{2}}}\right) \right| \quad (3.20)$$

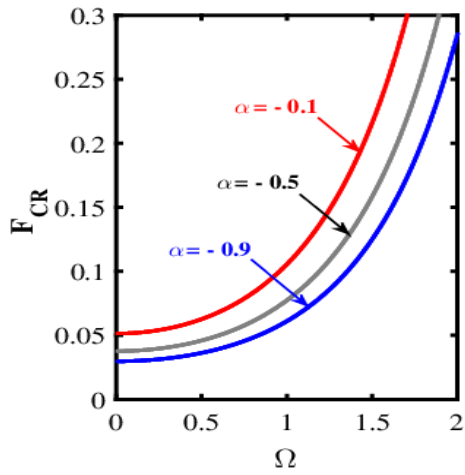
The criterion in Eq (3.20) defines the threshold value of F_{CR} for the appearance of a transverse intersection between the perturbed and the unperturbed manifolds. Such a condition is known as necessary for the existence of chaos. The threshold condition is plotted in Figure 3.6 as a function of the driving frequency Ω for different values of α (see Figure 3.6(a)), A (see Figure 3.6(c)) and $(\gamma + \varepsilon\beta)$ (see Figure 3.6(e)), as function of the parameter α (see Figure 3.6(b)), as function of A (see Figure 3.6(d)) and as function of the parameters $(\gamma + \varepsilon\beta)$ (see Figure 3.6(f)).

Figure 3.6(a) shows in the space (Ω, F_{CR}) , the lower bound for the appearance of heteroclinic bifurcation for several cases of α parameter. For (Ω, F_{CR}) taken below the lower bound line, the system displays a periodic motion, while possible chaotic motion is observed in the upper domain. It appears that: when α decreases the surface of the critical force increases consequently critical force decreases.

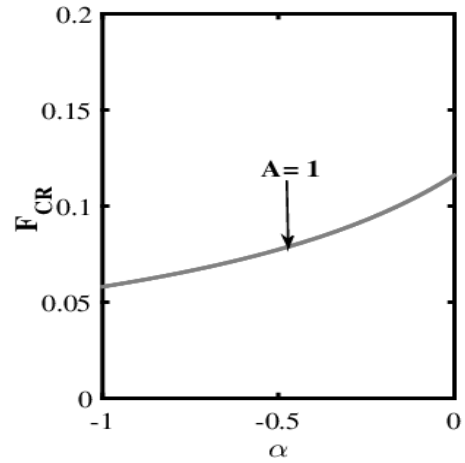
Figure 3.6(b) illustrates the effects of negative stiffness on the threshold value of F_{CR} , for $-1 < \alpha < 0$, the threshold increases, it appears that the control effect increases as α increases, this is a sign of the reinforcement of effectiveness of the control. The variations of the critical force as a function of α show that the parameter α plays a preponderant role in its efficiency.

Figures 3.6(c) and 3.6(e) show the critical external forcing amplitude for different values of A and $(\gamma + \varepsilon\beta)$ respectively. One can see (Figure 3.6(c)) that when the value of the parameter A increases, the thresholds of the critical values for heteroclinic bifurcation of the harmonic excitation F_{CR} decrease. The same effect is observed with the parameters $(\gamma + \varepsilon\beta)$ (Figure 3.6(e)). We conclude that the parameters A and $(\gamma + \varepsilon\beta)$ have the same effect on the critical value for chaotic motions.

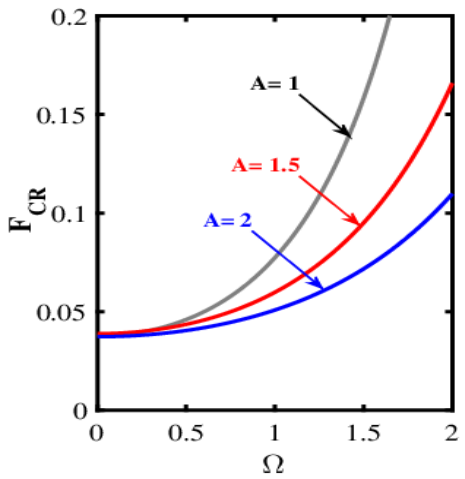
Figure 3.6(d) highlights the fact that as A increases the amplitude of the critical force decreases. Consequently, the choice of the parameter A relating to the reduction of the speed and amplitude of vibration or to the increase of the stability basin may be the starting point of a route leading to unpredictable behaviour. The same investigations are made in the case of Figure 3.6(f).



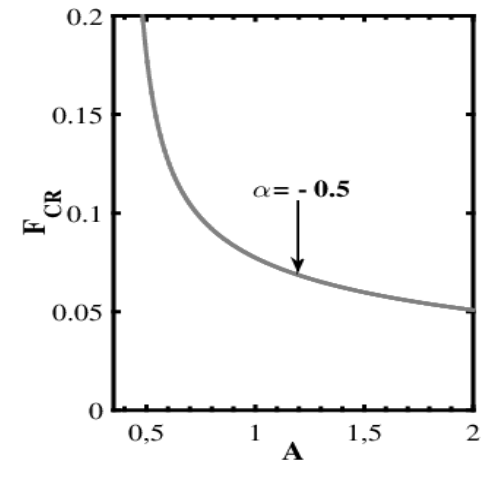
(a)



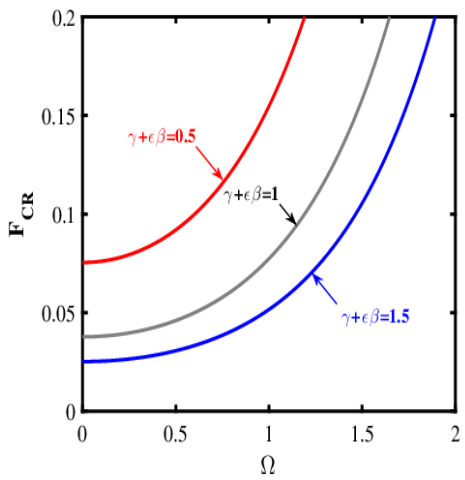
(b)



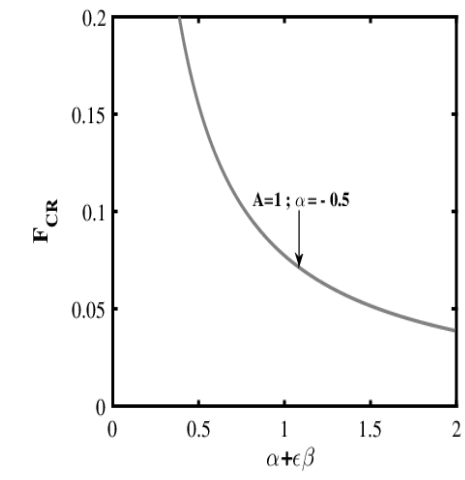
(c)



(d)



(e)



(f)

Figure 3.6: Evolution of the critical amplitude F_{CR} as a function of : Ω (a), (c) and (e) ; α (b) ; A (d) and $(\gamma + \epsilon\beta)$ (f) with $\epsilon = 1$.

3.2.4 Numerical investigation

The existence of a homoclinic or heteroclinic orbit for the detection of horseshoe chaos in physical systems is of paramount importance. Indeed, the choices of control parameters for obtaining the basin of attraction is not done in a random manner; Moreover, it is possible to determine the conditions for which heteroclinic orbit appears, while defining the limits of values of model parameters for which basins can be obtained. Of Equations (3.18), it is possible to find the conditions (see Equation 3.21) for which the parameters of the BW model, will allow to obtain each time a heroclinic orbit. Thus, if the conditions (I) and (II) of Equations (3.21) are satisfied, horseshoe chaos in the system can be predicted if only if:

$$A > 0; \quad -1 < \alpha < 0 \quad \text{with} \quad \left\{ \begin{array}{l} (I) \left\{ \begin{array}{l} \beta + \gamma > 0 \\ \gamma - \beta < 0 \end{array} \right. \\ (II) \left\{ \begin{array}{l} \beta + \gamma > \beta - \gamma \\ \beta - \gamma > 0 \end{array} \right. \\ (III) \text{All other cases} \quad \emptyset \end{array} \right. \quad (3.21)$$

To validate the accuracy of the proposed analytical predictions, we solve numerically Equation 3.9 by means of fourth order Runge Kutta algorithm. A particular characteristic of the Melnikov theory is the fractality [106, 108, 109] of the basin of attraction and the resulting unpredictability due to the dependence on the initial conditions.

The limit F_{CR} given by (3.20) is shown in Figure 3.7. These figures display the basin of attraction according to the evolution of external forces. Thus, it appears that the basin has a regular geometry (see Figure 3.7(a)), and completely fractal (see Figure 3.7(b) and Figure 3.7(c)) for higher values, sign of the establishment of chaos. In addition, from the appropriate parameters of the Bouc-Wen model, we can also control the appearance of chaos in the SDOF system (see Figure 3.8).

Figure 3.8 Shows how when playing with the parameters of BW model it is possible to control system or to cause chaos. Thus, for the same value of critical amplitude and for different parameters of the Bouc-Wen model, the attraction basin is chaotic (see figure 3.7(c)), at the Figure 3.8 the attraction basin can be controlled. It is viewed that for a small amplitude of the external force, the limits of the basin are regular. In the case of the soft system, the heteroclinical orbit is clear. Above a certain value, it becomes irregular, meaning the presence of Melnikov chaos in the case of the soft system.

To validate the accuracy of the restoring force, (3.2) is plotted in Figure 3.9, by

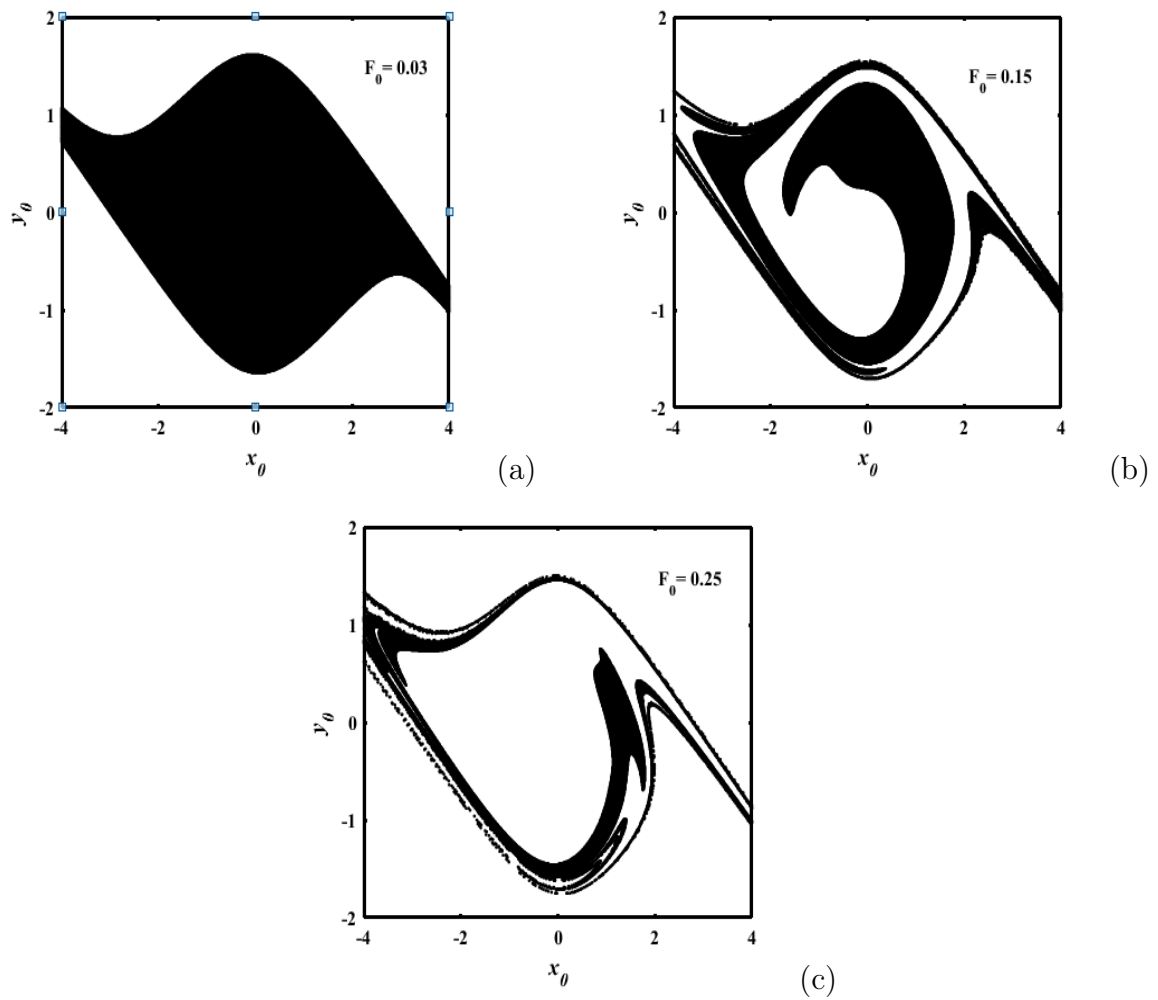


Figure 3.7: Basins of attraction showing the confirmation of the analytical prediction for $\varepsilon = 1$; $\alpha = -0.5$; $\beta = 0.95$; $\gamma = 0.05$; $\zeta = 0.02$ and $A = 1$.

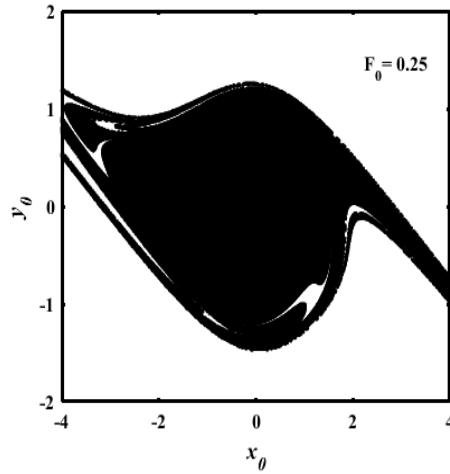


Figure 3.8: Effect of parameters $(\gamma + \varepsilon\beta)$, A and α , on the basin of attraction for $\Omega=1$; $\alpha=-0.4$; $\gamma + \varepsilon\beta = 0.9$ and $A = 0.7$

comparing the curves in this figure, we show that, the energy dissipated by the system can be considerably reduced when the system is controlled.

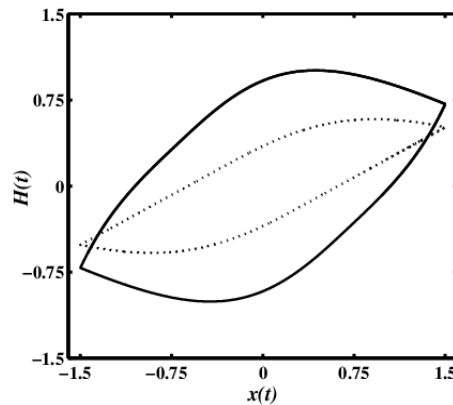


Figure 3.9: Response of BW model under cyclic excitation, with parameters used in Fig 3.7 without control and Fig 3.8 with control: — without control; ... with control

3.3 On Appearance of homoclinic chaos in a SDoF oscillator with Bouc-Wen hysteresis: Mathematical formalism and dynamics explanation

3.3.1 Bouc-Wen hysteresis model: New consideration

The following set of differential equations governs the motion of a SDoF oscillator with BW hysteresis [105]:

$$\ddot{x}(t) + 2\zeta\omega_0\dot{x}(t) + \alpha\omega_0^2x(t) + \omega_0^2(1 - \alpha)z(t) = F(t) \quad (3.22)$$

$$\dot{z} = D^{-1} [A - (\gamma + \text{sgn}(\dot{x}) \text{sgn}(z) \beta) |z|^n] \dot{x}, \quad (3.23)$$

where x , \dot{x} and \ddot{x} are displacement, velocity and acceleration respectively. α the rigidity ratio of post-yield to pre-yield and z the hysteretic displacement. With ζ the damping ratio of the system and ω_0 the natural frequency of the system without damping and hysteresis. The relative input of the hysteretic part is therefore controlled by the parameter α with $0 \leq \alpha \leq 1$. The non-linear restoring force is thus a function of the fictitious hysteretic displacement z rather than the total displacement x .

In this study, the case $A < 0$ of the classification table 2.1 of the BIBO-stable BW model and second principle of Thermodynamics are strictly adopted [70, 77] following these inequalities:

$$\beta > 0 \quad \text{and} \quad \beta \geq \gamma \quad (3.24)$$

Assuming that, the external excitation is harmonic i.e $F(t) = F_0 \sin(\omega t)$.

where F_0 and ω are respectively the amplitude and frequency of the excitation. We note that the phase space of the Bouc-Wen oscillator is three dimensional and is spanned by (x, \dot{x}, z) . Setting $\varepsilon = \text{sgn}(\dot{x}) \text{sgn}(z) = \pm 1$ with Sgn denotes the signum function, Eq (3.23) can be rewritten in the following form:

$$dz = D^{-1} [A - (\gamma + \varepsilon\beta) |z|^n] dx \quad (3.25)$$

3.3.2 Fixed points and their stability

To examine the stability of system, the equations (3.22) and (3.25) can be recast into state space form as:

$$\begin{aligned}
\dot{x} &= y \\
\dot{y} &= -2\varsigma\omega_0 y - \alpha\omega_0^2 x - (1 - \alpha)\omega_0^2 z \\
\dot{z} &= D^{-1} [A - (\gamma + \varepsilon\beta) |z|^n] y
\end{aligned} \tag{3.26}$$

Firstly, we obtain the fixed points by solving the general equation $F(\dot{u}) = 0$, where F is the nullcline and u is the vector space containing x , y and z . It appears that without purely hysteretic force ($\alpha = 1$), we have only one fixed point $P_0(0, 0, 0)$ and with hysteretic force, we have two fixed points namely $P_1(0, 0, 0)$ and $P_2\left(-\frac{(1-\alpha)A}{\alpha(\gamma+\varepsilon\beta)}, 0, \frac{A}{(\gamma+\varepsilon\beta)}\right)$. In both cases, by considering the Jacobian matrix of one of these equilibria and calculating their eigenvalues, we can investigate the stability of the equilibrium point based on the roots of the characteristic equation:

$$P^3 + a_2P^2 + a_1P + a_0 = 0, \tag{3.27}$$

where $a_2 = (\gamma + \varepsilon\beta) y_0 + \varsigma$, $a_1 = (\gamma + \varepsilon\beta) \varsigma y_0 + A\omega_0^2(1 - \alpha) - (\gamma + \varepsilon\beta)(1 - \alpha)\omega_0^2 z_0 + \alpha\omega_0^2$ and $a_0 = \alpha\omega_0^2(\gamma + \varepsilon\beta) y_0$

We know that the fixed points are stable if the real parts of the roots of the characteristics equation are all negative. Otherwise, the fixed points are unstable. Using Routh-Hurwitz criterion, for the sign of the real part of the roots, we obtain that the real parts of the roots are negative if and only if the conditions of Eq (3.28) are satisfies.

$$\begin{aligned}
a_2 &> 0, a_1 > 0, a_0 > 0 \\
a_2 a_0 - a_1 &> 0 \\
a_0 (a_2 a_0 - a_1) &> 0
\end{aligned} \tag{3.28}$$

Before analyzing the stability status of each point, it is important to consider the practical process of modeling system Eq (3.26). It is clear that A can take negative or positive values. Focussing on the fixed point P_1 and for $A < 0$, the analysis leads us to the conclusion that for $\left(\frac{-A}{1-A} < \alpha < 1\right)$ this fixed point can be stable (see fig. 3.11 (a)) or unstable (see fig. 3.11 (b)) if $\left(0 < \alpha < \frac{-A}{1-A}\right)$ depending on the choice of space parameter of the system. The other fixed points P_2 is always stable. Therefore the stability condition (see fig. 3.10) should be checked according to the criteria defined above before any use is made of the system.

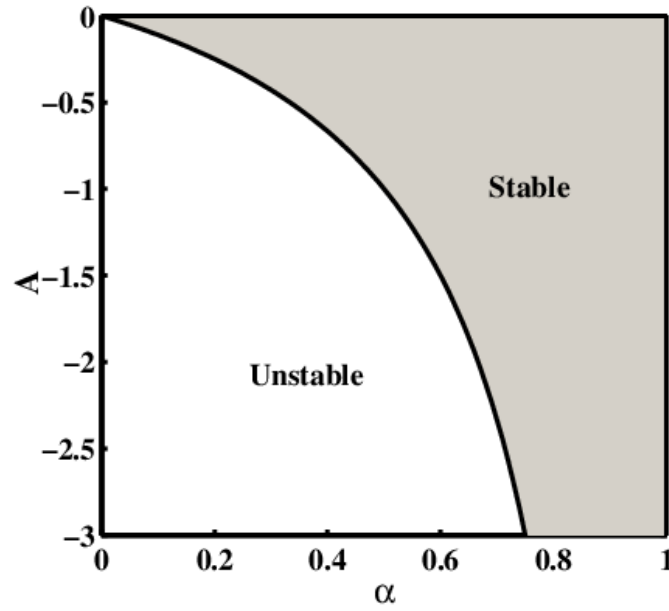


Figure 3.10: Stability curve of system: With hysteretic force at point P_1 class **III** and class **IV**

3.3.3 Appearance of separatrix

Without taking into account hysteretic force the potential energy of the system is harmonic and given by:

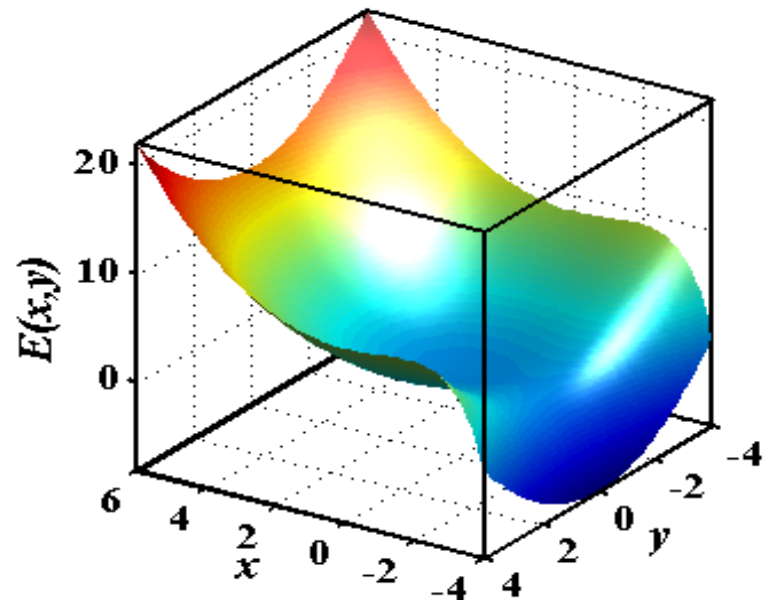
$$V(x) = \frac{1}{2}\alpha\omega_0^2x^2 \quad (3.29)$$

Taking into account the influence of the hysteretic force, this is modified in the following manner:

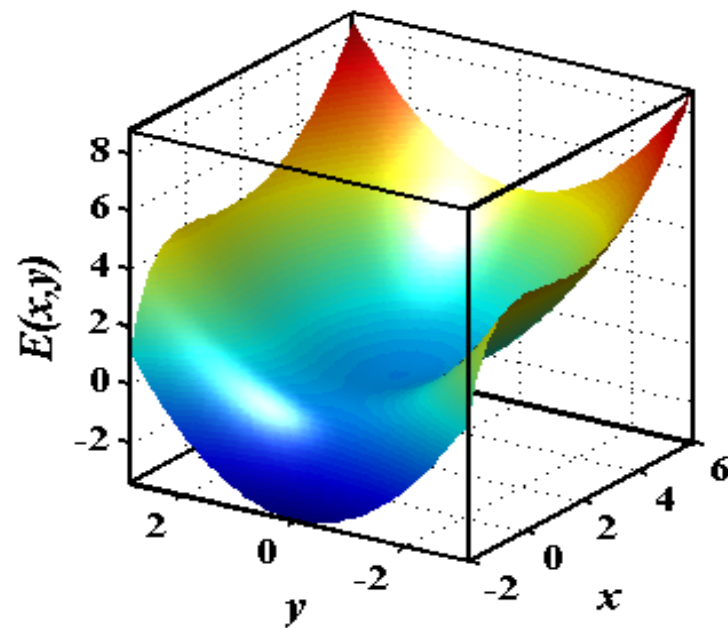
$$V(x) = \frac{1}{2}\alpha\omega_0^2x^2 + \omega_0^2(1-\alpha) \int_{x(0)}^{x(t)} z dx \quad (3.30)$$

The energy absorbed by the hysteretic element is thus the continuous integral of the hysteretic force and the total energy displacement. Equation (3.25) is integrated for $D = 1$ and $n = 1$. The initial conditions $x(0)$, $\dot{x}(0)$, $z(0)$ are known. For the sake of simplicity it is assumed that $x(0) = \dot{x}(0) = z(0) = 0$. It is claimed that the hysteretic force z can thus be derived explicitly and given by:

$$z = \frac{A}{(\gamma + \varepsilon\beta)} [1 - \exp(-(\gamma + \varepsilon\beta)x)], \quad (3.31)$$



(a)



(b)

Figure 3.11: Energy diagram of system for P_1 : a) Stable $\alpha = 0.85$, b) Unstable $\alpha = 0.5$ with $A = -2$; $\gamma = 0.05$; $\beta = 0.95$ and $\epsilon = 1$ (class *III*)

Then the complete potential of the system taking into account the hysteresis component is given by:

$$V(x) = \frac{1}{2}\alpha\omega_0^2x^2 + \frac{A\omega_0^2(1-\alpha)}{(\gamma+\varepsilon\beta)} \left[x - \frac{1-\exp(-(\gamma+\varepsilon\beta)x)}{(\gamma+\varepsilon\beta)} \right], \quad (3.32)$$

The representation of this potential shows that the presence of hysteretic force change the shape of potential : Without the hysteretic force, the potential (fig. 3.12(a)) shows one stable fixed point $(0, 0)$ in this case, the system can carry out symmetrical oscillations of large amplitude around the fixed point $(0, 0)$ meaning that in this case there is no possibility of homoclinic orbit appearance in the system, and with hysteretic force, the potentials (fig. 3.12(b) and 2(c)) show two fixed points: one unstable fixed point $(0, 0)$ and one other stable fixed point, leading to the appearance of homoclinic separatrix (see fig. 3.13(b)).

Fig. 3.12(b) also shows that as $(\gamma + \varepsilon\beta)$ increases, a particle inside the well gradually retracts from the unstable point. In the case of fig. 3.12(c) as $(\gamma + \varepsilon\beta)$ increases for the negative values, the same behaviour is observed. We conclude that when $A < 0$, the behaviour of soft system (**class III**) and hard system (**class IV**) could describe the same dynamic behaviour.

The critical amplitude P_u is obtained when the following conditions are satisfied:

$$V'(x) = 0 \quad \text{and} \quad V''(x) \geq 0 \quad (3.33)$$

In Eq (3.31) one assumes that $\beta = \xi\bar{\beta}$ and $\gamma = \xi\bar{\gamma}$ where ξ is a small positive constant. An expansion in power series of ξ allows to obtain an approximate description of the hysteresis loop by neglecting the ξ^3 and higher powers one obtains:

$$\begin{aligned} z(x) &= \frac{A}{(\varepsilon\beta+\gamma)} (1 - e^{-(\varepsilon\beta+\gamma)x}) \\ &= xA - \frac{(\varepsilon\beta+\gamma)A}{2}x^2 + 0(\xi^3) \end{aligned} \quad (3.34)$$

And by integration of Eq. (3.30), one obtains:

$$V_{ap}(x) = \frac{\omega_0^2}{2}((\alpha + (1 - \alpha)A))x^2 - \frac{\omega_0^2}{6}(A(1 - \alpha)(\gamma + \varepsilon\beta))x^3 \quad (3.35)$$

By approximation of this potential, fig. 3.13 (a) shows the correspondence between the approximated and the original potential. Thus, one obtains a stable fixed point $\left(0, \frac{2(\alpha+(1-\alpha)A)}{(1-\alpha)(\gamma+\varepsilon\beta)A}\right)$ and the other one unstable $(0, 0)$ for class III and a stable fixed point

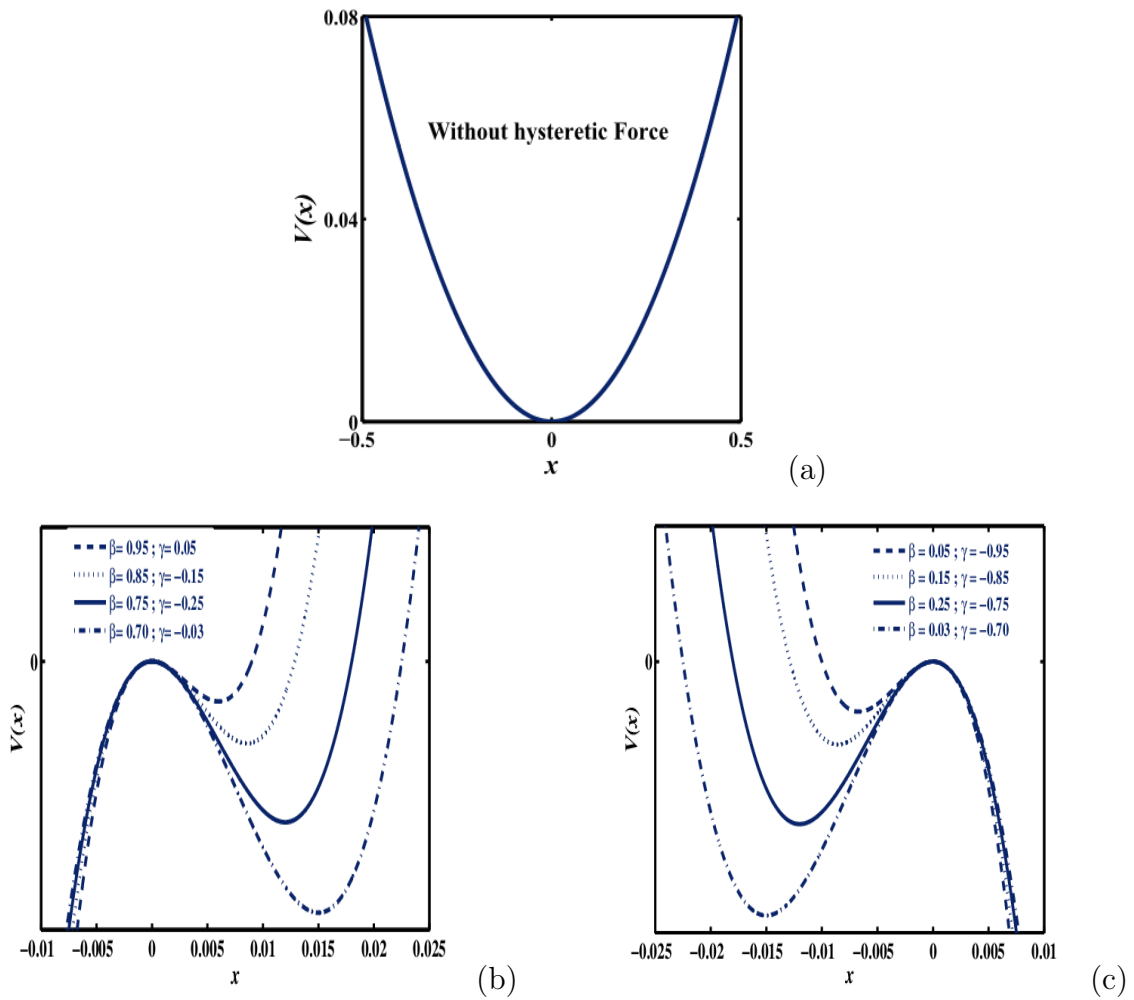
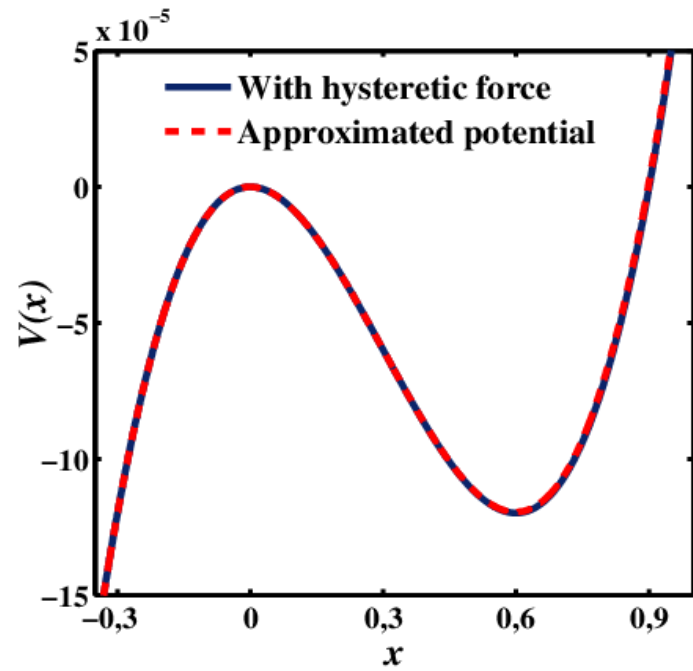
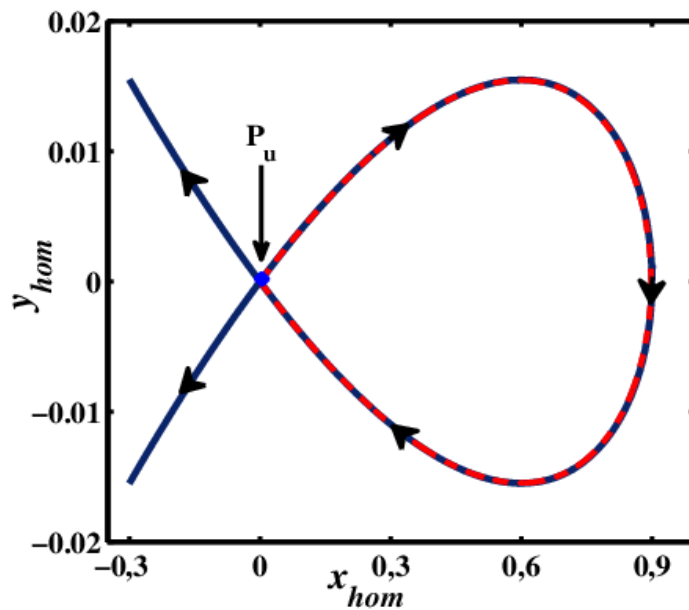


Figure 3.12: Potentials curves of system: Without hysteretic force (a) , with hysteretic force class *III* (b) and class *IV* (c) for $\varepsilon = 1$; $\alpha = 0.666$; $A = -2$



(a)



(b)

Figure 3.13: Potentials curves of system, separatrix and homoclinic orbit of unbounded monostable potential : (a) Original and approximated potential (b) Separatrix (solid line) and homoclinic orbit (dashed-dashed line): for $\varepsilon = 1$; $\alpha = 0.666$; $A = -2$; $\beta = 0.95$ and $\gamma = 0.05$

$\left(\frac{2(\alpha+(1-\alpha)A)}{(1-\alpha)(\gamma+\varepsilon\beta)A}, 0\right)$ and the other one unstable $(0, 0)$ for class IV.

In the case of $A < 0$ for class **III**, the separatrix (see fig. 3.13(b)) appears leading to the possible transverse intersection between perturbed and unperturbed homoclinic orbit. This means that the shape parameters of the hysteresis force have a direct link with the appearance of homoclinic orbit. Equation of the dynamic of this system is given by :

$$\ddot{x}(t) + 2\zeta\omega_0\dot{x}(t) + (\alpha + (1 - \alpha)A)\omega_0^2x(t) - \frac{1}{2}\omega_0^2A(1 - \alpha)(\gamma + \varepsilon\beta)x^2(t) = F_0 \sin(\omega t) \quad (3.36)$$

This homoclinic orbit can be evaluated analytically and we obtain:

$$x_{\text{hom}} = -3\eta \left(1 - \tanh^2 \left[\frac{\omega_0\tau}{2}\sqrt{\rho}\right]\right) \quad (3.37)$$

$$y_{\text{hom}} = 3\eta\sqrt{\rho}\operatorname{sech}^2 \left[\frac{\omega_0\tau}{2}\sqrt{\rho}\right] \tanh \left[\frac{\omega_0\tau}{2}\sqrt{\rho}\right] \quad (3.38)$$

with $\eta = \frac{\rho}{(1-\alpha)(\gamma+\varepsilon\beta)}$ and $\rho = -(\alpha + (1 - \alpha)A)$

3.3.4 Melnikov analysis

In order to analyse the effects of the parameters of the Bouc-Wen model of the dynamic response of the system, we take-in account the case where the point $P_1(0;0)$ is unstable in aim to determine the conditions for which this point could become stable. Fig. 3.11 confirms the analytical prediction given by Eq. (3.30), we observe the original homoclinic separatrix and the phase diagram of the system. Homoclinic orbits are solutions which are forward and backward asymptotic (in time) to a saddle-type fixed point (or a more general invariant set [98]). They occur at the intersection of the sets which are forward and backward asymptotic to the saddle point, i.e. the stable and unstable manifolds, respectively.

Related to this homoclinic orbit is the appearance of the typical *Smale horseshoe*. Chaotic motion, which occurs when the fractality of the basin of attraction appears and the Melnikov theory is satisfied [96, 98, 111, 132]. This theory can be easily evaluated in this case.

$$F_0 \geq F_{cr} = \left| \frac{4\zeta\eta\rho^{\frac{3}{2}}\omega_0^4}{5\pi\omega^2} \sinh \left[\frac{\pi\omega}{\omega_0\sqrt{\rho}} \right] \right| \quad (3.39)$$

here F_{cr} is the threshold amplitude for the onset of Melnikov chaos in the system.

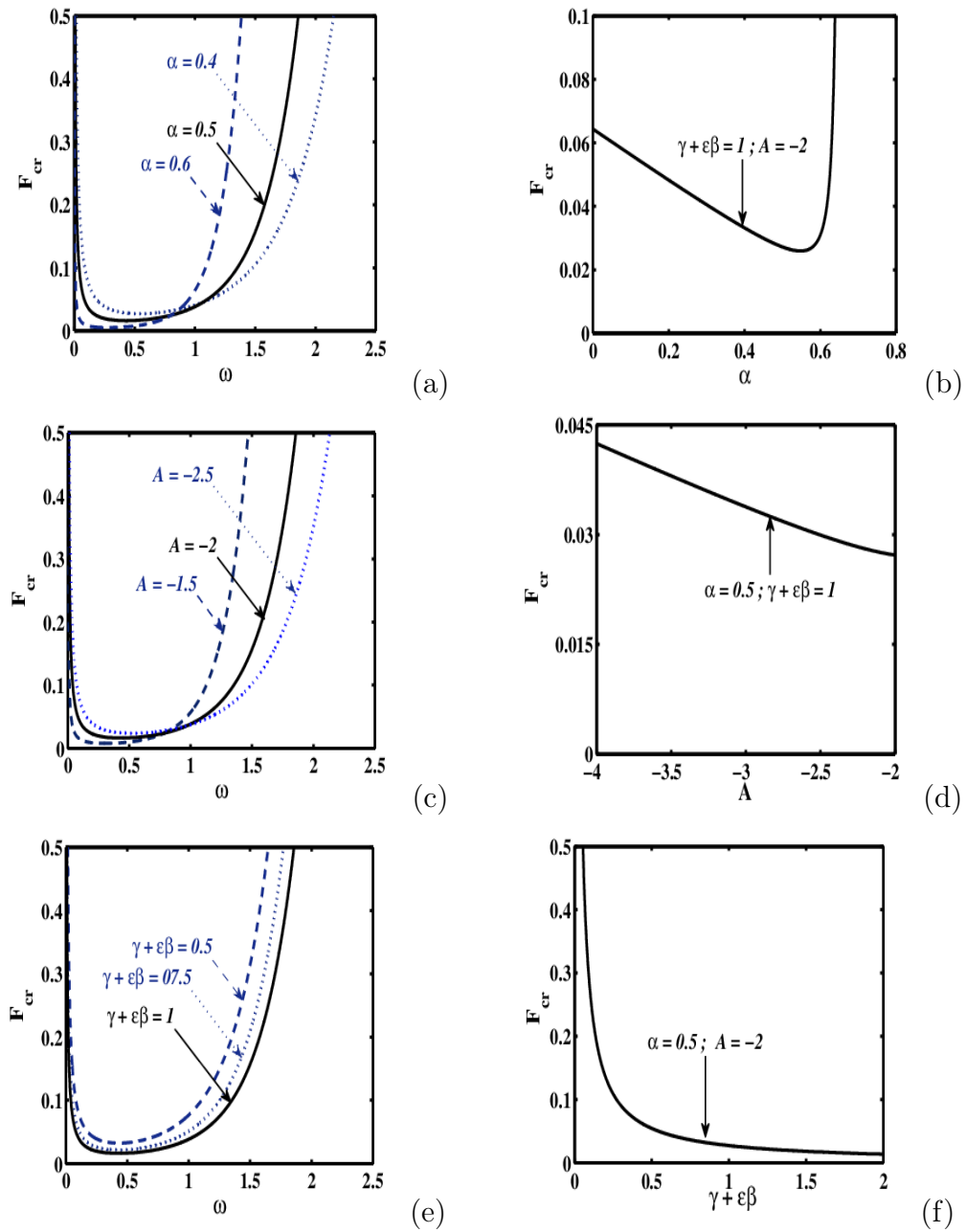


Figure 3.14: Evolution of the critical amplitude F_{cr} for appearance or disappearance of horseshoes chaos as a function ω for different values of α (a), A (c) and $\gamma + \epsilon\beta$ (e), as a function of α (b), A (d) and $\gamma + \epsilon\beta$ (f) : With $\epsilon = 1; \beta = 0.95; \gamma = 0.05; \alpha = 0.5; A = -2$ and $\zeta = 0.02$

The criterion in eq. (3.39) defines the threshold value of F_{cr} for the appearance of a transverse intersection between the perturbed and the unperturbed manifolds. Such a condition is known as necessary for the existence of chaos. The threshold condition is plotted in fig. 3.14 as a function of the driving frequency ω for different values of α (fig. 3.14(a)), A (fig. 3.14(c)) and $(\gamma + \epsilon\beta)$ (fig. 3.14(e)), as function of the parameter α (see fig. 3.14(b)), as function of A (see fig. 3.14(d)) and as function of the parameters $(\gamma + \epsilon\beta)$ (see fig. 3.14(f)).

Fig. 3.14(a) and (c) show in the space (ω, F_{cr}) , the lower bound for the appearance of homoclinic bifurcation for several cases of α and A parameters respectively. For (ω, F_{cr}) taken below the lower boundary line, the system displays a periodic motion, while possible chaotic motion is observed in the upper domain. It appears that: when α increases the surface of the critical force decreases consequently critical force decreases. The same investigations are made in the case of Fig. 3.14(c)

Fig. 3.14(b) illustrates the effects of α on the threshold value of F_{cr} , for $0 < \alpha < 0.51$, it appears that, the intensity of the critical force for the appearance of of Melnikov's chaos decreases when α increases and $0.51 < \alpha < 0.666$ the intensity increases, it appears that the control effect increases, this is a sign of the reinforcement of effectiveness of the control. The variations of the critical force as a function of α show that the parameter α plays a preponderant role in its efficiency.

Fig. 3.14(d) and (f) highlight the fact that as A and $(\gamma + \epsilon\beta)$ increase the amplitude of the critical force decreases. Consequently, the choice of these parameters relating to the reduction of the speed and amplitude of vibration or to the increase of the stability basin may be the starting point of a route leading to unpredictable behavior. The same observations were obtained by [120].

Fig. 3.14(e) shows the critical external forcing amplitude for different values of $(\gamma + \epsilon\beta)$. One can see that when $(\gamma + \epsilon\beta)$ increases, the thresholds of the critical values for homoclinic bifurcation of the harmonic excitation F_{cr} decrease. We conclude that, more and more as $(\gamma + \epsilon\beta)$ increases the control becomes less and less effective.

3.3.5 Basins of attraction

The existence of a homoclinic orbit for the detection of Melnikov chaos in physical systems is of paramount importance. Indeed, the choices of control parameters for obtaining the basin of attraction is not done in a random manner; Also, it is possible to determine the conditions for which homoclinic orbit appears, while defining the limits of values of model parameters for which basins can be obtained. Of eq. 3.37 we obtain:

$$A < 0; \alpha < \frac{A}{A-1} \text{ with } \left\{ \begin{array}{l} \text{Class III} \\ \text{Class IV} \\ \text{All other cases } \emptyset \end{array} \right. \quad (3.40)$$

These conditions describe well the hysteretic behaviour of softening systems. To validate the accuracy of the proposed analytical predictions, we solve numerically Eq. 3.36 by means of fourth order Runge Kutta algorithm. A particular characteristic of the Melnikov chaos is the fractality [112] of the basin of attraction and the resulting unpredictability due to the dependence on the initial conditions.

Fig. 3.15 displays the basin of attraction according to the evolution of external force. Thus, it appears that the basin has a regular geometry (see fig. 3.15(a)), fractal (see fig. 3.15(b), (c)) and completely fractal (see fig. 3.15(d)) for higher values, sign of the establishment of chaos. In addition, from the appropriate parameters of the Bouc-Wen model, we can also control the appearance or disappearance (see fig. 3.16) of chaos in the SDOF system. It is viewed that for a same amplitude of the external force, the basins are fractal (see fig. 3.16(a), (b) and (c)) or regular (see fig. 3.16(d)) by consideration of Melnikov investigation and playing on the Bouc-Wen parameter model.

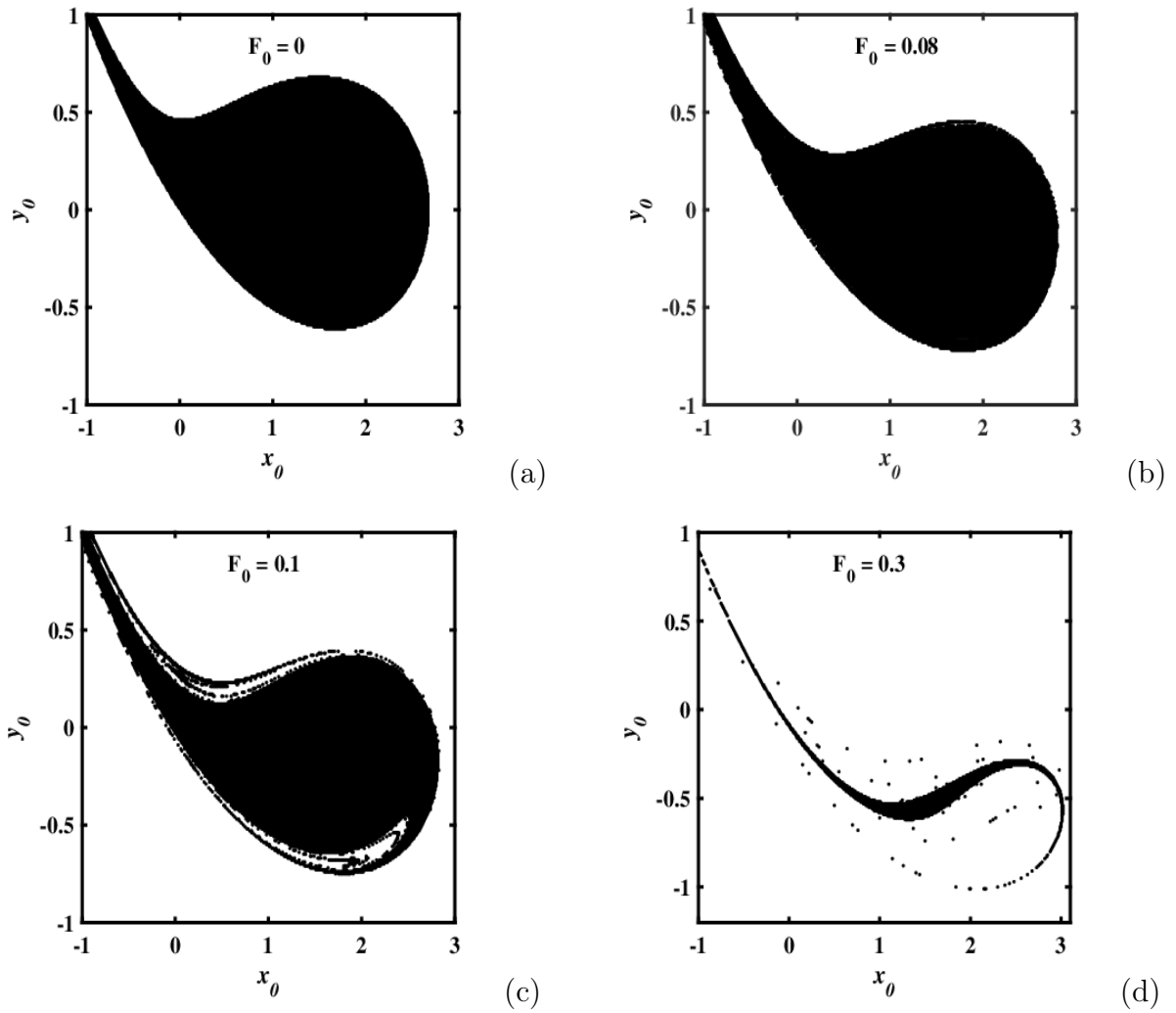


Figure 3.15: Basins of attraction showing the confirmation of the analytical prediction: $D = 1$; $n = 1$; $\varepsilon = 1$; $\omega = 0.85$; $\beta = 0.95$; $\gamma = 0.05$; $\alpha = 0.5$; $A = -2$ and $\zeta = 0.02$

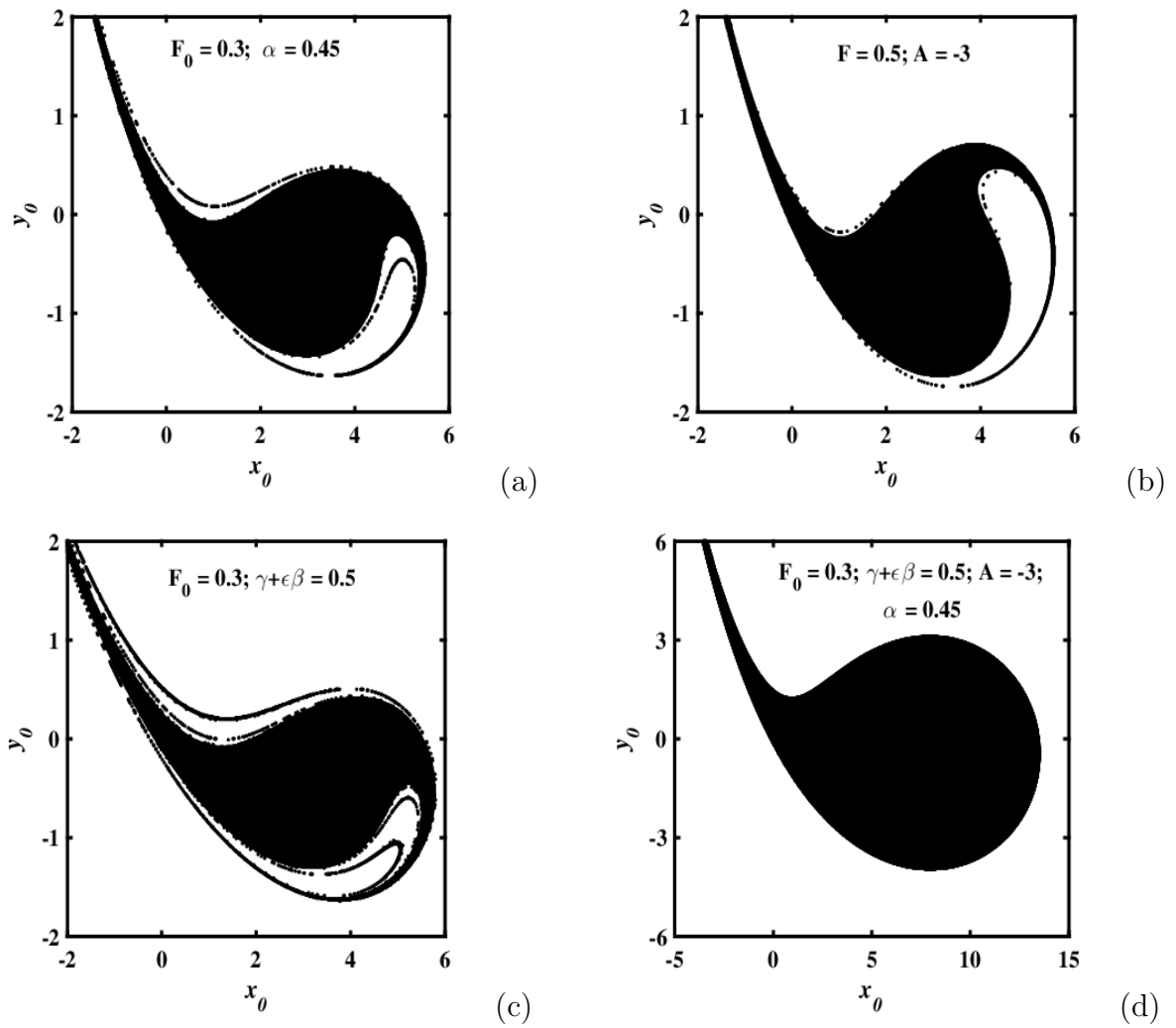


Figure 3.16: Basins of attraction showing the confirmation of the analytical prediction: $\varepsilon = 1$; $\omega = 0.85$; $\beta = 0.95$; $\gamma = 0.05$; $\alpha = 0.5$ and $\varsigma = 0.02$

3.3.6 Bifurcation Diagram and Lyapunov Exponent

A bifurcation diagram for the range of excitation amplitude $0.0 < F_0 < 6.0$ is shown in fig. 3.17(a) for damping ratio $\zeta = 0.02$; $\epsilon = 1$; $A = -2$; $\alpha = 0.666$; $\gamma = -0.54$; $\beta = 0.55$; $\omega_0 = 1$; $D = 1$; $n = 1$ and frequency of external excitation $\omega = 1$. The initial conditions are $x|_{t=0} = \dot{x}|_{t=0} = 0$ fig. 3.17(b) is corresponding diagram of the largest Lyapunov exponents. The stroboscopic time period used to map various transitions which appear in the model is $T = 2\pi/\omega$. Our investigations show that the model exhibits chaotic behavior (see fig. 3.18 (a)). These curves are obtained by numerically solving Eq. 3.22 and 3.23 and the corresponding variational equations. The one dimensional Lyapunov exponent is defined by:

$$Lya = \lim_{t \rightarrow \infty} \frac{\ln \left(\sqrt{dx^2 + dy^2 + dz^2} \right)}{t} \quad (3.41)$$

where dx, dy and dz are respectively the variations of x, \dot{x} , and \dot{z} . As the amplitude F_0 increases from zero, the amplitude of the quasi-periodic oscillations exists until $F_0 = 3.96$ where a chaotic orbit takes place. At $F_0 = 4.05$, the system bifurcates from a period-21 orbit to a chaotic orbit until $F_0 = 4.236$ where the chaotic orbit appears, the system remains until $F_0 = 4.54$ where it bifurcates to the period-1 orbit. Figures 3.18 presents the phase portrait \dot{x} versus x of the chaotic and periodic motions.

Remark The bifurcation diagram and Lyapunov Exponent of classes **III** and **IV** are the same, there is due in a negative value of **A** parameter. The same analysis is founded in section 3.

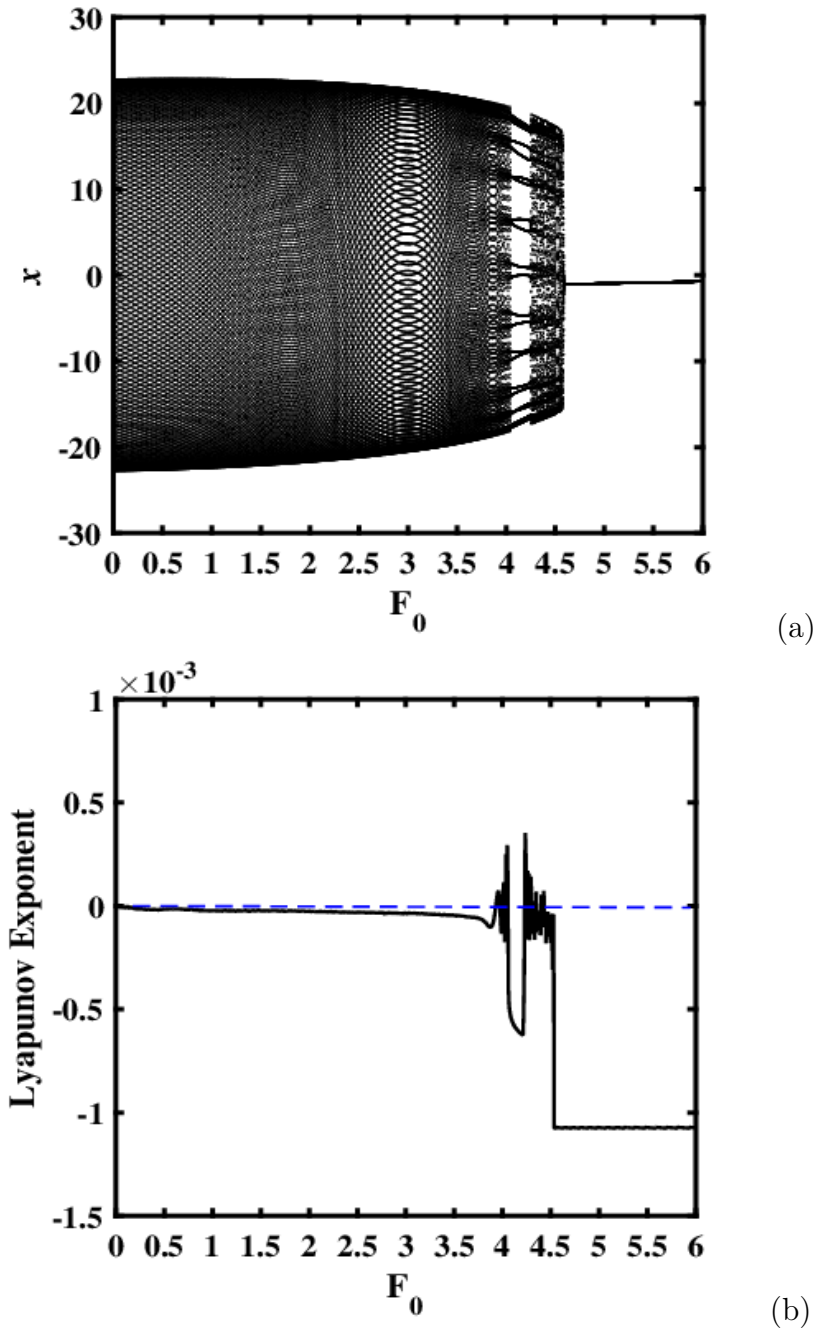
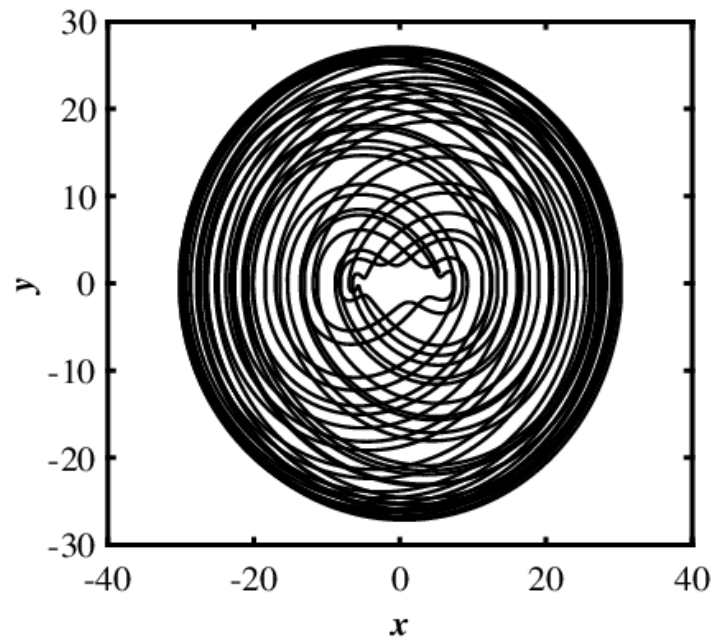
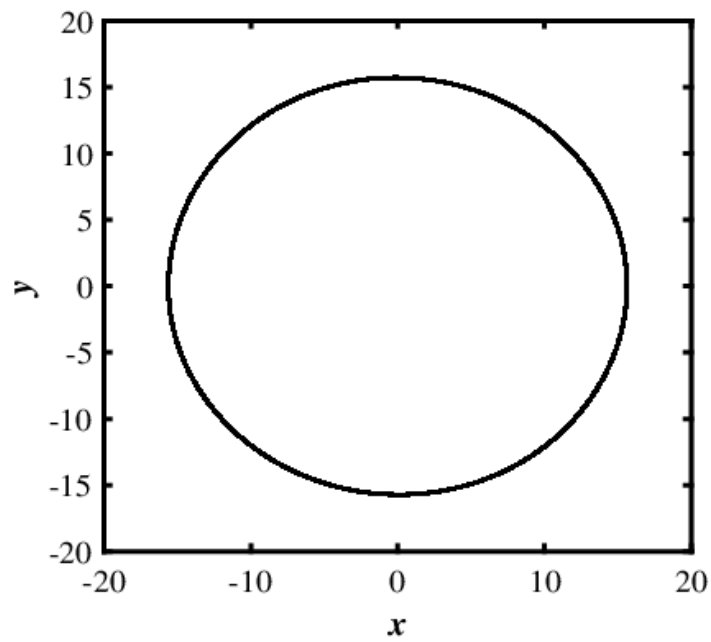


Figure 3.17: Bifurcation diagram (a) and Lyapunov exponent (b) vs the amplitude F_0 with the parameters of system: $D = 1$; $n = 1$; $\varepsilon = 1$; $\alpha = 0.666$; $A = -2$; $\beta = 0.55$ and $\gamma = -0.54$



(a)



(b)

Figure 3.18: Various phase portraits in some intermittency areas for different values of F_0 : $F_0 = 4.3$ (a); $F_0 = 5.5$ (b). With $D = 1$; $n = 1$; $\omega = 1$; $\omega_0 = 1$; $\varepsilon = 1$; $\alpha = 0.666$; $A = -2$; $\beta = 0.55$ and $\gamma = -0.54$.

3.4 Complex horseshoe chaos on a nonlinear oscillator with hysteretic Bouc-Wen force

A large number of studies have been dedicated to the nonlinear dynamic structures modelled by a classical Duffing oscillator with single and double well [90, 99, 113–115].

$$V(x) = \frac{a_0}{2}x^2 + \frac{b_0}{4}x^4, \quad (3.42)$$

where $V(x)$ is the potential: a and b are the constants, with $a_0 > 0$ and $b_0 < 0$ case of single well and $a_0 < 0$ and $b_0 > 0$ case of double well. The representation of these potentials shows that, this model describes a mass particle that can move in a symmetrical potential well [116]. Under harmonic excitation such systems can exhibit chaotic behavior, for structures subjected to extreme dynamic loads, a degrading, hysteretic restoring force model has been developed by Wen and Baber [4, 115, 117, 118]. Because of their large nonlinearities and discontinuities, hysteretic systems are complicated to investigate. This non-linear hysteretic behavior is typically found in processes where input-output dynamic relationships between variables involve memory effects. Many others researchers studied this potential by introducing an asymmetric term [112, 127, 128]. Diverse ideas have been analyzed, several aspects have been considered [127, 128] and experimental design [111]. Another interesting model takes into account the hysteretic energy due to hysteretic force, unfortunately, few analytical investigations have been done until now [110, 120].

$$V(x) = \frac{a_0}{2}x^2 + \frac{b_0}{4}x^4 + (1 - \alpha)\omega_0^2 \int_{x(0)}^{x(t)} g dx, \quad (3.43)$$

where g is the hysteretic displacement.

We Firstly show that by taking into account higher nonlinear contributions of the hysteretic force, the dynamics of a Duffing oscillator is described by the asymmetric potential. Secondly, the Melnikov theory is used to force the starting point for a successive route to chaotic dynamics taking to account homoclinic and heteroclinic orbits. Some complex behavior has also been investigated. We conclude in the last section.

3.4.1 General mathematical formalism

Bouc-Wen model of hysteresis [57, 78, 101, 121] commonly used in mechanical, civil and seismic engineering for the manufacture, design and control of structures, is a set of non-linear differential equation that reflect local history by introducing an additional state

variable. Here we consider the Duffing-Bouc-Wen oscillator as presented by Figure 3.19, with $H(g, t)$ is given by (3.44).

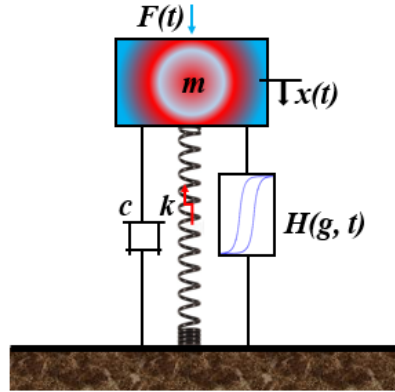


Figure 3.19: Physical model

$$\begin{cases} H(g, t) = k(1 - \alpha)g(t) \\ \dot{g} = D^{-1}(A\dot{x} - \beta|\dot{x}|g|g|^{n-1} - \gamma\dot{x}|g|^n), \end{cases} \quad (3.44)$$

where x , \dot{x} and H are displacement, velocity and purely hysteretic force. With $A > 0$, $\beta > 0$, γ and n are dimensionless quantities controlling the behavior of the model. Parameter A simply controls the hysteresis amplitude. Along with n , β and γ are parameters describing shape of hysteresis. k is a stiffness, α the rigidity ratio of post-yield to pre-yield, The relative input of the hysteretic part is therefore controlled by the parameter α with $0 \leq \alpha < 1$. In this study, thermodynamic admissibility issues impose the following inequality [77, 103, 104]:

$$\beta \geq \gamma \quad (3.45)$$

We impose $\begin{cases} A = 1 \\ \beta + \gamma > 0 \end{cases}$ This condition is a sufficient and necessary for strain-softening behavior [104]. Eqn. (3.44). is integrated for $D = 1$ and $n = 1$. It is claimed that the hysteretic displacement g can thus be derived explicitly and given by :

$$\begin{cases} \dot{g} = [A - (\gamma - \text{sgn}(\dot{x}) \text{sgn}(g) \beta) g] \dot{x} \\ g = \frac{A}{(\varepsilon\beta + \gamma)} (1 - e^{-(\varepsilon\beta + \gamma)x}), \end{cases} \quad (3.46)$$

with $\varepsilon = \text{sgn}(\dot{x}) \text{sgn}(g) = \pm 1$

Thus, the equation of motion of the SDOF system with asymmetric potential under an external excitation can be written as:

$$\ddot{x} + 2\zeta\dot{x} + a_{1,2}x + \lambda_{1,2}x^3 + \frac{(1 - \alpha)A\omega_0^2}{(\varepsilon\beta + \gamma)} (1 - e^{-(\varepsilon\beta + \gamma)x}) = F_0 \sin \Omega t, \quad (3.47)$$

with $\zeta = \frac{c}{2m\omega_0}$; $\omega_0^2 = \frac{k}{m}$ and $a_{1,2} = \pm\omega_0^2$, the parameters ζ , F_0 and Ω are respectively: the damping, the amplitude and the frequency of the excitation. t is the time and the dot over x stands for the time derivative. The Hamiltonian system from Eqn. (3.47) is as follow:

$$\begin{cases} \dot{x} = y \\ \dot{y} = -a_{1,2}x - \lambda_{1,2}x^3 - \frac{(1-\alpha)A\omega_0^2}{(\varepsilon\beta+\gamma)} (1 - e^{-(\varepsilon\beta+\gamma)x}), \end{cases} \quad (3.48)$$

and is Hamiltonian function given as:

$$H(x, y) = \frac{1}{2}y^2 + V(x) \quad (3.49)$$

with $V(x)$ the asymmetric potential:

$$V(x) = \frac{1}{2}a_{1,2}x^2 + \frac{1}{4}\lambda_{1,2}x^4 + \frac{A(1-\alpha)}{(\gamma+\varepsilon\beta)} \left[x - \frac{1 - e^{-(\gamma+\varepsilon\beta)x}}{(\gamma+\varepsilon\beta)} \right] \quad (3.50)$$

The total energy of our systems are plotted in 3D: for a_1 and λ_1 (see Figure 3.20(a)) one observes two stable and one unstable equilibrium points (see Figure 3.20(b)), and for a_2 and λ_2 (see Figure 3.20(d)) one observes two unstable and one stable equilibrium points (see Figure 3.20(e)).

The position $x = 0$ is a static equilibrium position, around which for a small amplitude vibration, Eqn. (3.46) (where $(\varepsilon\beta + \gamma) \succ 0$) can be expanded using a Taylor series:

$$g(x) = \frac{A}{(\varepsilon\beta + \gamma)} (1 - e^{-(\varepsilon\beta+\gamma)x}) = x(1-\alpha)A - \frac{(1-\alpha)(\varepsilon\beta + \gamma)A}{2}x^2 + 0(x^3), \quad (3.51)$$

where $0(x^3)$ represents the higher other terms, Of this approximation, the approximate potential is obtained at Eqn. (3.52)

$$V_{ap}(x) = \frac{1}{2}(a_{1,2} + (1-\alpha)A)x^2 + \frac{1}{3}\left(-\frac{1}{2}A(1-\alpha)(\gamma+\varepsilon\beta)\right)x^3 + \frac{1}{4}\lambda_{1,2}x^4 \quad (3.52)$$

Figure (3.21) gives the correspondence between approximated and the original potential. Thus, one obtains a two stables fixed point: case of double well (Figure 3.21 (a))

$$\left(\frac{\frac{1}{2}A(1-\alpha)(\gamma+\varepsilon\beta) \pm \sqrt{\left(\frac{1}{2}A(1-\alpha)(\gamma+\varepsilon\beta)\right)^2 - 4\lambda_1(a_1 + (1-\alpha)A)}}{2\lambda_1}, 0 \right) \text{ and one unstable } (0, 0).$$

and in the case of single well (Figure 3.21 (b)). **case (a)** two unstables fixed points:

$$\left(\frac{\frac{1}{2}A(1-\alpha)(\gamma+\varepsilon\beta) \pm \sqrt{\left(\frac{1}{2}A(1-\alpha)(\gamma+\varepsilon\beta)\right)^2 - 4\lambda_2(a_2 + (1-\alpha)A)}}{2\lambda_2}, 0 \right) \text{ and one stable } (0, 0).$$

and **case (b)** one unstable fixed point:

$$\left(\frac{\frac{1}{2}A(1-\alpha)(\gamma+\varepsilon\beta) - \sqrt{\left(\frac{1}{2}A(1-\alpha)(\gamma+\varepsilon\beta)\right)^2 - 4\lambda_2(a_2 + (1-\alpha)A)}}{2\lambda_2}, 0 \right) \text{ and one stable } (0, 0).$$

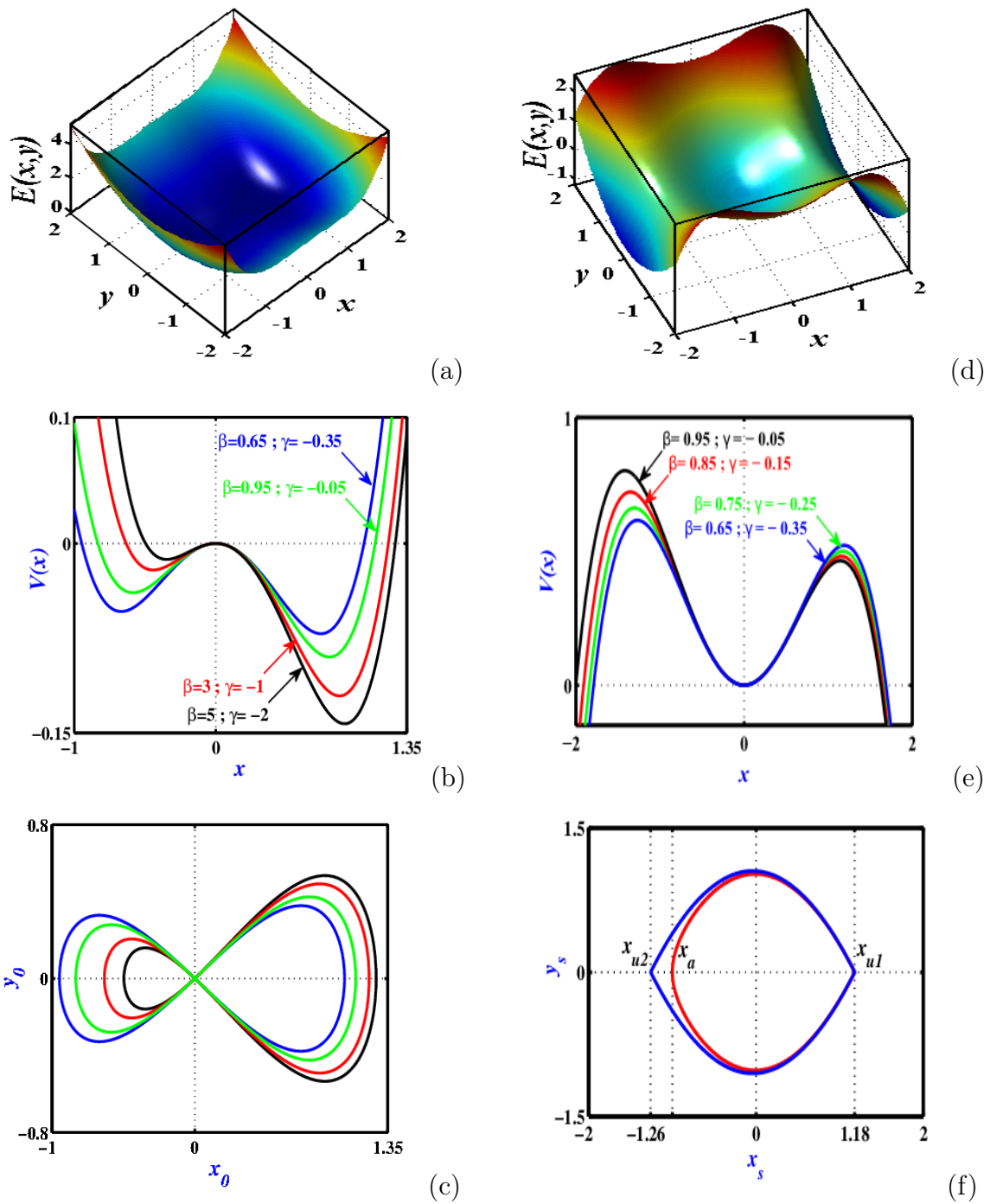


Figure 3.20: Phase space, Asymmetric potentials and separatrix due to the hysteretic force:(a) Phase space of double well, (b) Asymmetric potential of double well ,(c) Asymmetric separatrix of double well, (d) Phase space of single well, (e) Asymmetric potential of single well ,(f) Asymmetric separatrix of single well (Heteroclinic Blue and Homoclinic Red) . $A = 1, \lambda_1 = 1, a_1 = -1, \lambda_2 = -1, a_2 = 1, \alpha = 0.5, n = 1$ and $\varepsilon = 1$.

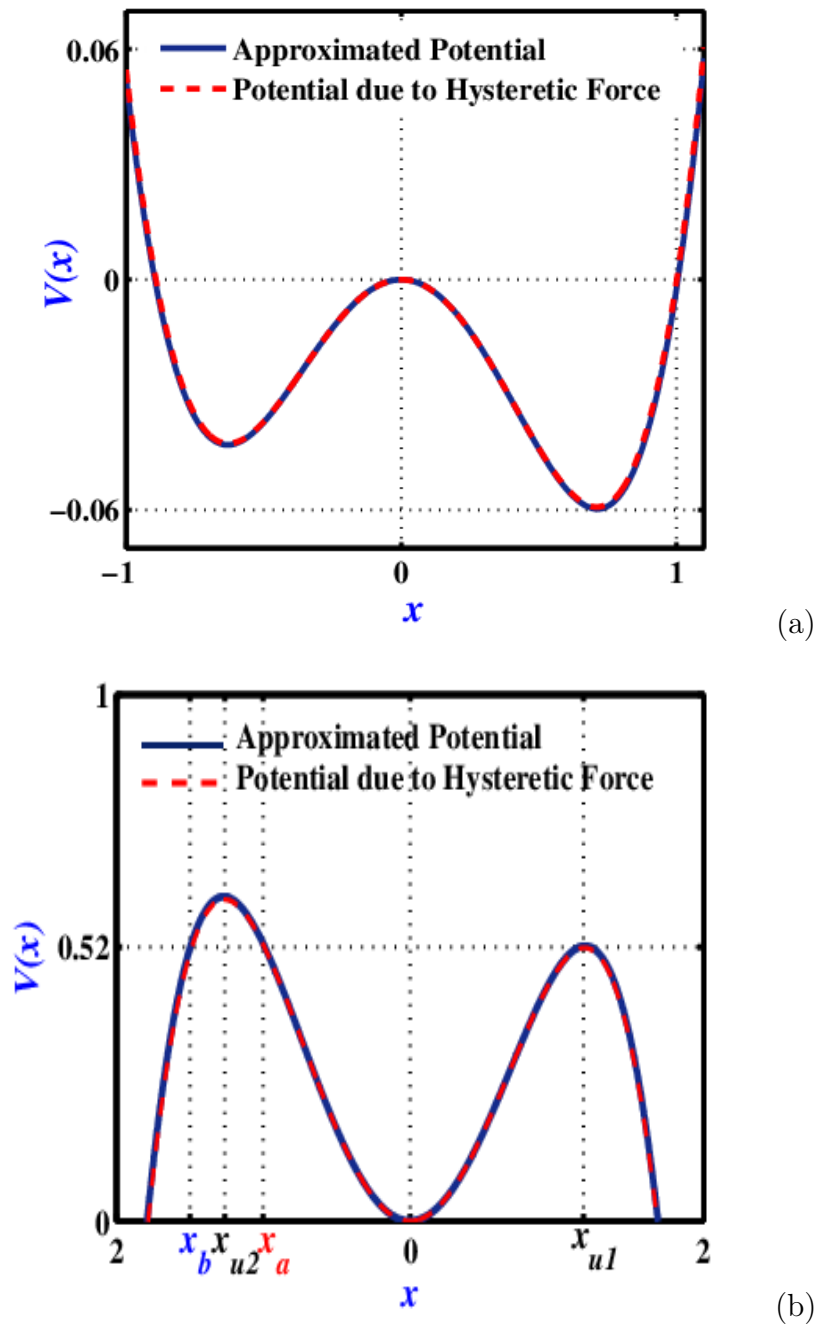


Figure 3.21: Perturbed potential due to hysteretic force for original and approximated potential: (a) Two wells, (b) Single well. for $A = 1$; $\lambda_1 = 1$; $a_1 = -1$; $\lambda_2 = -1$; $a_2 = 1$ $\beta = 0.65$; $\gamma = -0.35$; $\alpha = 0.5$; $n = 1$ and $\varepsilon = 1$.

3.4.2 Complex behaviour versus fractal

3.4.2.1 Melnikov theory

In this section, we used the Melnikov's theory to determine analytically the critical value of external force, where the Melnikov's chaos appears in our system. Consider the generalized dynamical equation of a given system written in vector form:

$$\dot{u} = g_0(u) + \varepsilon' g_p(u, t) , \quad (3.53)$$

where $u = (x, y)$, $(y = \dot{x})$ is the state vector, $g_0(g_1, g_2)$ is the vector field chosen Hamiltonian with the energy H_0 so that:

$$\begin{cases} g_1 = \frac{\partial H_0}{\partial \dot{x}} \\ g_2 = -\frac{\partial H_0}{\partial x} \end{cases} \quad (3.54)$$

and g_p is a periodic perturbation function. In our model, we have:

$$\begin{cases} g_0 = (y, -(a_{1,2} + (1 - \alpha) A) x - (-\frac{1}{2} A (1 - \alpha) (\gamma + \varepsilon \beta)) x^2 - \lambda_{1,2} x^3) \\ g_p = (0, -\zeta y + F_0 \sin \Omega t) \end{cases} \quad (3.55)$$

Let us assume that the unperturbed Hamiltonian system possesses saddle points connected by a separatrix or heteroclinic orbit $\bar{u}(t)$ or only one hyperbolic saddle point with a homoclinic orbit $\bar{u}(t)$. In the presence of the perturbation $g_p(u, t)$, the orbits are perturbed. When the perturbed and the unperturbed manifolds intersect transversally, the geometry of the basin of attraction may become fractal, indicating the high sensitivity to initial conditions, thus chaos. The Melnikov's theory which gives the condition for the fractal basin boundary can be given as follows [96, 133]. Let the Melnikov's function be defined as:

$$M(t_0) = \int_{-\infty}^{+\infty} g_0(\bar{u}(t)) \wedge g_p(\bar{u}(t), t + t_0) dt, \quad (3.56)$$

with $-\infty < t_0 < +\infty$. If $M(t_0)$ has simple zeros so that for a given t_0^l one has $M(t_0^l) = 0$ with $dM(t_0)/dt_0 \neq 0$ at $t = t_0^l$ (condition for transversal intersection), then Eq. (3.50) (for a_1 and λ_1) can present fractal boundaries for motions around different stable equilibrium points. To apply the Melnikov theorem to our model, we derive the equations for the homoclinic and heteroclinic orbits. Let us first consider the case of the potential with two wells (see Figure 3.20(b)). For this case, we have to find the homoclinic orbits connecting the unstable point (see Figure 3.20(c)) $x = 0$ to itself. Making use of

integrals tables [122] (see also [123]) and the method of residues, we obtain the homoclinic orbits defined by:

$$\begin{aligned} x_{ho}^{l,r} &= \frac{-2a_1}{-\frac{1}{3}A(1-\alpha)(\gamma+\varepsilon\beta)\pm\sqrt{\Delta}\cosh\sqrt{-a_1}t} \\ y_{ho}^{l,r} &= \frac{\pm 2a_1\sqrt{-a_1}\Delta\sinh\sqrt{-a_1}t}{\left[-\frac{1}{3}A(1-\alpha)(\gamma+\varepsilon\beta)\pm\sqrt{\Delta}\cosh\sqrt{-a_1}t\right]^2} \end{aligned} \quad (3.57)$$

, ,

with $\Delta = \frac{(A(1-\alpha)(\gamma+\varepsilon\beta))^2}{9} - 2a_1\lambda_1 > 0$ In the case of the potential with a single well (see Figure 3.20(e)), the heteroclinic orbit (see Figure 3.20(f)) connecting the unstable points x_{u2} and x_{u1} and the homoclinic orbit connecting the unstable point x_{u1} to itself. Making use of integrals tables [122], we obtain the heteroclinic orbit defined by the following equations:

$$\begin{aligned} x_{he} &= \frac{4x_1^2}{\left(4x_1 - e^{\left(\frac{t|x_1|}{\sqrt{2}}\right)}\right)} + x_{u1} \\ y_{he} &= \frac{\frac{4|x_1|^3}{\sqrt{2}}e^{\left(\frac{t|x_1|}{\sqrt{2}}\right)}}{\left(4x_1 - e^{\left(\frac{t|x_1|}{\sqrt{2}}\right)}\right)^2} \end{aligned} \quad (3.58)$$

,

and the homoclinic orbit defined by:

$$\begin{aligned} x_{ho} &= \frac{4x_1x_2e^{\left(t\sqrt{\frac{x_1x_2}{2}}\right)}}{-\left(x_1 - x_2\right)^2 - e^{\left(2t\sqrt{\frac{x_1x_2}{2}}\right)} + 2\left(x_1 + x_2\right)e^{\left(t\sqrt{\frac{x_1x_2}{2}}\right)}} + x_{u1} \\ y_{ho} &= \frac{4x_1x_2\sqrt{\frac{x_1x_2}{2}}e^{\left(t\sqrt{\frac{x_1x_2}{2}}\right)}\left(\left(x_1 - x_2\right)^2 - e^{\left(2t\sqrt{\frac{x_1x_2}{2}}\right)}\right)}{\left(-\left(x_1 - x_2\right)^2 - e^{\left(2t\sqrt{\frac{x_1x_2}{2}}\right)} + 2\left(x_1 + x_2\right)e^{\left(t\sqrt{\frac{x_1x_2}{2}}\right)}\right)^2} \end{aligned} \quad (3.59)$$

,

with $x_1 = x_a - x_{u1}$ and $x_2 = x_b - x_{u1}$ (see Figure 3.17(b))

with the expressions of Eqs. (3.57) and (3.58), we can calculate the Melnikov functions for each case. In the case of the potential with two wells, the calculations lead to the

following conditions for the appearance of fractal basin boundaries. For the homoclinic orbits, we have:

$$F_0 \geq F_{Cr} = \left| \frac{\varsigma I_1}{I_2} \right| = \varsigma \left| \frac{\frac{a_1^2 \sqrt{-a_1}}{15\Delta} {}_2F_1\left(1, 2; \frac{7}{2}; \xi\right)}{\frac{4\pi\omega^2}{\Delta \sinh \frac{\Omega\pi}{\sqrt{-a_1}}} {}_2F_1\left(\frac{1}{2} - J \frac{\omega\pi}{\sqrt{-a_1}}, \frac{1}{2} + J \frac{\omega\pi}{\sqrt{-a_1}}; \frac{3}{2}; \xi\right)} \right|, \quad (3.60)$$

with I_1 and I_2 are shown (see **Appendix**).

In the case of the potential with a asymmetric single well, we obtain for the hysteroclinic orbit:

$$F_0 \geq F_{Cr} = \left| \frac{\int_{-\infty}^{+\infty} y_{he}^2 dt}{\int_{-\infty}^{+\infty} y_{he} \sin[\omega(t+t_0)] dt} \right| \quad (3.61)$$

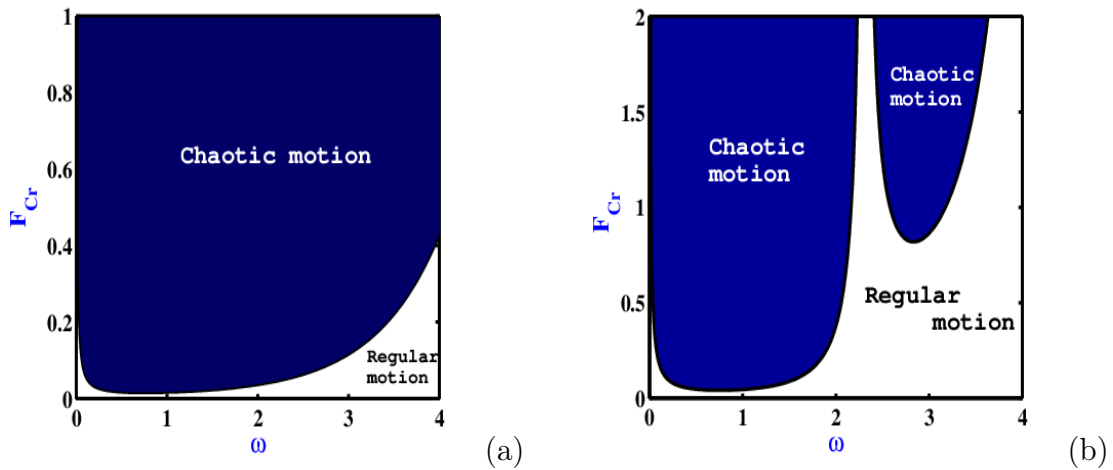


Figure 3.22: Melnikov criteria for the appearance of chaos in the ω - F_{Cr} plane. (a) Case of a homoclinic orbit (potential of Figure 3.17(a)). (b) Case of a single well potential (Figure 3.17(b)). for $A = 1$; $\lambda_1 = 1$; $a_1 = -1$; $\lambda_2 = -1$; $a_2 = 1$ $\beta = 0.65$; $\gamma = -0.35$; $\alpha = 0.5$; $n = 1$ and $\varepsilon = 1$.

The conditions given by Eqs. (3.60) and (3.61) show that some complex behaviors can appear in the system if the Melnikov boundary is crossed. A comparative study of Figure (3.22) for the same parameters of system clearly shows that: The critical force amplitude in the case of an asymmetrical single well potential is greater than that of the asymmetrical double well, and also the area of chaotic behaviours is less important than that observed in the two wells.

3.4.3 Fractal basin boundaries

In order to confirm the analytical predictions from Melnikov's theory, we analyse in this section the regular or irregular geometries of the attraction basins by numerical resolution of Eq. (3.57) by means of Runge-Kutta algorithm of the fourth order. This irregular geometry of the basin of attraction is characterized by the appearance of fractality [96, 98, 110, 132] on the boundary of basin of attraction which reflects the chaos, resulting indisputably from the greater sensitivity due to initial conditions. The influence of F_0 on the shape of the basins of attraction of Figures 3.23 and 3.24 are plotted for the values of Figure 3.22(a) and 3.22(b). For $\omega_0 = 1$, with the values of 3.22(a) and 3.22(b). The Melnikov theory shows that the fractal shape appears for $|F_{Cr}| \approx 0.0135$ as shown in Figure 3.23 (case of double well) and $|F_{Cr}| \approx 0.027$ as shown in Figure 3.24 (case of single well).

These figures display the basin of attraction according to the evolution of external forces. Thus, it appears that the basin has a regular geometry (see Figure 3.23(a) and 3.24(a)), and completely fractal (see Figure 3.23(c), (d) and Figures 3.24(c), (d)) for higher values, sign of the establishment of chaos. In addition, from the appropriate parameters of the BW model, we can also control the appearance of chaos in the SDOF system (see Figure 3.25). It is viewed that for a small amplitude of the external force, the limits of the basin are regular. Above a certain value, it becomes irregular, meaning the presence of Melnikov chaos.

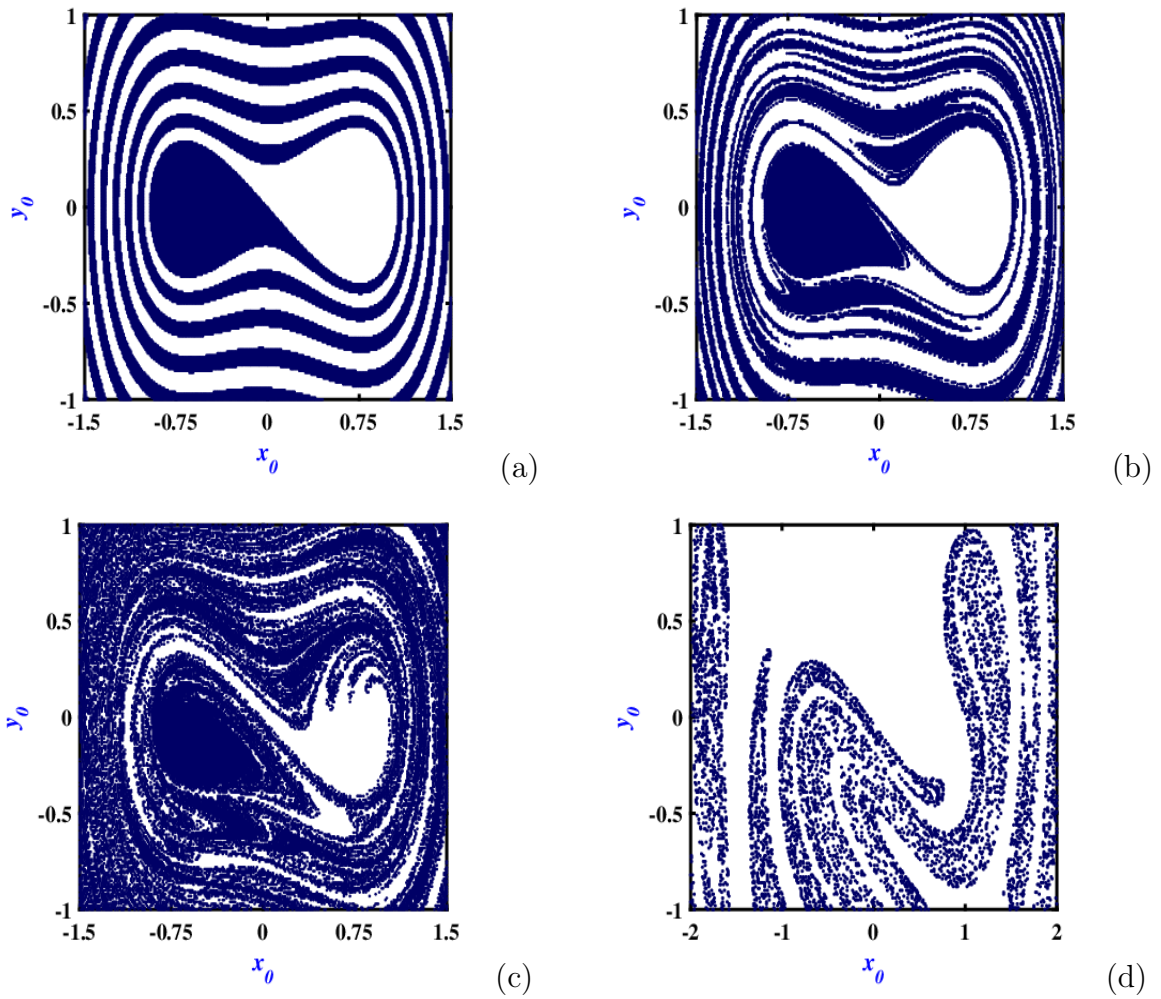


Figure 3.23: Basins of attraction showing the Melnikov predictions: Case of two wells at left well as f_0 increases for $\lambda_1 = 1$, $a_1 = -1$, $\alpha=0.5$, $\beta=0.65$, $\gamma=-0.35$, $\varsigma=0.02$ and $A=1$; a) $f_0 = 0$; b) $f_0 = 0.02$; c) $f_0 = 0.05$; d) $f_0 = 0.5$

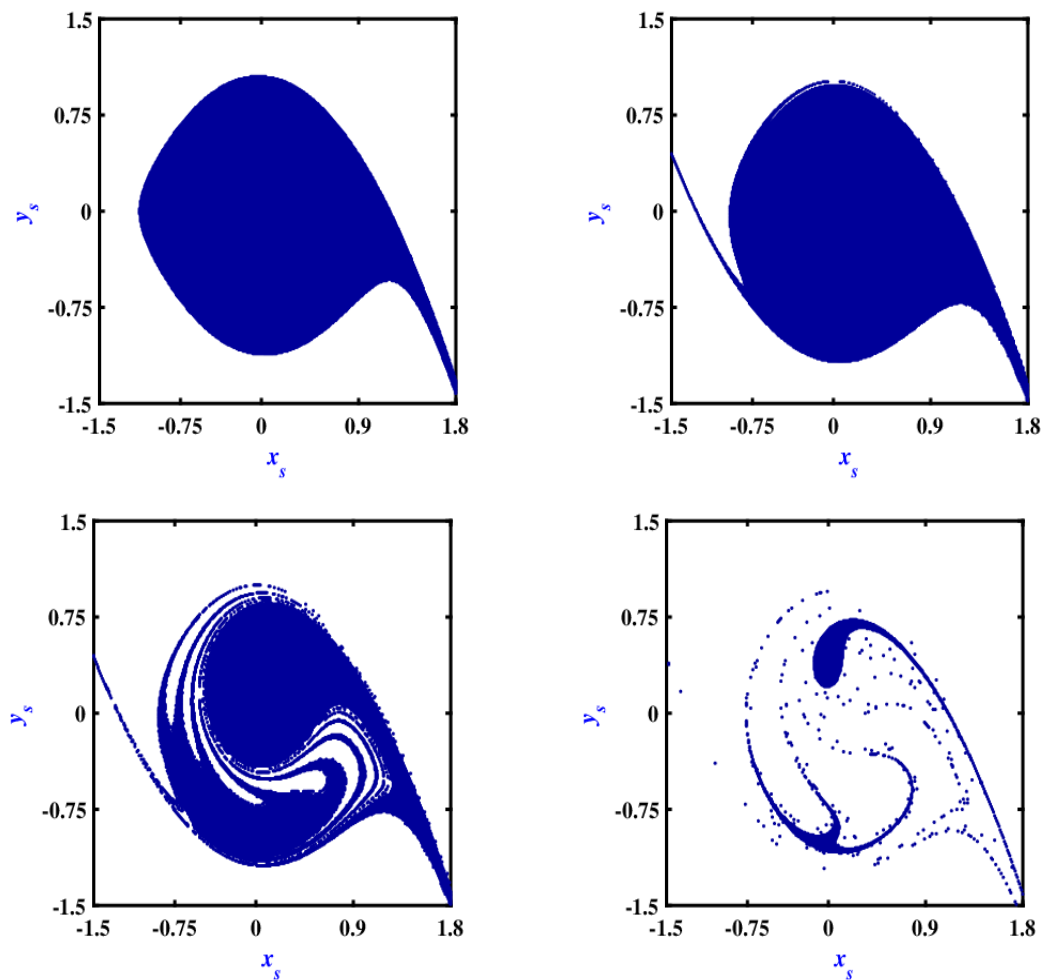


Figure 3.24: Basins of attraction showing the Melnikov predictions: case of single well as f_0 increases for $\lambda_2 = -1$, $a_2 = 1$, $\alpha=0.5$, $\beta=0.65$, $\gamma=-0.35$, $\zeta=0.02$ and $A=1$; a) $f_0 = 0$; b) $f_0 = 0.027$; c) $f_0 = 0.05$; d) $f_0 = 0.15$

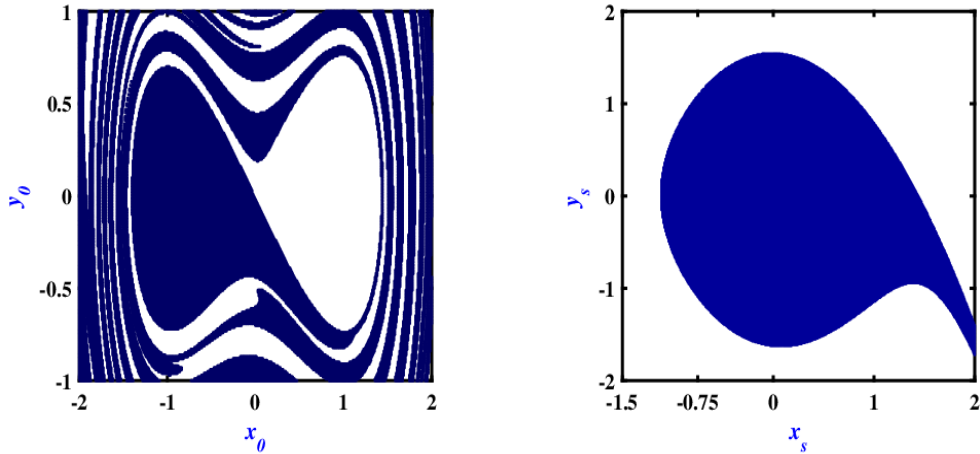


Figure 3.25: Effect of BW parameters A and α on the basins of attraction a) Case of two wells At left, b)case of single well. for $\Omega = 1$; $\alpha = 0.9$; $A = 0.2$ and $f_0 = 0.05$

3.5 Conclusion

In this chapter, we have studied the dynamic behaviors of a structure with one degree of freedom and strongly nonlinear and subjected to a periodic excitation. This nonlinearity is characterized by the BW-type hysteresis force on the one hand and the Bouc-Wen-Duffing type on the other hand. The results obtained were presented and discussed.

Firstly, an analytical approach to the dynamics of a negative stiffness SDOF system with hysteresis force under the effect of periodic loads was considered. As a brief summary, we have shown that the shape of the hysteresis curves and therefore the parameters of the BW model have a major impact on the appearance (fig. 3.2) or the disappearance (fig. 3.3) of the horseshoe chaos in the system. More interesting is the unexpected influence of negative stiffness on the control of chaos in the system (fig. 3.6(b)). To distinguish what we consider to be the most relevant finding, we focused on the effect of the parameters of the BW model on the energy dissipated by the system. Fig. 3.9 reveals an unexpected beneficial role of dissipated energy on system stability. The analytical approach was also verified with numerical simulations and the fairly good agreement between the two approaches was found.

Secondly, we have identified a homoclinic orbit in an SDOF system for a negative value of the \mathbf{A} parameter. We have found that a negative value of the \mathbf{A} parameter causes a threshold for the appearance of chaos in the model. Therefore, this model makes it possible to describe the real behavior of structures for *classes III* and *IV*, while allowing the

control community to guarantee new designs for the reinforcement of the structures.

Finally, we studied the effects of the BW-type hysteresis force on the classical Duffing oscillator. The main conclusion is: The force of hysteresis is responsible for the asymmetric shapes of the potential wells (fig. 3.21(a)) and (fig. 3.21(b)). Indeed, complex behaviors appear within the system as soon as the hysteresis phenomenon is taken into account.

The interesting conclusion is that the shapes of the hysteresis loops and hence the parameters of the BW model play a key role in the occurrence of chaotic dynamics called horseshoe chaos.

GENERAL CONCLUSION

This thesis focused on the dynamic analysis and vibratory control of mechanical structures with hysteresis of the Bouc-Wen type under the action of a periodic external force. The structures studied are considered buildings. These moving structures were modelled as cantilever beams. Specific analytical and numerical analysis methods have been formulated to assess the response of the latter. The Bouc-Wen hysteresis model was used to model the hysteresis force generated by the moving system. The main results obtained in this work are summarized as follows:

In the first chapter, a literature review on hysteresis phenomena and their impact on engineering systems was presented. We also briefly presented some mathematical systems of mechanical hysteresis and some applications of this phenomenon on biological and engineering systems.

In the second chapter, material and methods were presented and detailed, The B-W model is in the form of a PDE therefore, two mathematical considerations of this model were presented. More specifically, Four analytical techniques including Melnikov's theory to predict Smale's horseshoe-type chaos, the theory of residues for the calculation of complex integrals, the Routh-Hurwitz criterion to give the decision on the stability of the Bouc-Wen model and Taylor's development in series for approximations and reconciliation to reality and four numerical methods were presented: the RK4 algorithm to integrate the ODE, the predictor-corrector schemes of Newton-Raphson for non-linear POEs, the Euler method.

Finally, the third chapter was devoted to the dynamic behaviour of mechanical structures with hysteresis force of the Bouc-Wen type and subjected to periodic external force. Two considerations were considered and the main results obtained were presented and discussed. In the first series of results, the problem of the appearance of horseshoe chaos in a system at a degree of freedom in the presence of negative rigidity was considered. Based on the parameters $n = 2$ and $\alpha < 0$ of the B-W model and the energy method, we

demonstrated that the potential of the monostable system is catastrophic, and based on Melnikov's theory, we showed the conditions for the appearance of horseshoe chaos in the system and by playing with the parameters of the model we showed that it is possible to cancel out the chaos in the system.

A second approach was to consider $n = 1$ and $A < 0$ on the basis of the Routh-Hurwitz stability criterion and the energy method, we demonstrated that: for a value of parameter A taken in the stability zone, this system dissipates energy well and its behaviour describes well that of real structures. The analytical approach was also verified with numerical simulations and we observed a fairly good agreement.

In the third series of results, to increase the realism of the studies, we have included a non-linearity of the Duffing type, we have thus demonstrated that the presence of the force of hysteresis in the system leads to the appearance of complex phenomena (the asymmetry of the different forms of potential). Based on the residue theory, we calculated the complex integrals for determining the orbits of the system. we have demonstrated on the basis of Melnikov's theory that for the same values of the system parameters, the simple asymmetric well has a smaller chaotic domain than that of the asymmetric double well and a higher critical value of the amplitude of the external force. It appears that the presence of hysteresis force in the classic Duffing-oscillator makes it more unstable in the case of the double well.

This work leads to some prospective works which could be the improvement of the proposed model of this work: Despite multiple models available to predict it, mechanical hysteresis is often unpredictable. The forces caused by potential deformation and friction are not easy to predict ahead of time. Predicting mechanical hysteresis is different from estimating the amount of mechanical hysteresis that already exists in a system. Models like Bouc-Wen have limitations because they can't easily model highly dynamic systems. Artificial intelligence has led to some new ideas for predicting mechanical hysteresis. Neural networks may be able to predict mechanical hysteresis by learning how hysteresis works in a way that humans cannot directly observe. The accuracy of current mechanical hysteresis models depends on them being used in the proper engineering field, and universal prediction of mechanical hysteresis has remained elusive. Neural networks can model many hysteresis loops at once, allowing granular refinement of predictions with increased input.

Appendix: Special functions (the gamma (Γ) function, the associated Legendre function of the second kind and the Gauss hypergeometric function Eq.(3.57)

$$\Gamma\left(n + \frac{1}{2}\right) = (2n - 1)!! \frac{\sqrt{\pi}}{2^n} \quad (3.62)$$

$$\Gamma(n) = (n - 1)! \quad (3.63)$$

$$\int_0^{+\infty} \frac{\sinh^{2\nu} \tau}{\left(\chi + \sqrt{\chi^2 - 1} \cosh \tau\right)^{\mu+1}} d\tau = \frac{2^\nu e^{-J\nu\pi} \Gamma(\mu - 2\nu + 1) \Gamma\left(\nu + \frac{1}{2}\right)}{\sqrt{\pi} (\chi^2 - 1)^{\frac{\nu}{2}} \Gamma(\nu + 1)} Q_{\mu-\nu}^\nu(\chi) \quad (3.64)$$

$$[\operatorname{Re}(\mu - 2\nu + 1) \succ 0, \operatorname{Re}(\mu + 1) \succ 0] \quad (3.65)$$

$Q_{\mu-\nu}^\nu(\chi)$ is the associated Legendre function of the second kind.

$$Q_\mu^\nu(\chi) = \frac{e^{J\nu\pi} \Gamma(\nu + \mu + 1) \Gamma\left(\frac{1}{2}\right)}{2^{\mu+1} \Gamma\left(\mu + \frac{3}{2}\right)} (\chi^2 - 1)^{\frac{\nu}{2}} \chi^{-\mu-\nu-1} {}_2F_1\left(\frac{\mu + \nu + 2}{2}, \frac{\mu + \nu + 1}{2}; \mu + \frac{3}{2}; \frac{1}{\xi}\right) \quad (3.66)$$

$$M(t_0) = -4a_1^3 \Delta \varsigma I_1 + F_0 I_2 \quad (3.67)$$

with

$$\begin{aligned} I_1 &= \int_{-\infty}^{+\infty} y_{ho}^{l,r^2} dt \\ &= \int_{-\infty}^{+\infty} \frac{\sinh^2 \sqrt{-a_1} t}{\left[-\frac{1}{3} A(1-\alpha)(\gamma+\varepsilon\beta) \pm \sqrt{\Delta} \cosh \sqrt{-a_1} t\right]^4} dt = \frac{-81a_1^2 \Delta \sqrt{-a_1}}{\left[\frac{1}{2} A(1-\alpha)(\gamma+\varepsilon\beta)\right]^4} \frac{\Gamma(2)\Gamma(3/2)}{\sqrt{\pi}\Gamma(4)} \frac{\chi^4}{\sqrt{\chi^2-1}} Q_2^1(\chi) \end{aligned} \quad (3.68)$$

where χ is defined for the left and right side such that $\frac{\sqrt{\chi^2-1}}{\chi} = \pm \frac{3\sqrt{\Delta}}{A(1-\alpha)(\gamma+\varepsilon\beta)}$, $\Gamma(z)$ is the Gamma function, and $Q_m^n(z)$ is the associated Legendre function of the second kind. Using the definition and functional relation of the Gamma function and the associated Legendre function of the second kind listed, integral I_1 becomes:

$$I_1 = \frac{a_1^2 \sqrt{-a_1}}{15\Delta} {}_2F_1\left(1, 2; \frac{7}{2}; \xi\right) \quad (3.69)$$

where $\xi = \frac{18a_1\lambda_1}{18a_1\lambda_1 - (A(1-\alpha)(\gamma+\varepsilon\beta))^2}$ and ${}_2F_1(a, b; c; z)$ is the hyper-geometric function.

$$\begin{aligned} I_2 &= \int_{-\infty}^{+\infty} y_{ho}^{l,r} \sin \Omega t dt \\ &= \pm \frac{4\pi\Omega^2}{\Delta \sinh \frac{\Omega\pi}{\sqrt{-a_1}}} {}_2F_1\left(\frac{1}{2} - J \frac{\Omega}{2\sqrt{-a_1}}, \frac{1}{2} + J \frac{\Omega}{2\sqrt{-a_1}}; \frac{3}{2}; \xi\right) \end{aligned} \quad (3.70)$$

with $J^2 = -1$.

$${}_2F_1(a, b; c; \chi) = \sum_{n=0}^{+\infty} \frac{(a)_n (b)_n \chi^n}{(c)_n n!}, \quad |\chi| < 1, \quad (3.71)$$

then $b = \bar{a}$ one has

$${}_2F_1(a, \bar{a}, c; \chi) = \sum_{n=0}^{+\infty} \frac{(|a| |\bar{a}|)_n \chi^n}{(c)_n n!}, \quad |\chi| < 1, \quad (3.72)$$

This expression of ${}_2F_1(a, \bar{a}, c, z)$ is always a positive real number.

And the Pochhammer symbol is defined as

$$(a)_n = a(a+1)(a+2)\dots(a+n-1), \quad (a)_0 = 1 \quad (3.73)$$

Bibliography

Bibliography

- [1] **S. Mintz**, (2013), The Significance of Nonlinearity in the Natural Sciences, *Springer*.
- [2] **A. al Majid**, (2010), Dissipation of energy in vibratory mechanics, hysteresis operator, metrical phenomena, *PhD, insa Lyon Laboratory of Structural Mechanics*, pp. 6-65.
- [3] **R. Bouc**, (1966), Solution périodique de l'équation de la ferorésonance avec hystéérésis, *C. R. Acad. Sci. Paris, Serie A, vol. 263*, pp. 497-499.
- [4] **Y. K. Wen**, (1976), Method for random vibration of hysteretic systems, *Journal of the Engineering Mechanics Division*, 102(EM2), 246-263.
- [5] **I. D. Mayergoyz**, (1991), Mathematical Models of Hysteresis, *Springer, New York*.
- [6] **A. Visintin**, (1994), *Differential Models of Hysteresis*, Springer-Verlag, Berlin.
- [7] **M. Brokate and J. Sprekels**, (1996), Hysteresis and Phase Transitions, *Springer-Verlag, Berlin* .
- [8] **P. Krejci and V. Lovicar**, (1990), Continuity of hysteresis operators in Sobolev spaces, *Aplikace Matematiky, vol. 35, no. 1*, pp. 60-66.
- [9] **F. Preisach**, (1935), "Über die magnetische nachwirkung," *Zeitschrift für Physik, vol. 94*, pp. 277-302.
- [10] **A. M. Aly**, (2013), Vibration control of buildings using magnetorheological damper: a new control algorithm, *Journal of Engineering*.
- [11] **R. Bouc**, (1971), Modèle mathématique d'hystérésis (a mathematical model for hysteresis), *Acustica, 21*, 16-25.

-
- [12] **T. T. Nguyen and K. A. Kyoung**, A hysteresis functional link artificial neural network for identification and modelpredictive control of SMA actuator, *Journal of Process Control*, 22, 766-777
- [13] **S. Haykin**, (1994), Neural Networks, Maxwell Macmillan, *Ottawa, ON, Canada, 1994.*
- [14] **J. A. Ewing**, (1881), On the production of transient electric currents in iron and steel conductors by twisting them when magnetized or by magnetising them when twisted, *Proc. R. Soc. Lond.*, vol. 33, pp. 21-23.
- [15] **H. Kronmüller and M. Fähnle**, (2003), Micromagnetism and the Microstructure of Ferromagnetic Solids. *Cambridge, U. K. : Cambridge Univ. Press.*
- [16] **E. Madelung**, (1905), Über magnetisierung durch schnellverlaufende ströme und die wirkungsweise des rutherford-marconischen magnetdetektors, *Ann. Phys.*, vol. 17, pp. 861-890.
- [17] **P. Weiss**, (1907), Hypothesis of the molecular field and ferromagnetic properties, *J. Phys.*, vol. 4, no. 6, pp. 661-690.
- [18] **F. Preisach**, (1935), Über die magnetische nachwirkung, *Zeitschrift für Physik*, vol. 94, pp. 277-302.
- [19] **W. B. Haines**, (1930), Studies in the physical properties of soil: V. the hysteresis effect in capillary properties, and the modes of moisture distribution associated therewith, *J. Agricultural Sci.*, vol. 20, pp. 97-116.
- [20] **L. D. Landau**, (1937), *Phys. Z. Soviet Un.*, vol. 11, p. 26.
- [21] **M. Krasnoselskii and A. Pokrovskii**, (1989), Systems with Hysteresis. *New York: Springer-Verlag.*
- [22] **A. Dixit**, (1989), Hysteresis, import penetration, and exchange rate passthrough, *The Quart. J. Econ.*, vol. CIV, pp. 205-228.
- [23] **Johnson, R. Colin**. (2012), 'Missing link' memristor created: Rewrite the textbooks.
- [24] **M. Brokate and A. Visintin**, (1989), Properties of the Preisach model for hysteresis, *J. Reine und Angewandte Mathematik*, vol. 402, pp. 1-40.

- [25] **G. Bertotti**, (1998), Hysteresis in Magnetism: For Physicists, Materials Scientists, and Engineers, *Ed. Academic Press*.
- [26] **G. Lin, D. Yang, and R. O. Warrington**, (1992), A computational model of the shape memory alloys for the design and control of micro actuators, *Micromechanical Systems*, vol. 40, pp. 171-181.
- [27] **D. Hughes and J. T. Wen**, (1997), Preisach modeling of piezoceramic and shape memory alloy hysteresis, *Smart Materials and Structures*, vol. 6, no. 3, pp. 287-300.
- [28] **K. Kuhnen**, (2003), Modeling, identification and compensation of complex hysteretic nonlinearities: A modified Prandtl-Ishlinskii approach, *European Jour. of Cont.*, vol. 9, no. 4, pp. 407-418.
- [29] **M. A. Janaideh, J. Mao, S. Rakheja, W. Xie, and C. Y. Su**, (2008), Generalized Prandtl-Ishlinskii hysteresis model: Hysteresis modeling and its inverse for compensation in smart actuators, *Proc. IEEE Conf. Dec. Contr.*, pp. 5182-5187.
- [30] **A. K. Padthe, B. Drincic, J. Oh, D. D. Rigos, S. D. Fassois, and D. S. Bernstein**, (2008), Duhem modeling of friction-induced hysteresis: Experimental determination, of gearbox stiction, *IEEE Contr. Sys. Mag.*, vol. 28, pp. 90-107.
- [31] **C. Canudas de Wit, H. Olsson, K. J. Åström, and P. Lischinsky**, (1995), A new model for control of systems with friction, *IEEE Trans. Autom. Contr.*, vol. 40, no. 3, pp. 419-425.
- [32] **P. Dahl**, (1976), Solid friction damping of mechanical vibrations, *AIAA J.*, vol. 14, no. 2, pp. 1675-82.
- [33] **Jin Hyong Oh and D. S. Bernstein**, (2005), Semilinear Duhem model for rate-independent and rate-dependent hysteresis, *IEEE Trans. Autom. Contr.*, vol. 50, pp. 631-645.
- [34] **H. Olsson, K. J. Åström, C. Canudas de Wit, M. Gafvert, and P. Lischinsky**, (1998), Friction models and friction compensation, *European Journal of Control*, vol. 4, no. 3, pp. 176-195.
- [35] **H. Cho and J. R. Barber**, (1998) Dynamic behavior and stability of simple frictional systems, *Mathl. Comput. Modeling*, vol. 28, no. 4-8, pp. 37-53.

-
- [36] **Hanbum Cho, J. R. Barber**, (1999), Stability of the three-dimensional Coulomb friction law, *Proc. R. Soc. Lond. A*, vol. 455, pp. 839-861.
- [37] **P. Dahl**, (1976), Solid friction damping of mechanical vibrations, *AIAA J.*, vol. 14, no. 2, pp.16, 75-82.
- [38] **P. A. Bliman**, (1992), Mathematical study of the Dahl's friction model, *European J. of Mechanics and Solids*, vol. 11, no. 6, pp. 835-848.
- [39] **Y. Q. Ni, Z. G. Ying, J. M. Ko, and W. Q. Zhu**, (2002), Random response of integrable Duhem hysteretic systems under non-white excitation, *Int. J. NonLinear Mech.*, vol. 37, no. 8, pp. 1407-1419.
- [40] **J. Suhardjo, B. F. Spencer and M. K. Sain**, (1990), Feedback-feedforward control of structures under seismic excitation, *Struct. Safety*, 8, pp69-89.
- [41] **B. F. Spencer and S. Nagarajaiah**, (2003), State of the Art of Structural Control, *Journal of Structural Engineering* 129 845-856.
- [42] **U. E. Dorka**, (2014), Introduction to Earthquake Engineering: Introduction to Seismic Control, *published October 2014*.
- [43] **U. E. Dorka**, (1994), Hysteretic device systems for earthquake protection of buildings, *Proc. 5th US nat. conf. on earthq. eng., Chicago, USA*, 775-785.
- [44] **U. E. Dorka and G. A. Conversano**, (1995), Seismic retrofit of Allstate Building, *IABSE symposium, San Francisco, USA*, 145-150.
- [45] **I. S. Idrizi, U. E. Dorka and Z. S. Idrizi**, (2012), Application of HYDE structural control system for RC buidings, *15th World Conference on Earthquake Engineering, LISBOA 2012*.
- [46] **D. Okuyucu, U. E. Dorka and M. Sharifi**, (2009), Tendon Systems for Seismic Upgrading of Historical Masonry Buildings, A Preliminary Feasibility Study: Erzurum Double Minaret Madrasah, Symposium with International Participation on Strengthening and Preserving Historical Buildings and Cultural Heritage - II, *Diyarbakir, Turkey, 15th-17th October 2009*.

- [47] **B. R. Nana Nbandjo and U. E. Dorka**, (2016), Effect of tendon structural control on the appearance of horseshoes chaos on a cantilever beam due to seismic action, *Advances in Mechanical Engineering* DOI: 10.1177.
- [48] **M. G. Castellano, M. Indirli, A. Martelli, J.J Azedevo, G. E. Sincarian, D. Tirelli, V. Renda, G. Croci, M. Biritognolo, A. Bonci and A. Viskovic**, (1999), Seismic Protection of Cultural Heritage Using Shape Memory Alloy Devices- An EC Funded Project (ISTECH), *International Post-SmiRT Conference Seminar on Seismic Isolation, Passive Energy Dissipation and Active Control of Vibration of Structures, Cheju, Korea*.
- [49] **A. Ueda et al**, (1996), Why five story pagodas hardly collapsed, Shincho-sha, Japan.
- [50] **Y. Wu, X. Song, X. Gu and L. Luo**, (2018), Dynamic performance of a multi-story traditional timber pagoda, *Engineering Structures*, 159 277-285.
- [51] **T. Hanazato, D. Ayaki, Y. Ogiwara, R. Uchida, Sato, M. Misu, M. Takayama and I. Sakamoto**, (2012), Seismic Design and Construction of a Traditional Timber-Made Five-Storied Pagoda by Applying Coupled Vibration Control, *15th World Conference on Earthquake Engineering, LISBOA*.
- [52] **T. Bock, T. Linner and S. Miura**, (2011), Robotic High-Rise Construction of Pagoda Concept: innovative earthquake-proof Design for the Tokyo Sky Tree, *CT-BUH 2011 World Conference, Seoul, Korea*.
- [53] **M. L. Hodgdon**, (1988), Applications of a theory of ferromagnetic hysteresis, *IEEE Transactions on Magnetic*, 24(1), 218-221.
- [54] **M. L. Hodgdon**, (1967), Mathematical theory and calculations of magnetic hysteresis curves, *IEEE Transactions on Magnetic*, 24(6), 3120-3122.
- [55] **A. K. Padthe, B. Drincic, J. Oh, D. D. Rizos, S.D. Fassois, and D. S. Berstein**, Duhem modeling of friction induced hysteresis, (2008) *IEEE Control System Magazine*, vol. 28(5), 90-107.
- [56] **A. Rodriguez, N. Iwata, F. Ikhouane, and J. Rodellar**, (2009), Modeling and identification of a large-scale magnetorheological fluid damper, *Smart Material and Structures*, vol. 18, pp. 374379.

- [57] **R. Bouc**, (1967), Forced vibration of mechanical systems with hysteresis. *In: Proceedings of 4th Conference on Non-linear Oscillation, Prague, Czechoslovakia*
- [58] **M. Saatcioglu, G. Ozcebe**, (1989), Response of reinforced concrete columns to simulated seismic loading. *ACI Struct. J. 86(1)*, 3-12.
- [59] **S. P. Triantafyllou and V. K. Koumoussis**, (2011), Small and large displacement dynamic analysis of frame structures based on hysteretic beam elements. *J. Eng. Mech. 138(1)*, 36-49.
- [60] **I. D. Lefas and M. D. Kotsovos**, (1990), Strength and deformation characteristics of reinforced concrete walls under load reversals. *ACI Struct. J. 87(6)*, 716-726.
- [61] **A. Madan, A. M. Reinhorn and J. B. Mander**, (2008), Fiber-element model of posttensioned hollow block masonry shear walls under reversed cyclic lateral loading. *J. Struct. Eng. 134(7)*, 1101-1114.
- [62] **T. Sireteanu, M. Giuclea and A. M. Mitu**, (2010), Identification of an extended Bouc-Wen model with application to seismic protection through hysteretic devices. *Comput. Mech. 45(5)*, 431-441.
- [63] **G. Quaranta, G. C. Marano, R. Greco and G. Monti**, (2014), Parametric identification of seismic isolators using differential evolution and particle swarm optimization. *Appl. Soft. Comput. doi:10.1016/j.asoc.2014.04.039*
- [64] **G. C. Foliente**, (1995), Hysteresis modeling of wood joints and structural systems, *J. Struct. Eng. 121(6)*, 1013-1022
- [65] **N. Gerolymos, G. Gazetas**, (2006), Static and dynamic response of massive caisson foundations with soil and interface nonlinearities validation and results, *Soil Dyn. Earthq. Eng. 26*, 377-394.
- [66] **N. M. Kwok, Q. P. Ha, T. H. Nguyen, J. Li and B. Samali**, (2006), A novel hysteretic model for magnetorheological fluid dampers and parameter identification using particle swarm optimization. *Sens Actuators A 132*, 441-451
- [67] **S. Talatahari, A. Kaveh and N. M. Rahbari**, (2012), Parameter identification of Bouc-Wen model for MR fluid dampers using adaptive charged system search optimization, *J. Mech. Sci. Technol. 26(8)*, 2523-2534.

- [68] **W. Hoon, Y. K. Yoon, J. Haeil and N. L. Gwang**, (2001), Nonlinear rate-dependent stick-slip phenomena: modeling and parameter estimation, *Int. J. Solids Struct.* 38, 1415-1431.
- [69] **T. P. Gunstona, J. Rebelleb, M. J. Griffina**, (2004), A comparison of two methods of simulating seat suspension dynamic performance, *J. Sound Vib.* 278, 117-134.
- [70] **M. Ismail, F. Ikhoulane, J. Rodellar**, (2009), The hysteresis Bouc-Wen model, a survey. *Arch. Comput. Methods Eng.* 16(2), 161-188.
- [71] **S. P. Triantafyllou and V. K. Koumousis**, (2011), Bouc-Wen type hysteretic plane stress element, *J. Eng. Mech.* 138(3), 235-246 .
- [72] **S. P. Triantafyllou and V. K. Koumousis**, (2012), An hysteretic quadrilateral plane stress element, *Arch. Appl. Mech.* 82(10-11), 1675-1687.
- [73] **M. Ülker-Kaustell and R. Karoumi**, (2013), Influence of rate-independent hysteresis on the dynamic response of a railway bridge, *Int. J. Rail Transp.* 1(4), 237-257.
- [74] **P. A. BLIMAN**, (1990), Etude mathématique d'un modèle de frottement sec: le modèle de P. R. Dahl, Thèse de doctorat en mathématiques et automatique. Paris : *Université de Paris IX-Dauphine*, 179p.
- [75] **V. S. KOZJAKIN, M. A. KRASNOSEL'SKII and V. POKROVSKII**, (1972), A Vibrationally stable hysterons, *Soviet Math. Dokl.*, vol. 13, n° 5, pp. 1305-1309.
- [76] **A. V. POKROVSKII**, On the theory of hysteresis nonlinearities, *Soviet Math. Dokl.* 1973, vol. 14, n° 3, pp. 896-900.
- [77] **S. Erlicher, and N. Point**, (2004), Thermodynamic admissibility of Bouc-Wen-type hysteresis models, *C. R. Mécanique.*, 332(1), 51-57.
- [78] **F. Ikhoulane, V. Mañosa and J. Rodellar** (2007), Dynamic properties of the hysteretic Bouc-Wen model, *Syst Control Lett* 56:197-205.
- [79] **K. C. Valanis**, (1971), A theory of viscoplasticity without a yield surface. Part i: General theory. *Arch Mech* 23(4):517-533.

-
- [80] **Z. Bazant**, (1978), Endochronic inelasticity and incremental plasticity, *Int. J Solids Struct* 14:691-714.
- [81] **F. Casciati**, (1987), Nonlinear stochastic dynamics of large structural systems by equivalent linearization. In: Proc, 5th int conf on application of statistics and probability in soil and structural engineering, *ICASP5, Vancouver, Canada*.
- [82] **J. E. Hurtado and A. H. Barbat**, (1996), Improved stochastic linearization method using mixed distributions. *Struct Saf* 18(1):49-62.
- [83] **M. Sasani and E. P. Popov**, (2001), Seismic energy dissipators for RC panels: analytical studies. *J Eng Mech* 127(8):835-843.
- [84] **R. S. Thyagarajan and W. D. Iwan**, (1990), Performance characteristics of a widely used hysteretic model in structural dynamics. Technical report, *Proc 4th US nat conf on earthquake engrg, vol 2, EERI, Oakland, Calif, pp 177-186*.
- [85] **Y. K. Wen**, (1989), Methods of random vibration for inelastic structures. *Appl Mech Rev* 42(2):39-52.
- [86] **F. Carli**, (1999), Nonlinear response of hysteretic oscillator under evolutionary excitation. *Adv Eng Softw* 30(9-11):621-630.
- [87] **F. Casciati**, (1988), Smoothed plasticity laws and elasto-plastic analysis. Technical report, Dipartimento di Ingegneria Strutturale e Geotecnica. Università di Roma La Sapienza
- [88] **F. Casciati**, (1989), Stochastic dynamics of hysteretic media. *Struct Saf* 6:259-269.
- [89] **A. M. Mitu, M. Giuclea, G. Ghita and T. Sireteanu**, (2005), Portraing the hysteretic behaviur of materials and devices by Bouc-Wen models, International Symposium on Energy Dissipation. Acoustical, Vibratory and Seismic Processes, *Bucharest, paper on CD-ROM Proceedings*.
- [90] **A. H. Nayfeh, D. T. Mook**, (1979), Nonlinear oscillations. *Wiley-Interscience New York*.
- [91] **C. Hayashi**, (1964), Nonlinear oscillations in physical systems, *McGraw-Hill New-York*.

- [92] **N. N. Bogoliubov and Y. A. Mitropolsky**, (1961), Asymptotic Methods in the Theory of Nonlinear Oscillations, *Gordon and Breach New York*.
- [93] **M. Schreiber**, (1977), Differential Forms, *Springer-Verlag New York*.
- [94] **C. Von Westenholz**, (1981), Differential Forms in Mathematical Physics, *North Holland Amsterdam*.
- [95] **Taylor, Brook** (1715). Methodus Incrementorum Directa et Inversa [Direct and Reverse Methods of Incrementation] (in Latin). London. p. 21-23 (Prop. VII, Thm. 3, Cor. 2). Translated into English in Struik, D. J. (1969). A Source Book in Mathematics 1200-1800. *Cambridge, Massachusetts: Harvard University Press. pp. 329-332*.
- [96] **V. K. Melnikov**, (1963), On the stability of the center for time periodic perturbations, *Trans. Moscow Math. 12, pp. 1-57*.
- [97] **P. Holmes**, (1979), A nonlinear oscillator with a strange attractor, *Philos. Trans. R. Soc A292, pp. 419-418*
- [98] **S. Wiggins**, (1990), Introduction to Applied Nonlinear Dynamical Systems and Chaos. *Springer Verlag New York*.
- [99] **J. Guckenheimer and P. Holmes**, (1983), Nonlinear Oscillations, Dynamical Systems, and Bifurcations of Vector Fields, *Springer-Verlag New York*.
- [100] **H. Press, S. A. Teukolsky, W. T. Vetterling and B.P. Flannery**, (2007), Numerical Recipes: The Art of Scientific Computing, *Cambridge University Press ISBN 0521880688, August*.
- [101] **F. Ikhouane and J. Rodellar**, (2005), On the hysteretic Bouc-Wen model. Part I: Forced limit cycle characterization, *Nonlinear Dyn, 42 63-78*.
- [102] **F. Ikhouane, J. Hurtado and J. Rodellar**, (2007), Variation of the hysteresis loop with the Bouc-Wen model parameters, *Nonlinear Dyn, 48 361-380*.
- [103] **C. W. Wong, Y. Q. Ni and J. M. Ko**, (1994), Steady-state oscillations of hysteretic differential model. Part II: performance analysis, *Journal of Engineering Mechanics, 11 2299-2325*

-
- [104] **E. Aristotelis Charalampakis**, (2015), The response and dissipated energy of Bouc-Wen hysteretic model revisited, *Arch Appl Mech*, 85 1209-1223.
- [105] **H. G. Li and G. Meng**, (2007), Nonlinear dynamics of SDOF oscillator with Bouc-Wen hysteresis,101. *Chaos, Solitons and fractals* 34 337-343.
- [106] **L. M. Anague Tabejieu, B. R. Nana Nbandjo and U. Dorka**, (2017), Identification of horseshoes chaos in a cable stayed-bridge subjected to randomly moving loads, *International Journal of Non-Linear Mechanics*.
- [107] **B. R. Nana Nbandjo and P. Wofo**, (2011), Modelling of the dynamics of Eulers beam by φ^6 potential, *Mech. Res. Commun*, 38 542-545.
- [108] **B. R. Nana Nbandjo, Y. Salissou and P. Wofo**, (2005), Active control with delay of catastrophique motion and horseshoes chaos in a single well Duffing oscillator, *Chaos, Solitons and fractals*, 23 809-816.
- [109] **S. Li, Shaopu Yang and W. Guo**, (2004), Dynamic system and invariant manifolds, Investigation on chaotic motion in hysteretic non-linear suspension system with multifrequency excitations, *Mechanics Research Communications*, 31 229-236.
- [110] **O. N. Youtha Ngouoko, B. R. Nana Nbandjo and U. Dorka**, (2021), On the appearance of horseshoe chaos in a non-linear hysteretic systems with negative stiffness, *Arch Appl Mech*, 91, 4621-4630, doi.org/10.1007/s00419-021-02038-5.
- [111] **G. Cicogna and F. Pappoff**, (1987), Asymmetric duffing equation and the appearance of chaos, *Europhys. Lett* 16; 963-967.
- [112] **A. S. Oumarou, B. R. Nana Nbandjo and P. Wofo**, (2011) Appearance of horseshoes chaos on a buckled beam controlled by disseminated couple forces, *Communications in Nonlinear Science and Numerical Simulation* 16 3212-3218.
- [113] **Y. Ueda**, (1979), Randomly transitional phenomena in the system governed by Duffings equation, *J. Stat. Phys*, 20, 181196.
- [114] **F. C. Moon and P.J. Holmes**, (1979), A magetoelastic strange attractor, *J. Sound Vibr*, 65, 275296.
- [115] **J. M. Thompson and H. B. Stewart**, (1986), Non-Linear Dynamics and Chaos, *Wiley, New York*.

- [116] **R. Tchoukuegno R, B. R. Nana Nbandjo, and P. Wofo**, (2002), Resonant oscillations and fractal basin boundaries of a particle in φ^6 potential, *Physica A: Statistical Mechanics and its Applications*.
- [117] **Y. K. Wen**, (1980), Equivalent linearization for hysteretic systems under random.
- [118] **T. T. Baber and Y. K. Wen**, (1980), Stochastic equivalent linearization for hysteretic, degrading, multistory structures, *Civ. Engrg. Studies SRS No. 471, Dept. of Civ. Engrg., Univ. of Illinois, Urbana, 111*.
- [119] **T. T. Baber and Y. K. Wen**, (1981), Random vibration of hysteretic degrading systems, *Jour. Eng. Mech., ASCE, 107(6),1069-1087*.
- [120] **O. N. Youtha Ngouoko and B. R. Nana Nbandjo**, (2023) On appearance of homoclinic chaos in SDOF oscillator with Bouc-Wen hysteresis: Mathematical formalism and dynamics explanation, *Chaos Solitons and Fractals*. **Submitted**
- [121] **H. G. Li, J. V. Zang and B.C. Wen**, (2002), Chaotic behaviours of a bilinear hysteretic oscillator, *Mechanics research communications, 29,283-289*.
- [122] **I. S. Gradshteyn and I. M. Ryzhik**, (1975), Table of Integrals, Series and Products, *4th Edition, Academic, New York*.
- [123] **S. Lenci, G. Menditto and A.M. Tarantino**, (1999), *Int. J. Non-Linear Mech, 34, 615*.
- [124] '<https://www.chinasage.info/inventions.htm>'
- [125] '<https://www.alchimiadellepietre.it/magnetite-usi-proprieta-cristalloterapia/>'
- [126] **K. Nakahara, T. Hisatogu, T. Nagase and Y. Takahashi**, (2000), Earthquake response of ancient five-story pagoda structure of Horyu-ji temple in Japan, *12WCEE, 1229/11/A*.
- [127] **C. A. K. Kwuimy, C. Nataraj and G. Litak**, (2011), Melnikov's criteria, parametric control of chaos, and stationary chaos occurrence in systems with asymmetric potential subjected to multiscale type excitation, *Chaos 21, 043113*.
- [128] **G. Litak and M. Borowiec**, (2005), Oscillators with asymmetric single and double well potentials: transition to chaos revisited, *Acta Mech. 184, (47)*.

-
- [129] **J. E. Ott**, (2002), Chaos in Dynamical Systems, *Cambridge University Press, Cambridge*.
- [130] **T. Erneux**, (2009), Applied delay differential equations. *Springer New York*.
- [131] **E. Saaed, G. Nikolakopoulos, J. E. Jonasson and H. Hedlund**, (2015), A state of the-art review of structural control systems, *Journal of Vibration and Control* 21(5) 919-937.
- [132] **M. Siewe Siewe and B. C. Nono Dueyou**, (2014), Heteroclinic motion and energy transfer in coupled oscillator with nonlinear magnetic coupling, *Non Dyn* 77(5).
- [133] **I. S. Mokem Fokou, C. Nono Dueyou Buckjohn, M. Siewe Siewe and C. Tchawoua**, (2018), Circuit implementation of a piezoelectric buckled beam and its response under fractional components considerations, *Meccanica* (53)2029-2052.

List of publications

-
- 1- **O.N. Youtha Ngouoko**, B.R. Nana Nbandjo and U. Dorka, (2021), On the appearance of horseshoe chaos in a non-linear hysteretic systems with negative stiffness, *Arch Appl Mech*, doi.org/10.1007/s00419-021-02038-5.

Collection of the published papers



REVIEW

O. N. Youtha Ngouoko · B. R. Nana Nbandjo · U. Dorka

On the appearance of horseshoe chaos in a nonlinear hysteretic systems with negative stiffness

Received: 24 April 2021 / Accepted: 31 August 2021
© The Author(s) 2021

Abstract The problem of inhibition of horseshoe chaos in a nonlinear hysteretic systems using negative stiffness is investigated in this paper. The Bouc–Wen model is used to describe the force produced by both the purely hysteretic and linear elastic springs. The analytical investigation of the Hamiltonian shows that the appearance of separatrix in the system is directly related to the parameters of the hysteretic forces. This means that the transverse intersection between the perturbed and unperturbed separatrix can be controlled according to the shape parameters of the hysteretic model.

Keywords Horseshoe chaos · Hysteretic systems · Negative stiffness · Bouc–Wen model · Separatrix

1 Introduction

Nowadays, one of the constant challenges of mechanical systems is to design new reinforcement techniques for existing structures so that they offer a real comfort of safety for their occupant while ensuring the lifespan of the structure [1, 2]. Amongst that, many phenomenological models using hysteresis force for modelling or control of mechanical systems have been proposed [4–8]. It is well known that hysteresis is a typical nonlinear phenomenon. This nonlinear behaviour is encountered in a wide variety of processes in which the input–output dynamic relations between variables involve memory effects.

The idea of employing negative stiffness springs, or ‘anti-springs’, for the dissipation of a large fraction of the energy initially induced into the system can be traced in civil engineering [9–12] and the innovative paper by George Tsiatas and Aristotelis Charalampakis [13]. This spring can easily obtain negative stiffness for negative values of its parameter α , leading to a true softening behaviour. The central concept of these approaches is to significantly reduce the stiffness of the isolator and consequently of the natural frequency of the system even at almost zero levels.

This paper deals with the predictions of conditions for which horseshoe chaos appears in a class of systems with Bouc–Wen hysteresis. In fact, due to the strongly nonlinearity of the Bouc–Wen model, no analytical investigation has been done until now. Predicting the appearance of some dynamic states in the space parameters of the system remains a challenge for engineering application. If force is the input function, and total force versus displacement is considered, then the reduction of the hysteretic force results in total stiffness degradation only, whereas both total strength and total stiffness degrade if displacement is the independent variable. In fact,

O. N. Youtha Ngouoko (✉) · B. R. Nana Nbandjo
Laboratory of Modelling and Simulation in Engineering, Biomimetics and Prototypes, Faculty of Science, University of Yaounde I, P.O. Box 812, Yaounde, Cameroon
E-mail: ynonl@yahoo.fr

O. N. Youtha Ngouoko · B. R. Nana Nbandjo · U. Dorka
Steel and Composite Structures, University of Kassel, Kurt-Wolters-Strasse 3, Kassel 34125, Germany

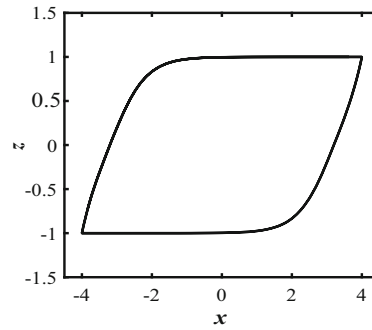


Fig. 1 Softening hysteresis loop generated by the model for $D = 1$, $n = 2$, $A = 1$, $\gamma = 0.05$ and $\beta = 0.95$

the hysteretic energy increases with linearly increasing force, the system degrades nonlinearly and is quite sensitive to the shape parameters of the systems. This sensitivity can give rise to the appearance of separatrix, meaning that the transverse intersection between the perturbed and unperturbed heteroclinic orbits can occur, thus the presence of horseshoe chaos [3, 16–20]. The appearance of horseshoe chaos in a physical system guarantees transient chaotic behaviour of the system. The control of this disturbance is fundamental to design an operation of these physical systems. This paper shows that by playing only on the shape parameters of the Bouc–Wen hysteresis one can predict and suppress the appearance of chaotic motion.

After the derivation of the equation, we show using some mathematical tools the transition from the nondegenerated to degenerated potential and then focus on the conditions for which horseshoe chaos can be suppressed on the system.

2 Mathematical modelling and analytical investigation

Equation of motion for single degree of freedom system consisting of a mass ($m > 0$) connected in parallel to a viscous damper ($c > 0$) with Bouc–Wen hysteretic spring is described by:

$$m\ddot{x}(t) + c\dot{x}(t) + H(x, z, t) = F(t) \quad (1)$$

where x , \dot{x} and \ddot{x} are displacement, velocity and acceleration, respectively, and the nondamping restoring force, H , is composed of both linear and hysteretic restoring forces. H is given by:

$$H(x, z, t) = \alpha kx(t) + k(1 - \alpha)z(t) \quad (2)$$

k is a stiffness, α the rigidity ratio of post-yield to pre-yield and z the hysteretic displacement. The relative input of the hysteretic part is therefore controlled by the parameter α . The nonlinear restoring force is thus a function of the fictitious hysteretic displacement z rather than the total displacement x . At larger displacements, for a nonpinching, nondegrading system the so-called Bouc–Wen model represents the true hysteresis in the form [5, 7, 14]:

$$\dot{z} = D^{-1}(A\dot{x} - \beta|\dot{x}|^n|z|^{n-1}z - \gamma\dot{x}|z|^n) \quad (3)$$

where \dot{z} denotes the time derivative, $n > 1$, $D > 0$, $k > 0$ and $A > 0$. A is the parameter controlling hysteresis amplitude β , γ and n are parameters describing shape and amplitude of hysteresis. In this study, thermodynamic admissibility issues impose the following inequality [23–25]:

$$\beta \geq \gamma \quad (4)$$

Based on (4), the hysteretic loop assumes a bulge shape (see Fig. 1) as opposed to a slim-S one (see Fig. 2).

$$\beta + \gamma \geq 0 \quad (5)$$

Equation (5) is a sufficient and necessary condition for strain-softening behaviour. The combination of β and γ dictates whether the model describes a softening (see Fig. 1) or hardening (see Fig. 2) load–slip relation.

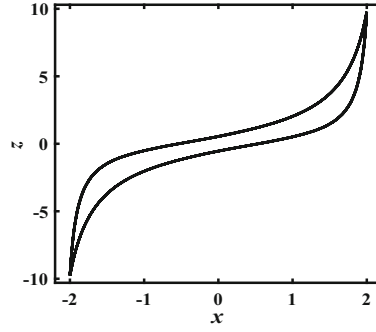


Fig. 2 Hardening hysteresis loop generated by the model for $D = 1$, $n = 2$, $A = 1$, $\gamma = -0.65$ and $\beta = 0.35$

These results are obtained assuming that the external excitation is harmonic, i.e. $F(t) = F_0 \sin(\Omega t)$, where F_0 and Ω are, respectively, the amplitude and frequency of the excitation. To derive the total energy of the system, it is convenient to rewrite the system equation in the form [4]:

$$\begin{aligned} \ddot{x}(t) + 2\zeta\omega\dot{x}(t) + \alpha\omega^2x(t) + \omega^2(1-\alpha)z(t) &= F(t) \\ \omega &= \sqrt{\frac{k}{m}}, \quad \zeta = \frac{c}{2m\omega}. \end{aligned} \quad (6)$$

where ω is a pre-yield natural frequency of the system and ζ a linear viscous damping ratio. The evolution of the hysteretic displacement z given by the following constitutive differential equation:

$$\dot{z} = D^{-1} [A - (\gamma + \text{sgn}(\dot{x}) \text{sgn}(z) \beta) |z|^n] \dot{x} \quad (7)$$

We note that the phase space of the Bouc–Wen oscillator is three dimensional and is spanned by (x, \dot{x}, z) . Setting $\varepsilon = \text{sgn}(\dot{x}) \text{sgn}(z) = \pm 1$ with Sgn denotes the Signum function; in order to integrate z , (7) can be rewritten in the following form:

$$dz = D^{-1} [A - (\gamma + \varepsilon\beta) |z|^n] dx \quad (8)$$

3 Appearance of separatrix and Melnikov analysis

Equations (6) and (8) can be recast in state space form as:

$$\begin{aligned} \dot{x} &= y \\ \dot{y} &= -2\zeta\omega y - \alpha\omega_0^2x - (1-\alpha)\omega_0^2z \\ \dot{z} &= D^{-1} [A - (\gamma + \varepsilon\beta) |z|^n] y. \end{aligned} \quad (9)$$

For $D = 1$ and $n = 2$, one obtains three fixed points $(0, 0, 0)$;

$$\left(-\frac{(1-\alpha)}{\alpha} \sqrt{\frac{A}{\gamma+\varepsilon\beta}}; 0; \sqrt{\frac{A}{\gamma+\varepsilon\beta}} \right) \text{ and } \left(\frac{(1-\alpha)}{\alpha} \sqrt{\frac{A}{\gamma+\varepsilon\beta}}; 0; -\sqrt{\frac{A}{\gamma+\varepsilon\beta}} \right)$$

Taking into account the influence of the hysteretic force, the potential energy of the system, is given by:

$$V(x) = \frac{1}{2} \alpha \omega^2 x^2 + \omega^2 (1-\alpha) \int_{x(0)}^{x(t)} z dx \quad (10)$$

The energy absorbed by the hysteretic element is thus the continuous integral of the hysteretic force and the total energy displacement.

Equation (8) is integrated for $D = 1$ and $n = 2$. The initial conditions $x(0)$, $\dot{x}(0)$, $z(0)$ are known. For the sake of simplicity, it is assumed that $x(0) = \dot{x}(0) = z(0) = 0$. It is claimed that the hysteretic displacement z can thus be derived explicitly and given by:

$$z = \frac{\sqrt{A}}{\sqrt{(\gamma + \varepsilon\beta)}} \tanh\left(\sqrt{A(\gamma + \varepsilon\beta)}x\right) \quad (11)$$

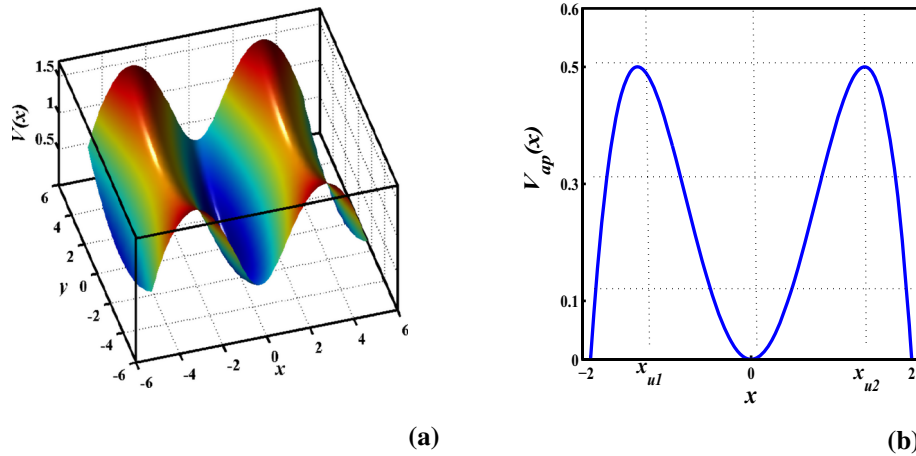


Fig. 3 **a** Phase space. **b** Potential curves of system for $\varepsilon = 1$

Then the complete potential of the system, taking into account the hysteresis component (see Fig. 3a) is given by:

$$V(x) = \frac{1}{2}\alpha\omega^2x^2 + \omega^2\frac{(1-\alpha)\sqrt{A}}{\sqrt{(\gamma+\varepsilon\beta)}}\ln\cosh\left(\sqrt{A(\gamma+\varepsilon\beta)}x\right) \quad (12)$$

The critical amplitude x_u is obtained when the following conditions are satisfied:

$$V'(x) = 0 \text{ and } V''(x) \geq 0 \quad (13)$$

But obtaining the analytical expression using the form given by (11) is quite impossible. To find an approximation solution, we carry out the expansion of $\tanh(\sqrt{A(\gamma+\varepsilon\beta)}x)$ and assume that $\beta = \xi\bar{\beta}$ and $\gamma = \xi\bar{\gamma}$ where ξ is a small positive constant. An expansion in power series of ξ allows to obtain an approximate description of the hysteresis loop by neglecting the ξ^3 and higher powers, and by integration of (10), one obtains:

$$V_{ap}(x) = \frac{1}{2}(\omega^2(\alpha + (1-\alpha)A))x^2 - \frac{1}{12}(\omega^2A^2(1-\alpha)(\gamma+\varepsilon\beta))x^4 \quad (14)$$

The representation of this potential shows that the presence of hysteretic force describes the unbounded monostable potential (see Fig. 3b).

Equation of the dynamic of this system is given by :

$$\ddot{x}(t) + 2\zeta\omega\dot{x}(t) + (\alpha\omega^2(t) + \omega^2(1-\alpha)A)x(t) - \frac{1}{3}\omega^2A^2(1-\alpha)(\gamma+\varepsilon\beta)x^3(t) = F_0\sin(\Omega t) \quad (15)$$

Figure 3 also shows that we have three fixed points: one stable $(0, 0)$ and the other two unstable $(\pm\sqrt{\frac{3(\alpha+(1-\alpha)A)}{(1-\alpha)(\gamma+\varepsilon\beta)A^2}}, 0)$ leading to the appearance of heteroclinic orbit (see Fig. 4). In this case, the separatrix appears leading to the possible transverse intersection between perturbed and unperturbed heteroclinic orbit. This means that the shape parameters of the hysteresis force have a direct link with the appearance of horseshoe chaos in the system. The presence of horseshoe chaos means the existence of a starting point for successive route to chaotic dynamics. This can be detected analytically using Melnikov theory.

4 Melnikov analysis

In the present section, we apply the Melnikov method [16,21,22,26] to detect analytically the effects of Bouc–Wen model parameters on the threshold condition for the inhibition of horseshoe chaos in the system and on the fractal basin boundaries. To apply this method, we introduce a small μ parameter in (15) and rewrite the governing system as the following set of first-order differential equations :

$$\begin{cases} \dot{x}(\tau) = y(\tau) \\ \dot{y}(\tau) = -\omega^2(\alpha + (1-\alpha)A)x(\tau) + \frac{1}{3}A^2\omega^2(\gamma + \varepsilon\beta)(1-\alpha)x^3(\tau) + \mu\Gamma(t) \end{cases} \quad (16)$$

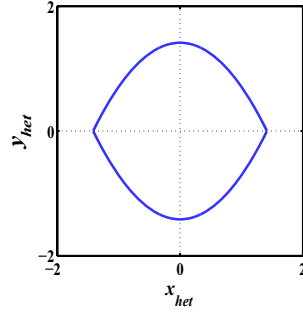


Fig. 4 Heteroclinic orbit of unbounded monostable potential

With $\Gamma(\tau) = -2\zeta\omega y(\tau) + F_0 \cos(\Omega\tau)$. For $\mu = 0$ and after assuming that $x = x(\tau)$; $y = y(\tau)$ the system of (16) is the Hamiltonian system with Hamiltonian function.

$$H(x, y) = \frac{1}{2}y^2 + \frac{1}{2}\omega^2(\alpha + (1-\alpha)A)x^2 - \frac{1}{4}\left(\frac{1}{3}(1-\alpha)(\gamma + \varepsilon\beta)\omega^2 A^2\right)x^4 \quad (17)$$

The saddle points (see Fig. 3) x_{u1} and x_{u2} are connected by heteroclinic orbits (see Fig. 4) that satisfied the following equation:

$$\begin{aligned} x_{het} &= \pm \sqrt{\frac{3(\alpha + (1-\alpha)A)}{(1-\alpha)(\gamma + \varepsilon\beta)A^2}} \tanh\left(\omega\sqrt{\frac{\alpha + (1-\alpha)A}{2}}\tau\right) \\ y_{het} &= \pm \frac{3(\alpha + (1-\alpha)A)\omega}{(1-\alpha)(\gamma + \varepsilon\beta)A^2} \sqrt{\frac{\alpha + (1-\alpha)A}{2}} \operatorname{sech}^2\left(\omega\sqrt{\frac{\alpha + (1-\alpha)A}{2}}\tau\right) \end{aligned} \quad (18)$$

The Melnikov theory defines the condition for the appearance of the so-called transverse intersection points between the perturbed and the unperturbed separatrix or the appearance of the fractality on the basin of attraction. This theory can be applied in the case of (15) by using the formula given by Wiggins [26] as follows:

$$\begin{aligned} M_Y(\tau_0) &= \int_{-\infty}^{+\infty} g_0(u_{het}(\tau)) \times g_p(u_{het}(\tau), \tau + \tau_0) d\tau \\ &= -2\zeta\omega \int_{-\infty}^{+\infty} y_{het}^2(\tau) d\tau + F_0 \int_{-\infty}^{+\infty} y_{het}(\tau) \sin(\Omega(\tau + \tau_0)) d\tau \\ &= I \pm Z(\tau_0) \end{aligned} \quad (19)$$

where

$$I = -24\zeta\omega^2 \sqrt{\frac{\alpha + (1-\alpha)A}{2}} \left(\frac{\alpha + (1-\alpha)A}{(1-\alpha)(\gamma + \varepsilon\beta)A^2} \right)^2$$

and

$$Z(\tau_0) = \frac{3F_0\Omega\pi(\alpha + (1-\alpha)A)\sin(\Omega\tau_0)}{\omega(1-\alpha)(\gamma + \varepsilon\beta)A^2 \sqrt{\frac{\alpha + (1-\alpha)A}{2}} \sinh\left(\frac{\Omega\pi}{2\omega\sqrt{\frac{\alpha + (1-\alpha)A}{2}}}\right)}$$

When the Melnikov function has a simple zero point, the stable manifold and the unstable manifold intersect transversally, and chaos in the sense of Smale horseshoe transform occurs. So let $M_Y(\tau_0) = 0$, one concludes that Melnikov chaos appears when:

$$F_0 \geq F_{CR} = \left| \frac{4\zeta\omega^3(\alpha + (1-\alpha)A)^2}{((\gamma + \varepsilon\beta)(1-\alpha)A^2)\Omega\pi\sin(\Omega\tau_0)} \sinh\left(\frac{\Omega\pi}{2\omega\sqrt{\frac{\alpha + (1-\alpha)A}{2}}}\right) \right| \quad (20)$$

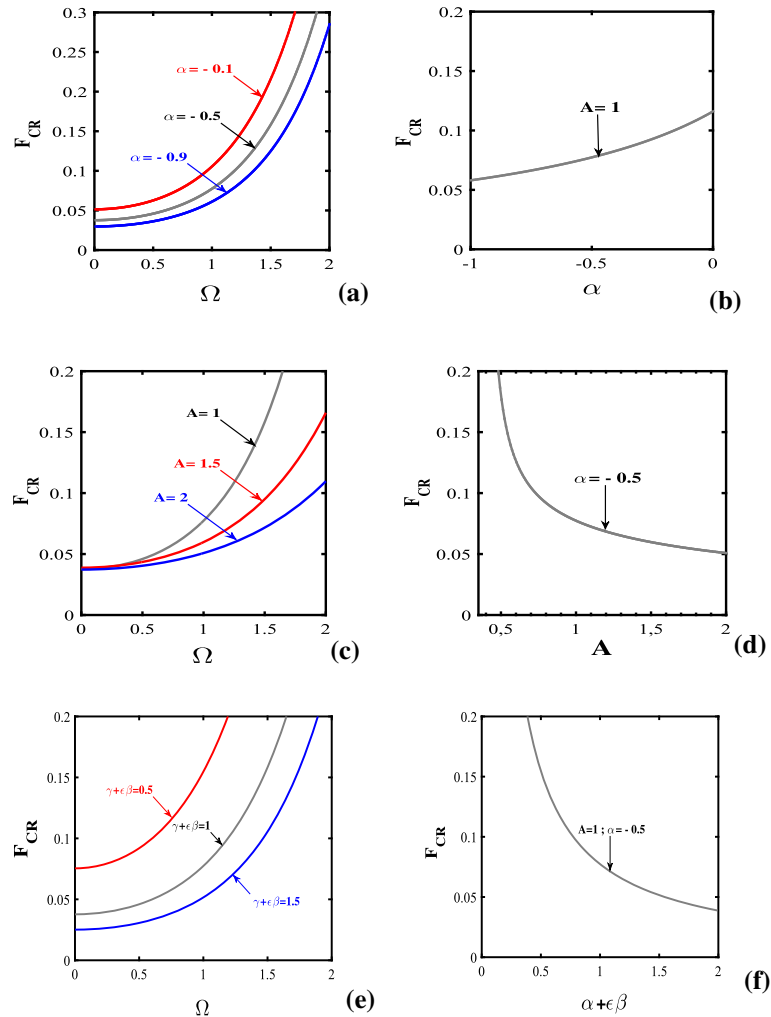


Fig. 5 Evolution of the critical amplitude F_{CR} as a function of : Ω (a), (c) and (e) ; α (b); A (d) and $(\gamma + \epsilon\beta)$ (f) with $\epsilon = 1$

The criterion in Eq. (20) defines the threshold value of F_{CR} for the appearance of a transverse intersection between the perturbed and the unperturbed manifolds. Such a condition is known as necessary for the existence of chaos. The threshold condition is plotted in Fig. 5 as a function of the driving frequency Ω for different values of α (see Fig. 5a), A (see Fig. 5c) and $(\gamma + \epsilon\beta)$ (see Fig. 5e), as function of the parameter α (see Fig. 5b), as function of A (see Fig. 5d) and as function of the parameters $(\gamma + \epsilon\beta)$ (see Fig. 5f).

Figure 5a shows in the space (Ω, F_{CR}) , the lower bound for the appearance of heteroclinic bifurcation for several cases of α parameter. For (Ω, F_{CR}) taken below the lower bound line, the system displays a periodic motion, while possible chaotic motion is observed in the upper domain. It appears that: when α decreases, the surface of the critical force increases; consequently, critical force decreases.

Figure 5b illustrates the effects of negative stiffness on the threshold value of F_{CR} , for $-1 < \alpha < 0$, the threshold increases, it appears that the control effect increases as α increases, this is a sign of the reinforcement of effectiveness of the control. The variations of the critical force as a function of α show that the parameter α plays a preponderant role in its efficiency.

Figure 5c and e shows the critical external forcing amplitude for different values of A and $(\gamma + \epsilon\beta)$, respectively. One can see (Fig. 5c) that when the value of the parameter A increases, the thresholds of the critical values for heteroclinic bifurcation of the harmonic excitation F_{CR} decrease. The same effect is observed with the parameters $(\gamma + \epsilon\beta)$ (Fig. 5e). We conclude that the parameters A and $(\gamma + \epsilon\beta)$ have the same effect on the critical value for chaotic motions.

Figure 5d highlights the fact that as A increases the amplitude of the critical force decreases. Consequently, the choice of the parameter A relating to the reduction of the speed and amplitude of vibration or to the

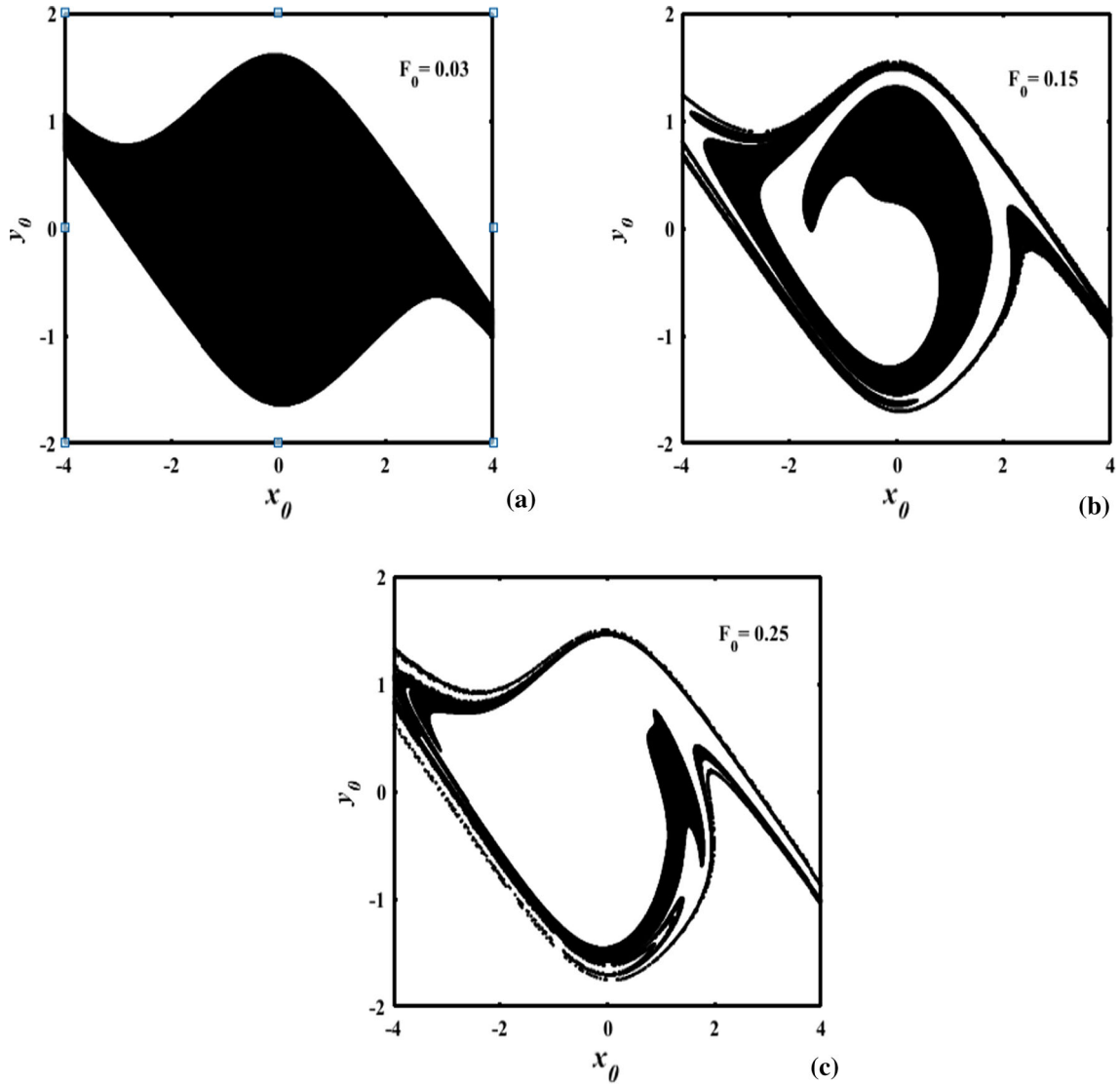


Fig. 6 Basins of attraction showing the confirmation of the analytical prediction for $\varepsilon = 1$, $\alpha = -0.5$, $\beta = 0.95$, $\gamma = 0.05$, $\zeta = 0.02$ and $A = 1$

increase of the stability basin may be the starting point of a route leading to unpredictable behaviour. The same investigations are made in the case of Fig. 5f.

5 Numerical investigation

The existence of a homoclinic or heteroclinic orbit for the detection of horseshoe chaos in physical systems is of paramount importance. Indeed, the choices of control parameters for obtaining the basin of attraction are not done in a random manner. Moreover, it is possible to determine the conditions for which heteroclinic orbit appears, while defining the limits of values of model parameters for which basins can be obtained. Of Eq. (18), it is possible to find the conditions (see Eq. 21) for which the parameters of the Bouc–Wen model will allow to obtain each time a heteroclinic orbit. Thus, if the conditions (I) and (II) are satisfied, horseshoe chaos in the system can be predicted.

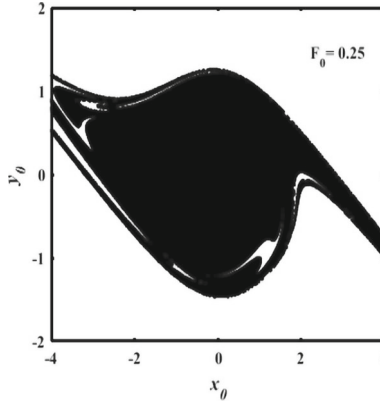


Fig. 7 Effect of parameters $(\gamma + \varepsilon\beta)$, A and α , on the basins of attraction for $\Omega = 1$, $\alpha = -0.4$, $\gamma + \varepsilon\beta = 0.9$ and $A = 0.7$

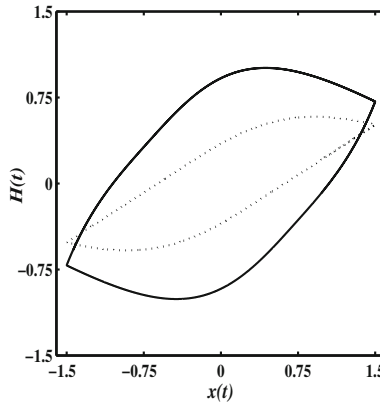


Fig. 8 Response of Bouc–Wen model under cyclic excitation, with parameters used in Fig. 6 without control and Fig. 7 with control: – without control; ... with control

$$A > 0; \quad -1 < \alpha < 0 \quad \text{with} \quad \begin{cases} (I) \begin{cases} \beta + \gamma > 0 \\ \gamma - \beta < 0 \end{cases} \\ (II) \begin{cases} \beta + \gamma > \beta - \gamma \\ \beta - \gamma > 0 \end{cases} \\ (III) \text{All other cases} \quad \emptyset \end{cases} \quad (21)$$

To validate the accuracy of the proposed analytical predictions, we solve numerically Eq. 9 by means of fourth-order Runge–Kutta algorithm. A particular characteristic of the Melnikov theory is the fractality [15, 17, 21] of the basin of attraction and the resulting unpredictability due to the dependence on the initial conditions.

The limit F_{CR} given by (20) is shown in Fig. 6. These figures display the basin of attraction according to the evolution of external forces. Thus, it appears that the basin has a regular geometry (see Fig. 6a), and completely fractal (see Figs. 6b, c) for higher values, sign of the establishment of chaos. In addition, from the appropriate parameters of the Bouc–Wen model, we can also control the appearance of chaos in the SDOF system (see Fig. 7).

Figure 7 shows how when playing with the parameters of Bouc–Wen model it is possible to control system or to cause chaos. Thus, for the same value of critical amplitude and for different parameters of the Bouc–Wen model, the attraction basin is chaotic (see Fig. 6c); in Fig. 7 the attraction basin can be controlled. It is viewed that for a small amplitude of the external force, the limits of the basin are regular. In the case of the soft system, the heteroclinic orbit is clear. Above a certain value, it becomes irregular, meaning the presence of Melnikov chaos in the case of the soft system.

To validate the accuracy of the restoring force, (2) is plotted in Fig. 8; by comparing the curves in this figure, we show that the energy dissipated by the system can be considerably reduced when the system is controlled.

6 Conclusion

We have presented an analytical and numerical solution to describe the link between the presence of horseshoe chaos and hysteretic loop in a SDOF system. The hysteretic behaviour has been modelled by the constitutive differential equation of the first-order so-called Bouc–Wen model. Based on Melnikov theory, the approximate analytical solution has been obtained and we have studied the effects of some main parameters of the system such as α , A , β and γ on the chaotic dynamic of the system on its stability. It appears after dynamics analysis that the shape parameters of the hysteresis force play a key role in the occurrence of chaotic dynamics so-called horseshoe chaos. Thus, taking into consideration a selective situation on the hysteresis function one could be able to quench the appearance of Melnikov chaos in the system. Those predictions are confirmed and complemented by the numerical simulations from which we illustrate the regular nature of the basin of attraction. The analysis has also allowed to estimate the condition for the possible appearance of horseshoe chaos in the system. The main conclusion is that this condition depends strongly of Bouc–Wen parameters in the case of softening system.

Acknowledgements Part of this work was completed during a research visit of Prof Nana Nbandjo at the University of Kassel in Germany. He is grateful to the Alexander von Humboldt Foundation.

Funding Open Access funding enabled and organized by Projekt DEAL.

Open Access This article is licensed under a Creative Commons Attribution 4.0 International License, which permits use, sharing, adaptation, distribution and reproduction in any medium or format, as long as you give appropriate credit to the original author(s) and the source, provide a link to the Creative Commons licence, and indicate if changes were made. The images or other third party material in this article are included in the article's Creative Commons licence, unless indicated otherwise in a credit line to the material. If material is not included in the article's Creative Commons licence and your intended use is not permitted by statutory regulation or exceeds the permitted use, you will need to obtain permission directly from the copyright holder. To view a copy of this licence, visit <http://creativecommons.org/licenses/by/4.0/>.

Declarations

Conflict of interest The authors declare that they have no conflict of interest.

References

1. Majid, B., Xiaojie, W., Faramarz, G.: Modeling of a new semi-active/passive magnetorheological elastomer isolator. *Smart Mater. Struct.* **23**, 1 (2014)
2. Marano, G.C., Pellicciari, M., Cuoghi, T.: Degrading Bouc-Wen Model Parameters Identification Under Cyclic Load. *Int. J. Geotech. Earthq. Eng* (2017)
3. Oumarou, A.S., Nana Nbandjo, B.R., Wofo, P.: Appearance of horseshoes chaos on a buckled beam controlled by disseminated couple forces. *Commun. Nonlinear Sci. Numer. Simul.* **16**, 3212–3218 (2011)
4. Li, H.G., Meng, G.: Nonlinear dynamics of SDOF oscillator with Bouc Wen hysteresis. *Chaos Solitons Fract.* **34**, 337–343 (2007)
5. Ikhoulane, F., Rodellar, J.: On the hysteretic Bouc-Wen model. Part I: forced limit cycle characterization. *Nonlinear Dyn.* **42**, 63–78 (2005)
6. Li, H.G., Zang, J.V., Wen, B.C.: Chaotic behaviours of a bilinear hysteretic oscillator. *Mech. Res. Commun.* **29**, 283–289 (2002)
7. Ikhoulane, F., Mañosa, V., Rodellar, J.: Dynamic properties of the hysteretic Bouc-Wen model. *Syst. Control Lett.* **56**, 197–205 (2007)
8. Mohammed, I., Ikhoulane, F., Rodellar, J.: The Hysteresis Bouc-Wen Model, a Survey. *Arch. Comput. Methods Eng.* **16**, 161–188 (2009)
9. Winterflood, J., Blair, D., Slagmolen, B.: High performance vibration isolation using springs in Euler column buckling mode. *Phys. Lett. A* **300**, 122–130 (2002)
10. Virgin, L., Santillan, S., Plaut, R.: Vibration isolation using extreme geometric nonlinearity. *J. Sound Vib.* **315**, 721–731 (2008)
11. Liu, X., Huang, X., Hua, H.: On the characteristics of a quasi-zero stiffness isolator using Euler buckled beam as negative stiffness corrector. *J. Sound Vib.* **332**, 3359–3376 (2013)
12. Antoniadis, I., Chronopoulos, D., Spitas, V., Koulocheris, D.: Hyper-damping properties of a stiff and stable linear oscillator with a negative stiffness element. *J. Sound Vib.* **346**, 37–52 (2015)
13. Geo, C., Charalampakis, E.: A new Hysteretic Nonlinear Energy Sink (HNES). *Commun. Nonlinear Sci. Numer. Simul.* **60**, 1–11 (2018)
14. Ikhoulane, F., Hurtado, J., Rodellar, J.: Variation of the hysteresis loop with the Bouc-Wen model parameters. *Nonlinear Dyn.* **48**, 361–380 (2007)
15. Nana Nbandjo, B.R., Salissou, Y., Wofo, P.: Active control with delay of catastrophique motion and horseshoes chaos in a single well Duffing oscillator. *Chaos Solitons Fract.* **23**, 809–816 (2005)

16. Melnikov, V.K.: On the stability of the center for time periodic perturbations. *Trans. Moskow Math. Soc.* **12**, 1–57 (1963)
17. Li, S., Yang, S., Guo, W.: Dynamic system and invariant manifolds, Investigation on chaotic motion in hysteretic non-linear suspension system with multi-frequency excitations. *Mech. Res. Commun.* **31**, 229–236 (2004)
18. Biagio, C., Walter, L.: Dynamic Response of Nonlinear Oscillators With Hysteresis. In: *International Conference on Multi-body Systems. Nonlinear Dynamics and Control*, Boston, Massachusetts, USA (2015)
19. Thompson, J.M.T., Stewart, H.B.: *Nonlinear Dyn chaos*. Wiley, London (1986)
20. Angelo, M.T., José, M.B., Jorge, L.P.F.: On elimination of chaotic behavior in a non-ideal portal frame structural system, using both passive and active controls. *J. Vib. Control* **19**, 803–813 (2012)
21. Anague Tabejieu, L.M., Nana Nbandjo, B.R., Dorka, U.: Identification of horseshoes chaos in a cable stayed-bridge subjected to randomly moving loads. *Int. J. Non-linear Mech* (2017)
22. Nana Nbandjo, B.R., Wofo, P.: Modelling of the dynamics of Eulers beam by $\Phi 6$ potential. *Mech. Res. Commun.* **38**, 542–545 (2011)
23. Erlicher, S., Point, N.: Thermodynamic admissibility of Bouc–Wen type hysteresis models. *C.R. Mec.* **332**, 51–57 (2004)
24. Wong, C.W., Ni, Y.Q., Ko, J.M.: Steady-state oscillations of hysteretic differential model. Part II: performance analysis. *J. Eng. Mech.* **11**, 2299–2325 (1994)
25. Aristotelis, C.E.: The response and dissipated energy of Bouc-Wen hysteretic model revisited. *Arch. Appl. Mech.* **85**, 1209–1223 (2015)
26. Wiggins, S.: *Introduction to Applied Nonlinear Dynamical Systems and Chaos*. Springer, New York (1990)

Publisher's Note Springer Nature remains neutral with regard to jurisdictional claims in published maps and institutional affiliations.